FRICTION CHARACTERIZATION & MODELING OF 4-CYLINDER I.C.E.

CHARACTERIZATION AND MODELING OF RUBBING FRICTION IN A MOTORED FOUR-CYLINDER INTERNAL COMBUSTION ENGINE

By

JEFFREY RAYMOND SYLVESTER, B.A.Sc.

A Thesis

Submitted to the School of Graduate Studies

in Partial Fulfillment of the Requirements

for the Degree of Master of Applied Science in the

Department of Mechanical Engineering,

McMaster University, Hamilton, ON

Canada

MASTER OF APPLIED SCIENCE (2011) McMaster University
(Mechanical Engineering) Hamilton, Ontario

TITLE: Characterization and Modeling of Rubbing Friction in a Motored Four-cylinder Internal Combustion Engine

AUTHOR: Jeffrey Raymond Sylvester, B.A.Sc. (University of Windsor)

SUPERVISOR: Professor S. R. Habibi

NUMBER OF PAGES: xiv, 143

Abstract

Internal combustion engines (I.C.E.s) are widely used across many industries to power a vast array of equipment. The fuel efficiency of these engines is almost always an important factor in their success, and as such it has seen continuous improvement. This is especially true in the case of consumer passenger vehicles where fuel efficiency is both a legislated mandate and a crucial sales feature. While many aspects of the engine contribute to this efficiency, internal friction warrants special attention due to the relatively large degree of losses it represents, as well as a nearly universal application to all engines. Internal friction is therefore an important consideration in the design of modern engines and will remain so in the conventionally powered and hybrid vehicles of the near future.

Measurement and characterization of internal engine friction is a significant first step towards engine modeling, attempts to reduce friction, and further applications related to engine condition monitoring or control. In order to measure the friction losses internal to a Ford 2.0L 4-cylinder engine a dedicated dynamometer test stand was designed and constructed. This test stand allowed the direct measurement of the frictional losses encountered by the engine in the motored state from low to moderate speeds. This data was then used to update and fit a physical, component-based friction model to the engine. A complete engine model known as the mean value engine model (MVEM) was then augmented with the verified friction model for simulation of the running engine. Its predictions were compared to a limited amount of available fired-engine data, demonstrating a general fit which could be improved with additional data.

The dynamometer test stand created is a viable tool for future engine friction testing, especially with partial engine disassembly or varying engine oil (operating) temperatures, or for future investigations of other rotating equipment.

Acknowledgements

The author would like to express his most sincere gratitude to his supervisor, Dr. S.R. Habibi, for his guidance and support throughout this research project and during the writing of this thesis. Further appreciation is expressed to Mr. Mark Mackenzie, Mr. Joseph Verhaeghe, Mr. Ron Lodewyks, Mr. Jim McLaren, and Mr. J.P. Talon for technical expertise shared.

Financial support provided by the School of Graduate Studies, the Department of Mechanical Engineering, and the Green Auto Powertrain Project is gratefully acknowledged.

Further gratitude is expressed to all research colleagues with whom the author has worked during the course of this project for the knowledge and insight they shared, as well as the assistance and support they provided.

Above all, the author's family and friends are thanked for their encouragement and support throughout this project, and all the others.

Table of Contents

Abstract iii
Acknowledgements iv
Table of Contents v
Index of Figures viii
Index of Tables x
Nomenclature xi
Declaration of Academic Achievement xiv
1. Introduction to the Thesis 1
1.1 I.C.E. Operation and Efficiency Considerations 2
1.2 Engine Losses 3
1.3 Research Objective 5
1.4 Outline of the Thesis 6
2. Engine Friction 7
2.1 Basic S.I. Engine Construction and Operation 7
2.2 Engine Friction Terminology 18
2.3 Engine Friction Fundamentals 21
2.4 Total Rubbing Friction Test Methods 25
2.5 Engine Friction Breakdown 28
2.6 Piston-Assembly Friction Measurements 30
2.7 Independent Test Rigs 34
3. Engine Modeling 35
3.1 Introduction to the MVEM 35
3.2 MVEM Basics 36
3.2.1 Time Scaling 38
3.2.2 Physical Overview of the MVEM 38
3.3 Composing System State Equations 41
3.3.1 Manifold Fuel Flow Equation 42
3.3.2 Manifold Air Flow Equation 44
3.3.3 Crankshaft Equation 46
3.4 Composing Instantaneous Engine Variable Equations 48
3.4.1 Fuel Film Variables and Parameters 49

3.4.2 Manifold Pressure Variables and Parameters 49
3.4.3 Crankshaft Variables and Parameters 51
3.5 Detailed Engine Friction Modeling 52
3.5.1 Crankshaft Group 54
3.5.2 Reciprocating Assembly Group 56
3.5.3 Valvetrain 58
3.5.4 Auxiliary Friction 60
3.5.5 Air Pumping Losses 60
3.5.6 Total Engine fmep 61
4. Experimental Setup of Motoring Test Stand 62
4.1 Experimental Requirements 63
4.2 Experimental Components and Specifications 63
4.2.1 Drive Motor 64
4.2.2 Unico Motor Drive 65
4.2.3 Crank Angle Sensor 67
4.2.4 Torque Sensor 69
4.2.5 Mechanical Alignment & Couplers 71
4.2.6 Engine Heating & Temperature Measurement 77
4.2.7 Mechanical Considerations of the Engine 79
4.2.8 Physical Enclosure 79
4.2.9 Data Acquisition 79
4.3 Software Environment 81
4.4 Data Collection 82
4.5 Data Processing 83
4.6 Test Data 85
4.6.1 Data Collection Limitations 90
4.6.2 Selected Data Range 92
4.6.3 Engine Disassembly Data 94
5. Simulations and Results 97
5.1 Fitting the Friction Model 97
5.1.1 Friction Model Adjustments 103
5.1.2 Demonstration of Friction Model Fit 114

5.2 Fitting the MVEM 121
5.2.1 Fired Engine Test Data 121
5.2.2 Modified Fuel Flow Equation 123
5.2.3 Modified Air Flow Equation 125
5.2.4 Modified Crankshaft Equation 126
5.2.5 Volumetric and Thermal Efficiencies 127
5.3 Power Test Simulation 129
6. Conclusions and Recommendations for Future Research 133
6.1 Conclusions 133
6.2 Recommendations for Future Research 135
References 138
Appendix A: Electrical wiring diagram 141
Appendix B: Select component specifications 143

Index of Figures

Figure 2-1: Sample engine block 8
Figure 2-2: Sample crankshaft 9
Figure 2-3: Sample connecting rod 10
Figure 2-4: Sample piston assembly 11
Figure 2-5: Cutaway view demonstrating typical relation of inlet and exhaust valves to the combustion chamber 13
Figure 2-6: The four strokes of the S.I. engine cycle 16
Figure 2-7: A sample P-V diagram. 20
Figure 2-8: Schematic representation of generic Stribeck diagram 24
Figure 2-9: Energy and friction breakdown in a fired engine 29
Figure 2-10: Grasshopper linkage 32
Figure 3-1: Schematic block diagram of a CFI engine 37
Figure 3-2: MVEM overview 39
Figure 3-3: Depiction of MVEM subsystems and energy flow 42
Figure 3-4: Physical depiction of MVEM fuel flow subsystem.. 43
Figure 3-5: Physical depiction of MVEM air flow subsystem 45
Figure 3-6: Physical depiction of crankshaft equation. 48
Figure 4-1: Primary components of the experimental setup 64
Figure 4-2: Reliance RPM AC electric drive motor 65
Figure 4-3: Unico 2400 motor controller and charging unit 66
Figure 4-4: Crankshaft position sensor and wheel on Ford 2.0L engine 68
Figure 4-5: Honeywell Model 1228-2k torque sensor 70
Figure 4-6: Honeywell Model 1228-2k torque sensor characteristic 71
Figure 4-7: Electric drive motor support stand 73
Figure 4-8: Supporting base with mounted electric drive motor and engine support cradle 73
Figure 4-9: Lovejoy SX-6 disc couplings 74
Figure 4-10: Types of shaft misalignment 75
Figure 4-11: Flexible couplings and torque sensor mounted between drive motor and engine 77
Figure 4-12: Engine coolant heating system used to bring the engine/oil temperature to operating conditions 78
Figure 4-13: National Instruments PCI-6229 DAQ card usage and availability 81
Figure 4-14: Sample cyclic torque data before and after digital filtering 85
Figure 4-15: Motoring test data from 10 datasets for Ford 2.0L engine with manifolds removed 87
Figure 4-16: Mean vale motoring test data from 10 datasets for Ford 2.0L engine with manifolds removed - error bars correspond to +/- 1 standard deviation 88
Figure 4-17: Motoring test data from 2 consecutive datasets for Ford 2.0L engine with manifolds in place 89
Figure 4-18: Motoring test comparison with and without manifolds 90
Figure 4-19: Full range of motoring test data depicting erroneous drop in measured torque

signal above 2700 RPM 92
Figure 4-20: Full range of mean value motoring test data for the Ford 2.0L engine demonstrating increased variability below 1500 RPM and above 2600 RPM 93
Figure 4-21: A closer look at the mean value motoring test data for the Ford 2.0L engine demonstrating repeatability over this speed range 94
Figure 5-1: Simple cutaway of a generic 4-cylinder engine depicting the main components responsible for engine friction as modeled 98
Figure 5-2: Individual component group losses for the motored Ford 2.0L engine as predicted by the uncalibrated model 100
Figure 5-3: Total friction losses for the motored Ford 2.0L engine as predicted by the uncalibrated model 103
Figure 5-4: Motored friction mean effective pressure vs engine speed for engine breakdown tests on a four-cylinder S.I. engine 106
Figure 5-5: Total friction losses with reduced auxiliary friction for the motored Ford 2.0L engine as predicted by the uncalibrated model 107
Figure 5-6: Comparison of total friction losses predicted by the uncalibrated model to the motored engine loss data 108
Figure 5-7: Model sensitivity to changes in the friction coefficient found within the reciprocating friction and valvetrain flat-follower and oscillating mixed groups 111
Figure 5-8: Model sensitivity to changes in the piston ring tension ratio, $F_t/F_{t0,}$ found within the reciprocating friction and piston gas pressure loading groups 113
Figure 5-9: Model sensitivity to changes in the piston roughness constant, $C_{r,}$ found within the reciprocating friction group 114
Figure 5-10: Individual component group losses for the motored Ford 2.0L engine as predicted by the uncalibrated and calibrated model 115
Figure 5-11: Stacked individual component group losses for the motored Ford 2.0L engines as predicted by the uncalibrated and calibrated model 116
Figure 5-12: Comparison of total friction losses predicted by the uncalibrated model, calibrated model, and the motored engine loss data 117
Figure 5-13: Comparison of total friction losses predicted by the uncalibrated model, calibrated model, and the motored engine loss data over the full speed range 118
Figure 5-14: Schematic of modified MVEM for power-test simulation 123
Figure 5-15: Volumetric and thermal efficiency trends as fit to data provided by Ford for the fired engine power test data 128
Figure 5-16: MVEM simulated and actual brake power 130
Figure 5-17: MVEM simulated and actual brake torque 131
Figure A-1: Experimental setup electrical wiring diagram 145

Index of Tables

Table 3-1: Constants for valvetrain mechanism terms 60
Table 4-1: Acceptable maximum misalignment of Lovejoy SX-6 coupling 75
Table 5-1: Initial parameter values used to apply friction model to the 2.0L engine..... 101
Table 5-2: Parameter values used to apply final suggested friction model to the 2.0L engine 120
Table B-1: Honeywell Model 1228-2k torque sensor specifications 143
Table B-2: Omega DMD-465 signal conditioner specifications 143

Nomenclature

Symbol	Definition	Unit/ Value
$\dot{m}_a$	rate of change of air mass in volume V within engine	kg/s
$\dot{m}_{ap}$	air mass flow rate into cylinder	kg/s
$\dot{m}_{at}$	air mass flow rate past throttle plate	kg/s
$\dot{m}_f$	cylinder port fuel mass flow	kg/s
$\dot{m}_{ff}$	fuel film (liquid) mass flow	kg/s
$\dot{m}_{fi}$	injected fuel mass flow	kg/s
$\dot{m}_{fv}$	fuel vapor mass flow	kg/s
B	cylinder bore diameter	mm
C_{ff}	flat follower valvetrain constant	
C_{oh}	oscillating hydrodynamic valvetrain constant	
C_{om}	oscillating mixed valvetrain constant	
C_r	piston roughness constant	
C_{rf}	roller follower valvetrain constant	
C_t	flow coefficient of throttle body throat	
D	diameter of throttle body throat	m
D_{bj}	diameter of journal bearings	mm
D_{bm}	diameter of main bearings	mm
F_t/F_{t0}	piston ring tension ratio	
H_u	fuel heating value	kJ/kg
I	total moment of inertia loading engine	kg m^2
k_b	engine loading parameter	kg m^2
L_{bj}	length of journal bearings	mm
L_{bm}	length of main bearings	mm
L_{th}	stoichiometric air/fuel ratio for gasoline (by mass)	14.67
L_v	maximum valve lift	mm
n	crankshaft speed	RPM

n_{bc}	number of camshaft bearings	
n_{bj}	number of journal bearings	
n_{bm}	number of main bearings	
n_{cyl}	number of engine cylinders	
n_v	total number of valves	
n_{ve}	number of exhaust valves	
n_{vi}	number of intake valves	
p_{amb}	ambient pressure	bar
P_b	load power	W
p_{exh}	exhaust gas pressure	bar
P_f	frictional power	W
P_i	indicated power	W
p_{man}	manifold pressure	bar
P_p	pumping power	W
p_r	ratio of manifold pressure to ambient pressure	
R	universal gas constant	
r_c	compression ratio	12:1
r_e	diameter of exhaust valves	mm
r_i	diameter of intake valves	mm
S	piston stroke length	mm
S_p	mean piston speed	m/s
t	time	s
T_{amb}	ambient temperature	K
T_{exh}	exhaust gas temperature	K
T_F	friction torque	
T_g	instantaneous torque due to gas pressure	
T_{irc}	instantaneous torque due to reciprocating masses	
T_{irt}	instantaneous torque due to rotating masses	
T_L	load torque	
T_{man}	manifold (air) temperature	K

V	manifold and port passage volume	m^3
V_d	engine displacement	m^3
W_a	accessory work	J
W_p	pumping work	J
W_{rf}	rubbing friction work	J
W_{tf}	total friction work	J
X	fraction of injected fuel deposited on the manifold wall as liquid film	
α	throttle plate angle	degrees
η_i	indicated (thermal) efficiency	
η_{vol}	volumetric efficiency (based on intake conditions)	
θ	spark advance angle	degrees
κ	ratio of the specific heats (for air)	1.4
λ	air/fuel equivalence ratio = $\dot{m}_a/(\dot{m}_f L_{th})$	
μ	oil viscosity for current model predictions	
μ_0	oil viscosity for original model calibration	
ρ	air density	kg/m^3
τ_d	time constant associated with the delay between fueling and the change in crankshaft speed	s
τ_f	time constant associated with the evaporation of fuel from the manifold wall	s

Declaration of Academic Achievement

This is a declaration that the content of the research contained within this document including the design and build of the experiments described was prepared by Jeffrey Sylvester and recognizes the guidance of Dr. S. R. Habibi during the research process and completion of the thesis.

Chapter 1

1. Introduction to the Thesis

Throughout modern history the internal combustion engine (I.C.E.) has been tasked with powering an impressively vast and varied range of machinery. Created in all sizes and countless variations, employing all viable combustible fuels, they have been used nearly everywhere across land, sea, and sky. Modifications in design and build have produced engines optimized for the needs of many industries. In the transportation sector and many others, this has sometimes required a difficult balance between fuel efficiency and power. This is especially true in the case of consumer passenger vehicles where extensive competition has confused the issue of how the industry's products should best be optimized. Dozens of vehicle configurations have been produced by dozens of manufacturers often with multiple engine choices on offer. While a small number of these engines may have been built to be powerful above all else, today most powertrain designers must strive for outstanding fuel efficiency despite a given vehicle's required level of performance. Recently these efforts have led to powertrain configurations which employ both conventional engines and an alternate means of storing and delivering power. At the time of this writing the only commercially successful examples employ batteries and electric motors in addition to the engine. Termed 'hybrids', these vehicles achieve significant improvements in fuel efficiency by relying on their alternative systems when the combustion engines are not required and would otherwise be at an inefficient operating point. The present work focuses on the I.C.E. within the passenger vehicle

segment and it is important to note that especially in hybrid vehicles, they may be expected to remain a primary component for decades, [1]. With continuous improvement, the I.C.E. will maintain advantages related to high power density, low cost of manufacture, recyclability, and existing infrastructure.

Specifically, the research documented in this thesis applies to a new Ford 2.0L four-cylinder gasoline engine with potential application to hybrid vehicles. This engine is tested to obtain the characteristics of one of the greatest losses within any engine: rubbing friction.

1.1 I.C.E. Operation and Efficiency Considerations

The function of the I.C.E. is to convert the chemical energy contained within its fuel into rotational motion. Precisely controlled combustion of the fuel and durable mechanical transfer of the resulting power to rotating equipment are standard. A balance of the required amount of fuel to produce the required motion defines the efficiency of the engine in the ordinary manner. For consumer vehicles, this is carried forward into the marketed overall efficiency of the vehicle by way of the standardized rating system. The vehicle is put through a testing sequence representing driving cycles and efficiency is calculated in terms of distance traveled per volume of fuel required. Many aspects of the vehicle play a role in this important metric, however the engine presents a reasonable case for special focus. The fuel of course is consumed directly by the engine and where other vehicle refinements may not universally apply to all vehicles, the engine remains an area for possible improvement so long as the performance requirements are met. The four main stages of engine operation include the introduction of air and fuel, the compression

of the air or air/fuel mixture, combustion, and finally the expelling of the gaseous products of combustion. Only the combustion stage produces power while the other stages rely on this power to complete.

Engines run cyclically, and most have multiple combustion chambers such that the four stages of operation occur in repetitive and overlapping sequences. From an efficiency standpoint, any restriction to the gaseous flow into or out of the engine can and should be minimized where possible. Control of event timing related to the combustion, known as the tune of the engine, allows a degree of control over the efficiency of the burn process itself. In this way specific engine designs are tweaked to use as little fuel as possible within their operating windows. However requirements of the vehicle or its operation may impose further restrictions on possible improvements in these areas. For example the air intake system is also designed for filtration and the minimization of audible noise within the vehicle. The next section details an area whereby improvements to engine fuel efficiency are unlikely to be at odds with any other design constraints: engine losses.

1.2 Engine Losses

Any energy produced by the engine that does not pass further down the line into the vehicle's drivetrain (i.e. into the transmission) or power critical engine auxiliaries may be considered a loss. The coolant and oil pumps are typically built-in components essential to engine operation. As such they are normally considered to be a part of the basic engine, [2]. In testing cases additional loads from vehicle components such as the power steering pump, electrical generator, and air conditioning compressor among others

may either be considered critical auxiliary components or engine losses. Some degree of reduction of these losses is possible through improvement of the auxiliary components and this will directly improve the efficiency of the engine package. Two remaining categories of engine loss may be defined as, [2]:

Pumping Work: The work done by the piston on the in-cylinder gases during the inlet and exhaust strokes (defined for four-stroke engines).

Rubbing Friction Work: The work dissipated in overcoming the friction due to the relative motion of adjacent components within the engine.

While pumping losses may be reduced via a careful consideration of intake and exhaust manifolds and valve layout, the pumping of air would still require energy and this loss cannot be totally eliminated. Likewise, an engine cannot operate without parts moving across one-another. However, these rubbing frictional losses are merely a secondary consequence of the engine mechanics and could well be reduced to their minimums. A number of aspects of any good engine design are employed to do just that, including more advanced selection of materials, surface finishes, coatings, and lubrication. Advancements in these key areas may be applied to all I.C.E.s, thus reducing this key form of power loss and subsequently improving fuel efficiency for many engines regardless of most other design parameters or requirements.

1.3 Research Objective

Having noted the importance of internal combustion engines to the consumer vehicle industry and the importance of rubbing friction to the I.C.E. we arrive at the issue around which this research is centered: determination of engine friction. Creating the proper test-conditions for testing any aspect of an engine can be difficult. Testing can either be completed on a dynamometer in an appropriately configured test stand or the engine may be instrumented with additional sensors and data-logging equipment within a vehicle. This initial choice must be made based on available resources and the objective of the testing. In the case of rubbing friction the research objective is most often a reduction of this loss through improved design. As this design may involve only a single component or component group within the engine, the testing scheme and hardware may be built only to track improvement in this particular area. If the objective of testing is only a reduction of power loss, then it is often not important that the testing be conducted such that the points tested accurately represent their values under operating conditions of the engine. While many examples of such testing exist throughout the literature, attempts to characterize the total friction internal to a running engine are somewhat more rare. The research described herein likewise does not attempt to make direct measurements in the firing mode as will be discussed in Chapter 2. Instead, testing is conducted on a purpose-built motoring dynamometer to measure the torque required to overcome friction in the non-firing engine over a range of speed. This data is then used to refine and optimize a mathematical model for the engine such that firing operation may be simulated with a fair representation of the internal friction. The resultant model is expected to be suitable to

simulate the engine in future research while the method used investigates the sufficiency of collecting only motored data in its creation.

1.4 Outline of the Thesis

Chapter 2 begins with background information regarding the construction and operation of spark ignition (S.I.) engines, including descriptions of the components that contribute to engine friction. Discussion then proceeds towards fundamental friction terminology and categories as they apply to engines. A review of various methods for measuring full engine and component friction concludes the chapter. In Chapter 3 the Mean Value Engine Model (MVEM) is described in detail. Chapter 4 describes the design and build of the experimental test stand and experimental testing sequence. Chapter 5 determines the motored friction characterization and details the adaptation of the MVEM to the Ford engine. The porting of the measured friction data into the engine model is described. Lastly, Chapter 6 provides conclusions and suggested future work.

Chapter 2

2. Engine Friction

In this chapter the basics of spark ignited (S.I.) internal combustion engines are presented and the basics of friction as applicable to these engines are described. The discussion remains generic and applies to many engine designs. It includes four-cylinder, four-stroke S.I. engines that are specifically being studied in this research. The characteristics of friction and the methods used to measure friction in both motoring and firing modes of the internal combustion engine are then discussed.

2.1 Basic S.I. Engine Construction and Operation

This opening section is intended to explain the general mechanics and operation of a typical gasoline engine. The primary focus lies with the components which are in relative motion with each other such that rubbing friction exists between them. In the case of most components there are many options for specific type and layout. There is neither the space nor the motivation to discuss them here. As such only representative components are described presenting a reference and one possible solution. This section provides a basic understanding of the task that components must accomplish and some insight into their contribution to friction. The discussion will proceed in the order in which an engine is physically assembled.

Engine block. The first and largest piece of any engine is the engine block. This precisely machined casting forms the basic layout of the engine and all other components are assembled to it. The engine block consists of the cylinder bores which the pistons act

within, provision for support of the crankshaft, and liquid passages for lubrication oil and coolant. If the block is made of steel the cylinder bores will be cut directly into the block and carefully honed. More commonly on modern engines the block is made of aluminum alloy and the pistons work within steel cylinder liners which are fit into the block. The layout of the pistons/cylinders can vary greatly from engine to engine, and so the basic shape of the engine block also varies. Two of the most common layouts entail having the cylinders lined up straight in a single row, or being inclined on an angle opposed to one another in two rows. These are referred to as *inline* and *"V"* configurations respectively. The Ford engine used in this research is a 4-cylinder inline type. Figure 2-1 gives an example of an engine block for 4 cylinder inline engine. Note the locations of the housing for the main bearings which support the crankshaft. This particular engine design houses the camshaft within the engine block as opposed to the 'overhead' cam position that would locate it in the cylinder head.

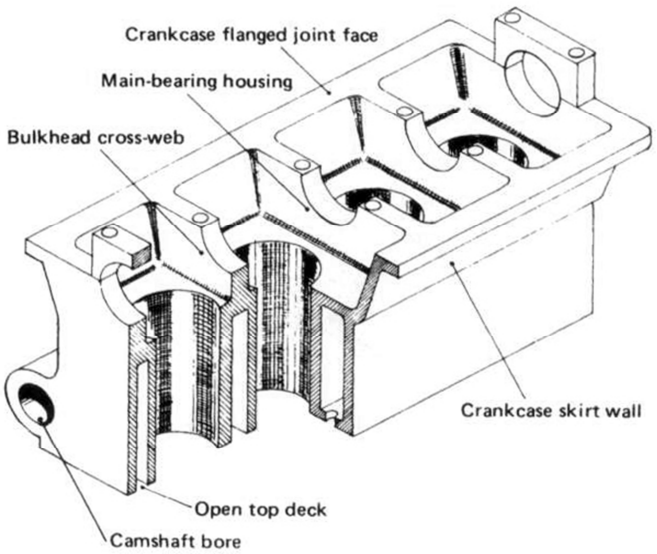

Figure 2-1: Sample engine block, [3]

Crankshaft. The crankshaft is a circular-sectioned bent shaft which connects indirectly to the pistons through the connecting rods. The unbent portion of the shaft provides the main journals about which it rotates. The bent portions extend to the *big-end journals* which connect to the connecting rods. The front of the crankshaft connects to the front end accessory drive system to drive engine/vehicle auxiliary components while the rear of the crankshaft typically connects to a flywheel or otherwise provides connection to engine output. Oil seals are present at both of these locations as the crankshaft passes through the engine block. See figure 2-2.

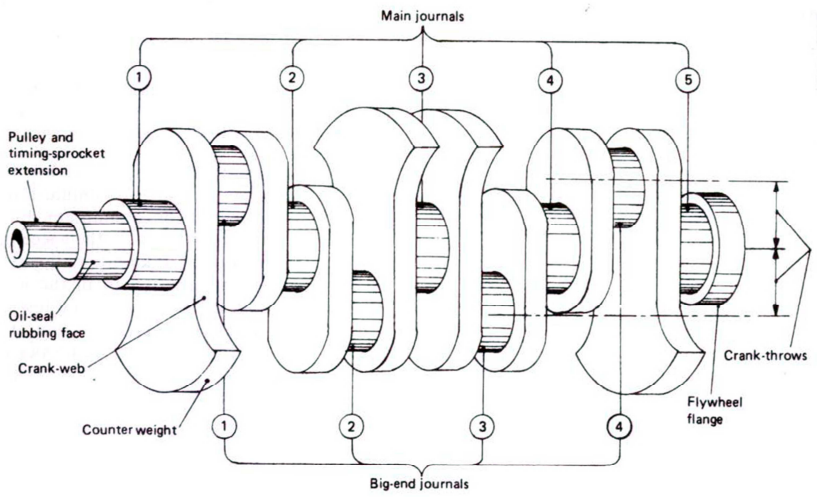

Figure 2-2: Sample crankshaft, [3]

Connecting rods. The connecting rods connect the pistons to the crankshaft. The connecting rods oscillate back and forth as the reciprocating motion of the pistons is transmitted and converted to rotational motion at the crankshaft. The *small end* of the connecting rod refers to the hinged joint formed with the piston. A hole is machined into this end of the crankshaft into which the *piston pin* is inserted through the bottom edges

of the piston so that it may pivot on this pin. The *big-end* of the connecting rod refers to the joint between it and the crankshaft. A typical two-piece automotive engine bearing is used for this joint. The connecting rod itself is typically manufactured first as a solid piece and then broken at this joint to allow insertion of the bearing while maintaining a perfectly matched union. See figure 2-3.

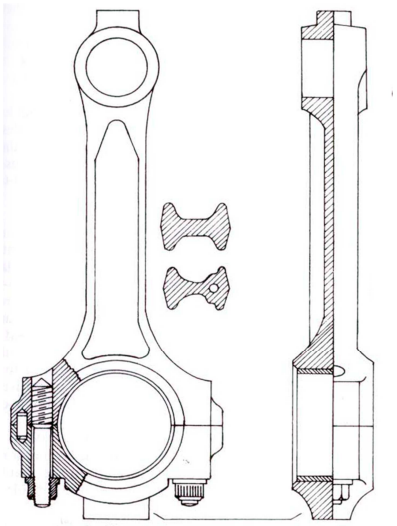

Figure 2-3: Sample connecting rod, [3]

Pistons. The pistons are essentially plungers that act within the cylinder bores. They are subjected to the gas pressure that occurs with combustion and transfer this pressure into force along the connecting rods. The top of the piston is grooved for the piston rings, while the two sides of the pistons adjacent to the piston pin are smooth and known as the *piston skirt*. The piston skirt at the bottom of the piston contacts the cylinder walls directly. See figure 2-4.

Piston rings. These circular, split rings fit into grooves in the top of the piston and are responsible for creating an air-tight seal to contain the combustion gases and to control lubrication on the cylinder wall. Differing number and types of piston rings are used to do so, though a typical arrangement may be considered to be two compression (air sealing) rings on top, with an oil control ring below them. Figure 2-4 gives an example of a piston assembly clearly showing the piston, piston rings, and pin to attach it to the connecting rod.

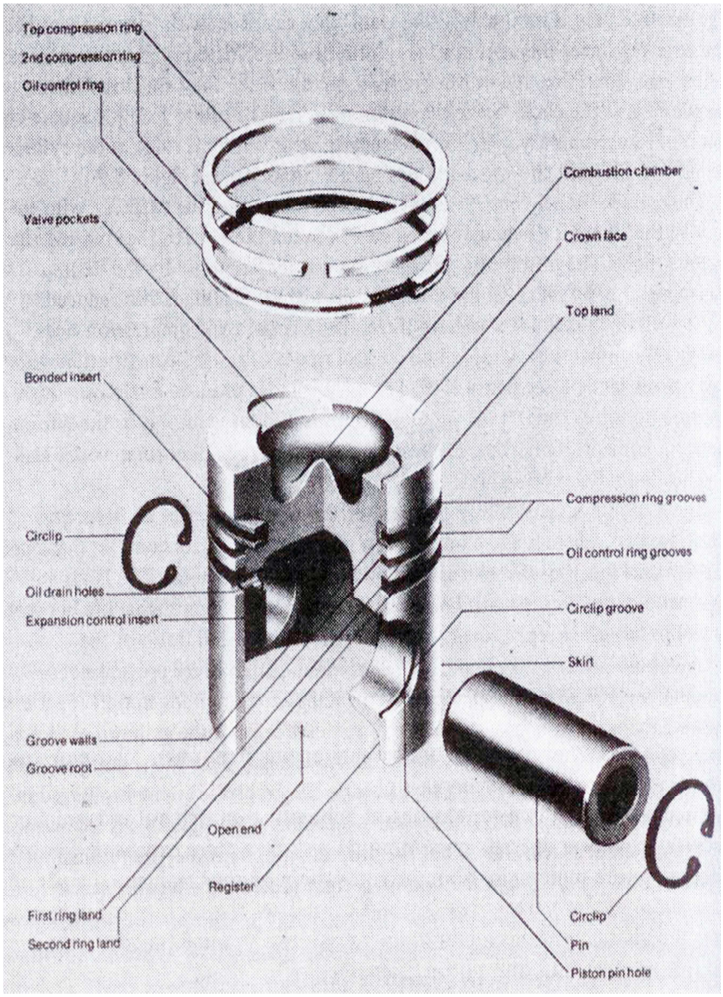

Figure 2-4: Sample piston assembly, [4]

Collectively when assembled along with associated items the above components form the *short block*. This refers to the bottom portion of the engine and at this point of assembly turning the crankshaft would cause the pistons to reciprocate in sequence within the cylinders. Friction exists between the piston rings/skirt and cylinder walls, at both joints of the connecting rods, and at all of the bearings and to a lesser degree oil seals where the crankshaft is supported in the block.

Cylinder head(s). Easily the second largest component is the cylinder head(s) that bolt onto the top of the engine block. Like the engine block these are large steel or aluminum castings with passages for oil and coolant and which the remainder of the engine components assemble on. The top portion of the combustion chambers above the pistons are cast into the cylinder heads. An inline engine has one cylinder head, a "V" configuration has two, and more exotic configurations may have more. The cylinder head usually supports the engine's camshafts (though these can also be located in the engine block), inlet and exhaust valves, and associated mechanical connections. Fresh air and exhaust gases are both routed through the cylinder heads on their way to or from the engine.

Camshaft(s). The camshafts rotate within the cylinder heads providing cams via which the valves are actuated. A common configuration has one camshaft for the inlet valves and one for the exhaust valves. The specific mechanics that lead to the valves opening and closing with the cams varies greatly, and is generally referred to as the valvetrain. Friction exists at this point regardless of how the motion is transferred from the cams to

opening and closing the valves. Likewise there is friction at the stems of the valves themselves which slide within guides in the cylinder heads. The camshafts are supported by a number of journal bearings and these represent a slightly more significant portion of friction.

Inlet and exhaust valves. Poppet style valves control the flow of gas into and out of the combustion chambers. A minimum of one inlet and one exhaust valve per cylinder is necessary, though having more than this is certainly commonplace. More flow area is required on the inlet side leading to the selection of additional and/or larger inlet valves. See figure 2-5 for a simple cutaway.

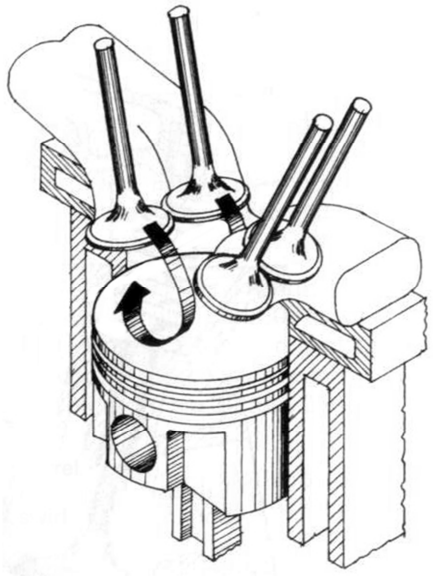

Figure 2-5: Cutaway view demonstrating typical relation of inlet and exhaust valves to the combustion chamber, [3]

Timing belt or chain. The camshafts are driven by the crankshaft by way of a timing belt or chain and sprockets on each shaft. This component is responsible for keeping the

camshafts in proper phase with the crankshaft. In this way the critical timing between the valves and the pistons is ensured. Keeping proper tension on the belt or chain contributes to its friction.

Lubrication system. The lubrication system ensures lubricating oil is delivered where needed within the engine. A pump driven by the crankshaft takes up oil from the oil pan attached to the bottom of the engine block. The oil is then pumped through internal passages in the engine block and cylinder head(s), where it is passed through holes or squirted through nozzles to the required points. Key lubrication areas include all bearings and the cylinder walls. For the latter, oil is either splashed or squirted towards the bottom of the pistons and the oil control ring and cylinder bore surface finish ensure the proper amount of oil remains on the cylinder walls. In addition to providing necessary lubrication for interacting parts, the engine oil also removes much of the heat from the combustion process before transferring this heat to the engine coolant. In similar fashion to the oil, engine coolant is pumped through internal passages in the engine. In this way the oil temperature is passively controlled by controlling the temperature of the coolant, which is cooled in a controlled manner by adjusting its flow through the vehicle's radiator. The viscosity of the oil must be appropriate for the engine's design to ensure correct lubrication without additional frictional losses resulting from overly viscous oil. The required grade is specified by the engine manufacturer. Since viscosity changes with temperature, the engine experiences higher losses until it reaches operating temperature. Variations of temperature with operating conditions also cause variations in viscosity, and thus variations in total engine rubbing friction. While it is difficult to accurately quantify

this effect in general terms, it is generally accepted that the total mechanical friction losses of a cold engine at 20˚C are approximately 2 times those at a typical engine operating temperature of 90˚C. Deviation of 10˚C from operating temperature may result in a change to total mechanical friction on the order of 10%, [5].

Basic engine operation. While many components are not specifically listed above, the basic components of the engine have been described and it has been shown that turning the engine will actuate the pistons within their cylinders while opening and closing the inlet and exhaust valves in a defined sequence. Mechanically these are the minimum requirements to allow the engine to run. The events that control combustion of the fuel in a running naturally-aspirated 4-stroke spark ignited engine are described briefly in the following paragraphs.

Referring to figure 2-6, one complete cycle of a running 4-stroke engine involves 4 discrete strokes. Each stroke is defined by the motion of a single piston over the extremes of its motion. When the piston is at the top of its travel this position is known as top dead center (TDC). Conversely the bottom of its travel is bottom dead center (BDC). Beginning from the TDC position, the four strokes occur as follows:

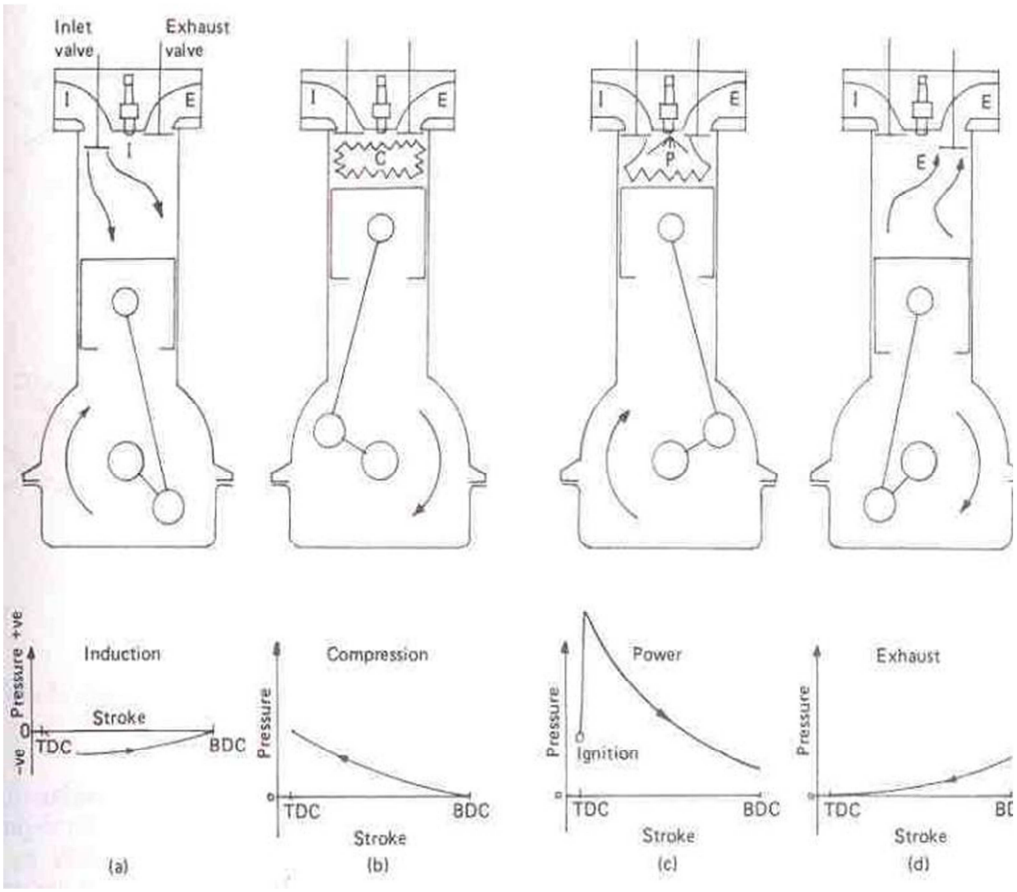

Figure 2-6: The four strokes of the S.I. engine cycle, [4]

Induction stroke {figure 2-6(a)}: With inlet valve(s) open and exhaust valve(s) closed the piston moves down to BDC. The downward motion of the piston reduces pressure vs. atmospheric such that fresh air and atomized fuel flow into the combustion chamber. Properly metered fuel is sprayed into the air intake system upstream such that an air/fuel mixture very near stoichiometry is already available.

Compression stroke {figure 2-6(b)}: With both valves closed the piston moves back toward the TDC position. As it does so it forces the induced air/fuel charge into the small area left between the piston and the top of the combustion chamber at TDC. The

compression that occurs is commonly within a range of 10:1 to 12.5:1 compared to the original volume of the cylinder.

Power stroke {figure 2-6(c)}: As all valves remain closed, events leading to this stroke begin slightly before the piston reaches TDC on the compression stroke. At this time, a spark plug produces a spark within the combustion chamber, igniting the compressed charge. Just as the piston reaches TDC the charge begins to burn, rapidly raising the temperature and pressure and forcing the piston back to BDC.

Exhaust stroke {figure 2-6(d)}: With the inlet valve(s) closed and the exhaust valve(s) opened the piston returns to TDC. Most of the burnt gases to be exhausted from the engine exit the exhaust valve(s) due to their existing pressure and energy while those remaining are expelled by the motion of the piston.

The crankshaft travels through 2 complete rotations, or 720° as this cycle completes. The events for each cylinder are typically equally spaced along this 720° such that the cycle occurs continuously in all cylinders and power is delivered as smoothly as possible. The timing of events including production of the spark, and timing and duration of valve openings is not as simplistic as the above description would imply, nor is the metering and delivery of fuel. These parameters have a significant impact on the efficiency of the burn process, the way the engine runs, and the emissions it produces.

2.2 Engine Friction Terminology

In this section, the basic terminology of engine power and friction losses are defined to facilitate further discussion of engine friction. Pumping work, rubbing friction work, and accessory work were discussed in chapter 1. These may be denoted as W_p, W_{rf}, and W_a, with the sum of these representing the total friction work denoted by W_{tf}. It is common to discuss engine output in terms of the *mean effective pressure*, mep, which is defined as the work per cycle per unit displaced volume. The mean effective pressures can then be considered for each of the quantities of work above. For example the pumping-mean-effective-pressure becomes:

$$pmep = \frac{W_p}{V_d}, \tag{2.1}$$

where V_d is the displaced volume.

Likewise rubbing-friction-mean-effective-pressure, accessory-mean-effective-pressure, and total-friction-mean-effective-pressure may be defined and denoted rfmep, amep, and tfmep respectively, where:

$$rfmep = \frac{W_{rf}}{V_d}, \tag{2.2}$$

$$amep = \frac{W_a}{V_d}, \tag{2.3}$$

$$tfmep = \frac{W_{tf}}{V_d}. \tag{2.4}$$

The terms *brake* and *indicated* are regularly used to describe quantities referring to total torque, power, etc. within engines. In this context that yields both a brake mean effective pressure (*bmep)* and an indicated mean effective pressure (*imep)*. The term *brake* refers to the power (for example) that would be measured during a typical running

dynamometer test and is the usable power that the engine delivers to its load. Conversely, the term *indicated* is derived from in-cylinder pressure data in order to calculate the work transfer from the gas to the piston. This is accomplished by generating a graph of the cylinder pressure vs. the corresponding cylinder volume, known as an indicator diagram or a p-V diagram for short. Integration of this plot yields the area enclosed by the curve and is the *indicated work* per cycle. Two definitions of this quantity are commonly used leading to the possibility of some ambiguity. A sample p-V diagram as shown in figure 2-7(b) is referred to for clarification. More commonly, the ***gross*** *indicated work per cycle* is defined as the work delivered to the piston over only the compression and expansion strokes. This work appears as the top (larger) loop in figure 2-7. The alternative definition, the ***net*** *indicated work per cycle*, is the work delivered to the piston over all four strokes of the engine cycle. This definition now includes the lower (smaller) loop as well, which shows the pumping work. For naturally aspirated engines this pumping work transfer will occur from the piston to the cylinder gases as it represents a loss to the engine as already described. It is therefore a negative quantity to be subtracted from the area of the top loop. It is necessary to explicitly state whether one is employing the gross or net definition wherever the term *indicated* is used. Unless otherwise specified gross indicated quantities will be used herein.

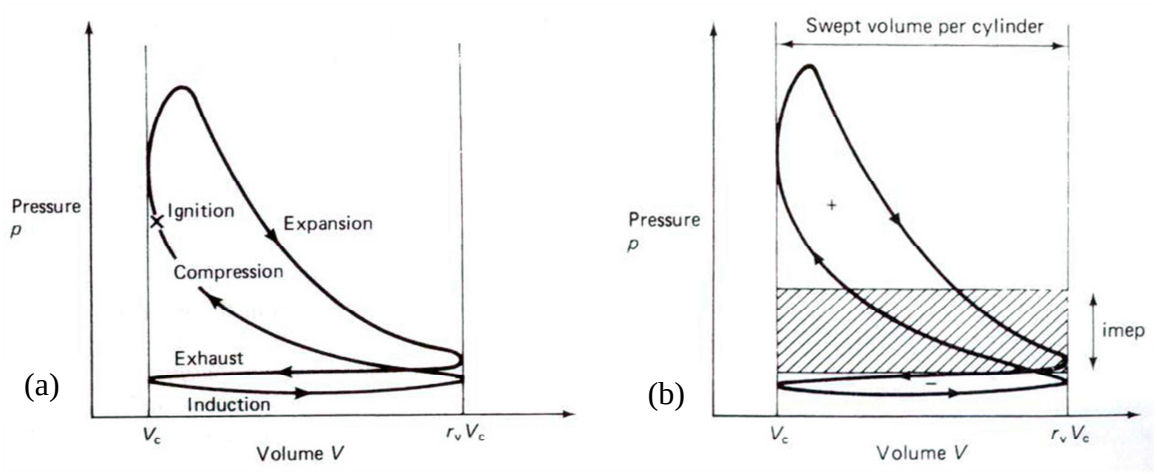

Figure 2-7: A sample P-V diagram. (a) Identifying the four strokes of the engine cycle. (b) Indicating the indicated work; the shaded portion shows equivalent net area under the curve, [3].

The following definitions have been stated by Heywood [2], and will be used as follows:

Gross indicated mean effective pressure, $imep_g$. The work delivered to the piston over the compression and expansion strokes, per cycle per unit displaced volume.

Net indicated mean effective pressure, $imep_n$. The work delivered to the piston over the entire four strokes of the cycle, per unit displaced volume.

While the following definition may be restated for convenience:

Brake mean effective pressure, bmep. The usable work generated by the engine and delivered to its load, per cycle per unit displaced volume

The terminology provided thus far may be summarized by considering the following equations:

$$imep_g = imep_n + pmep, \tag{2.5}$$

$$tfmep = pmep + rfmep + amep, \tag{2.6}$$

$$bmep = imep_g - tfmep, \tag{2.7}$$

$$bmep = imep_n - rfmep - amep, \tag{2.8}$$

These equations hint at the reason why alternate definitions of *indicated* are commonly used. When attempts are made to measure engine friction through motoring tests, *tfmep* is approximated according to equation (2.6). Then the easily measured *bmep* is the difference between the gross indicated *mep* and this quantity. When accurate in-cylinder pressure data is available over the entire cycle *pmep* may be calculated directly from this data, while the net indicated *mep* may be found by integration as represented by the area enclosed within the p-V diagram. The difference between this quantity and the measurable *bmep* is then the sum of *rfmep* and *amep* (rubbing friction and accessory work) according to equation (2.8).

2.3 Engine Friction Fundamentals

If the friction of auxiliary components essential to engine operation is considered separately, engine friction can be broken down into the two categories of pumping work and rubbing friction work. These two categories lend themselves immediately to two additional categories under which all engine friction falls: lubricated friction and turbulent dissipation. The former applies to rubbing friction where two surfaces move relative to each other separated by a lubricant, while the later exists wherever a fluid is pumped through a flow restriction. Both types occur within any engine. Resulting from either lubricated rubbing friction or turbulence, friction work in the engine is ultimately dissipated as heat. In addition to the direct losses faced by the engine this additional heat also impacts the sizing of the engine cooling system. With both direct frictional losses and additional loading imposed upon the cooling system, it is apparent that an effective

engine must minimize friction wherever possible. Doing so is not straightforward however due to the widely varying magnitude of forces realized by different components. This variation in force results in several possible lubrication regimes which cause altered friction behavior between different components and different operating conditions as detailed below, [2]:

Boundary Lubrication: In this regime the lubricating film is reduced to a few molecular layers or less and can no longer prevent metal-to-metal contact at surface asperities. The properties of dry friction are approached in this regime. Friction here is dependent both on surface properties of the components in relative motion and properties of the lubricant. Within engines boundary lubrication occurs during starting and stopping at the bearings, pistons, and rings. It also occurs under normal operating conditions at the piston ring – cylinder interface at top center and bottom center crank positions. Lastly it may be experienced between heavily loaded and/or slowly moving parts. These may include such items as valve stems, rocker arms, and crankshaft timing gears and chains.

Hydrodynamic Lubrication (Fluid-Film Lubrication): Also referred to as *viscous* or *thick-film* this lubrication regime occurs whenever the lubricating film is of sufficient thickness to completely separate the two surfaces in question. Maintaining this separation requires sufficient pressure in the liquid film which can be generated with the proper conditions of geometry and relative motion between the surfaces. In this regime it is not surface interactions that affect friction but rather the shear forces within the lubricant film that resist motion. Hydrodynamic

lubrication occurs in engine bearings, between piston skirt and cylinder wall, and for high sliding velocities at the piston rings and cylinder wall.

Mixed Lubrication (or Mixed-Film/Partial Lubrication): The final regime exists in the space between the two extremes presented by the other two cases. When the fluid film thickness approaches the height of surface asperities hydrodynamic lubrication begins to break down and the mixed lubrication regime is entered. Metal-to-metal contact intermittently occurs at the peak of the asperities and switching between boundary and hydrodynamic friction occurs. The transition into mixed lubrication is partly dictated by surface texture, but may also be brought on due to sudden variation in speed and/or load. In engines, mixed lubrication occurs in connecting rod and crankshaft bearings as well as between piston rings and cylinders at typical operating speeds.

Naturally the different lubrication regimes heavily impact the friction characteristics of engine components and the engine as a whole. Furthermore, the lubrication may alter the wear behavior of the part possibly leading to an increase in rubbing friction. Characterization of the relationship between friction and these three primary lubrication regimes is usually accompanied by a curve called a Stribeck diagram such as the generic one shown in figure 2-8. For a given pair of surfaces in relative motion the Stribeck diagram relates the coefficient of friction to a dimensionless duty parameter based on the lubricant viscosity, speed of motion, and loading (which must consider the actual surface in contact). The Stribeck diagram clearly shows the general behavior of each of the above lubrication regimes. For high values of the duty parameter, hydrodynamic

lubrication takes place and the coefficient of friction is seen to increase linearly as the friction is related to viscous dragging in the lubricant. When either the load increases or the oil viscosity and/or velocity of motion decrease the duty parameter also decreases. As this happens the mixed lubrication regime is entered and the friction coefficient is seen to increase as metal-to-metal contact increasingly occurs. Further decrease of the duty parameter shows the behavior as lubrication breaks down into the boundary regime. It is easy to see that with such a curve applying to each dynamic engine component and the engine speed, load, and oil viscosity varying with both operating point and conditions, the characterization of rubbing friction becomes complicated. Various test methods to do so for the whole or partial engine will be described in the following sections.

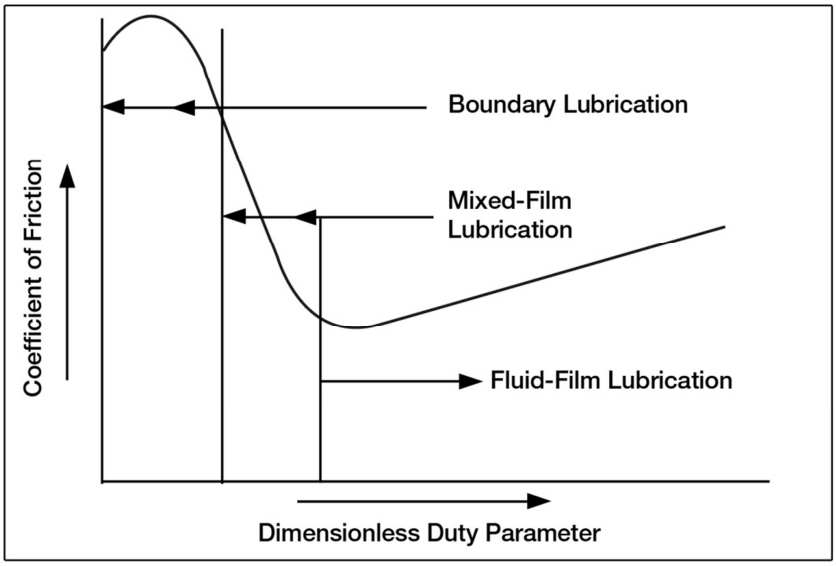

Figure 2-8: Schematic representation of generic Stribeck diagram, [44]

2.4 Total Rubbing Friction Test Methods

Nearly all attempts within the literature to measure engine friction in a spark ignition (i.e. gasoline) combustion engine fall into one of the first 4 of the following 5 types:

1. **Measurement of fmep from imep.** Perhaps the most direct and technically difficult methodology, this type of test requires that accurate and in phase pressure and volume data be collected for each cylinder, ensuring that the cylinder positions in time are also known. This is accomplished by inserting pressure transducers into each combustion chamber and collecting their data along with that of a crank angle sensor. Pressure vs. crank angle is thus collected, while volume vs. crank angle may be calculated. It is then possible to calculate $imep_g$ and *pmep*. Having simultaneously measured *bmep*, the sum of the rubbing friction and auxiliary power requirements may be calculated. This method has the advantage of measuring the true friction in a running engine, but collecting adequate *imep* data is difficult due in part to cylinder-to-cylinder and cycle-to-cycle variability. The method also requires the cylinder heads be modified to add the pressure transducers. Gish et. al. [6] may be credited with describing the methods used during one of the earliest executions of this method.

2. Direct motoring tests. As the name implies this type of test measures the power requirements to motor the engine, rather than the true friction within the engine while it is firing. The power to motor the engine as measured will include the pumping requirements. To closely approximate the running conditions of the engine, oil and coolant temperature may be maintained by heaters. Alternatively, if the test stand is

capable of firing the engine it may be brought up to operating temperature just prior to removing the source of ignition and conducting the motoring test. This technique is known as a *grab-motoring* test. Progressive disassembly of the engine is commonly carried out with direct motoring tests for investigation of friction requirements of specific components. One such experiment conducted by Shayler et. al. [7] investigated the piston rings and skirt under a range of modifications. Examples of such tests for investigation or verification of specific components are commonplace.

3. Morse test. In this test a running engine on a test stand has ignition removed from an individual cylinder such that the remaining cylinders are essentially motoring the cut cylinder. The reduction in *bmep* is monitored and frictional losses may be inferred. The difficulty with this method lies within the engine control as removing a cylinder must be possible without significantly altering the fueling and running behavior of the others.

4. P-ω method. Different from the other methods which investigate the *mep* and *fmep* or equivalent power, the P- ω method is based on a balance of torques. First proposed in 1984 by Rezeka and Henein [8] this method considers the fact that the instantaneous angular acceleration of the crankshaft is dependent upon the instantaneous torque acting on it. Similarly to the measurement of *imep*, this test requires pressure transducers to be fitted into each combustion chamber and the crankshaft position accurately tracked. Combining these measurements with knowledge of the geometry and masses of engine components the *friction torque* may be calculated according to the following summary of the method:

$$T_F = T_g - T_{irc} - T_{irt} - T_L, \quad (2.9)$$

where, T_F = friction torque,

T_L = load torque,

T_{irc} = instantaneous torque due to reciprocating masses,

T_{irt} = instantaneous torque due to rotating masses, and

T_g = instantaneous torque due to gas pressure

A primary benefit of this method is that it delivers a friction characterization as a function of crank angle as opposed to the average value as a function of engine speed provided by the other methods. This method proved to be distorted by structural deformation and torsional vibrations in the crankshaft such that careful modeling of the crankshaft assembly was required [9], [10]. Determining an effective rigid-body speed signal for the crankshaft therefore is a primary difficulty with the method. Sensors at each end of the crankshaft were used by Taraza et. al. [11] while filtering of the angular motion of the crankshaft was added by Nehme et. al. [12] to improve the method. Further improvement was achieved by Kfoury et. al. [13] through the implementation of a nonlinear sliding mode observer to estimate the motion of the relevant dynamics.

5. Willan's line method. This method is mentioned to complete the list, but does not apply to throttled engines. For compression ignition (typically diesel) engines this test measures and plots the fuel consumption vs. *bmep* from no load to full load at a constant engine speed. This plot is then extrapolated backward to intercept the horizontal (*bmep*) axis. In this way the negative *bmep*, the frictional losses including pumping, are found. This is assumed to be the value of friction at that engine speed regardless of load.

A throttled engine would require the throttle to be actuated essentially from closed to fully open to complete the test, thus changing the pumping losses considerably and varying the friction measured with this method with respect to engine load, [14].

2.5 Engine Friction Breakdown

Due to the substantial differences between engine designs the relative contribution of individual components to friction can vary greatly. As manufacturers continuously improve their designs this information constantly changes. Furthermore, this breakdown changes with engine load and speed. The total frictional losses of an engine can range from somewhere near 10% of the indicated power at full load to 100% when the engine is at idle (no-load) conditions. An approximation of the breakdown of friction within an engine is dependent on many factors including the chosen load, so it is perhaps better to present a range of values. This is provided graphically in figure 2-9 below as reproduced from Kurbet and Malagi [15]. Comparing the wide ranges presented in this breakdown to those given elsewhere in the literature confirms they are a suitable approximation. It is especially important to note within this breakdown that the piston assembly (piston, piston rings, and connecting rods) are dominant within total engine mechanical friction. The majority of the remaining mechanical friction terms are dissipated within the pumping work, while remaining components including the auxiliaries and the valvetrain contribute the last roughly 20% [2].

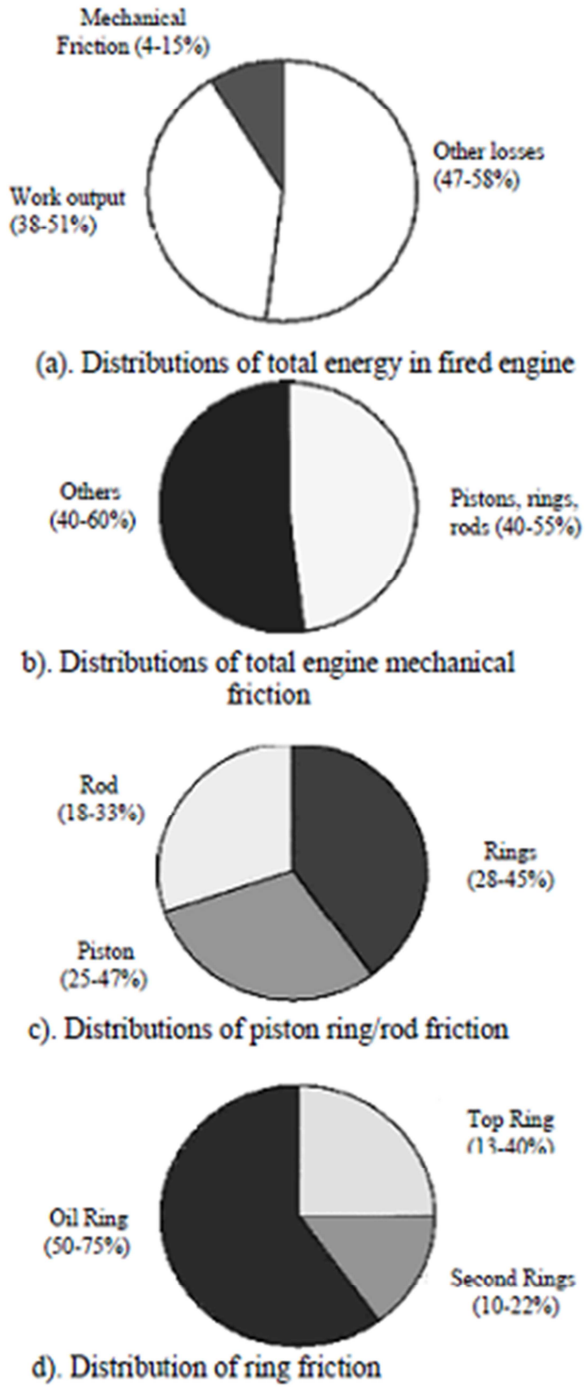

Figure 2-9: Energy and friction breakdown in a fired engine, [15]

2.6 Piston-Assembly Friction Measurements

Due to its dominant contribution to rubbing engine friction, the piston-assembly has received special attention in the literature. The piston-assembly friction mainly occurs between the piston rings/piston skirt and the cylinder walls, though the connecting rod joints are also considered. Investigation of the friction in this area within a running engine is of particular interest due to the high pressures which act directly on the assembly only during fired conditions. During attempts to evaluate the friction between the piston rings, piston skirt, and the cylinder walls two popular methods have been proposed. These are the *floating liner* method, and an adaptation of the *fmep* from *imep* method for total engine friction usually denoted simply as the *IMEP method.* Requiring extensive modification to the engine, the floating liner method isolates the cylinder liner from the engine block such that it is allowed to move axially under the force of the piston-assembly friction. This force is then typically measured directly with strain gages mounted at the liner's axial support. Forbes and Taylor [16], may be credited with the first attempt to measure the piston-assembly friction in a firing engine in a similar method. They supported the cylinder liner elastically, allowing a small degree of movement, and recorded the movement of the liner under the friction forces photographically. This work was carried on by Leary and Jovellanos [17], and later by Livengood and Wallour [18]. Over three decades, later Furuhama and Takiguchi [19], measured the piston-assembly frictional force in an operating diesel engine with the floating liner method axially supported by a Piezo electric pickup. They described many of the common problems encountered by the method and their solutions. These include sealing the high pressure

gas at the top of the rig without altering the force to be measured, eliminating deformation of the cylinder head and block, and the effects of piston side forces on the axial force sensor. This measurement technique has been the focus of many studies including that by Richez et al. [20], Parker et al. [21], Sherrington and Smith [22], Cerrato et al. [23], Wakuri et al. [24], and Kikuchi et al., [25]. All faced similar problems and the potential consequence that the gas-sealing apparatus at the interface between the cylinder head and liner in their respective test engines causes deviations from the actual firing engine [26]. Cho et al. [27] used this method with a strain-gage-type load cell under motored conditions.

While the floating liner method measures the friction force directly, the much less invasive IMEP method determines it indirectly through measurement of the forces acting on the piston assembly and the connecting rod. Like measuring total *fmep* from *imep* this method relies on an accurate in-cylinder pressure trace. To this is added measurement of the connecting rod strain. With this data, the actual force within the connecting rod is subtracted from the axial forces calculated from the cylinder pressure and piston inertia. The difference represents the friction in the assembly. This method must be carried out very accurately to achieve useful results, however it has the advantage of not modifying the engine in any way that would alter the measured piston-assembly friction. This method was pioneered by Uras and Patterson [28], who designed an arrangement they denoted as the grasshopper linkage (a later adaptation of this style linkage is shown in figure 2-10). In this method, wires from the connecting rod strain gages are lead to the side of the crankcase and then passed outside the engine. Their experiment was

ultimately limited with regards to engine speed and load because the wires within this linkage broke at high speeds. Mufti and Priest [26], successfully used this method to achieve results at realistic engine speeds and loads using an upgraded grasshopper linkage that was designed and developed by Federal Mogul Technology. This linkage, shown in figure 2-10, included special high-strength steel (Kapton®) wires to overcome breakage at high speeds. Furthermore the differences between motored and fired conditions were investigated in their work, concluding that the average piston-assembly friction was higher under fired than motored conditions mainly because of cylinder pressure and temperature.

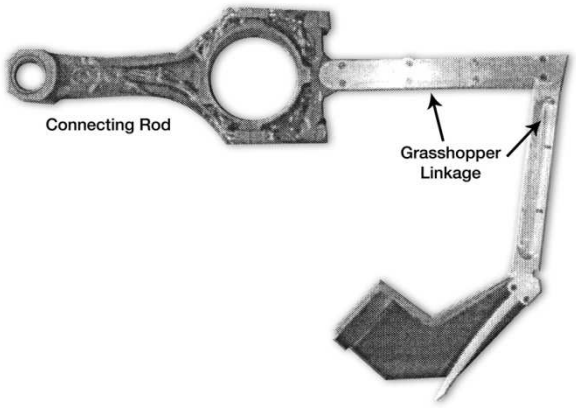

Figure 2-10: Grasshopper linkage employed by Mufti and Priest to pass strain gage wires from the connecting rod outside the engine, [26]

What could be considered a compromise between the floating liner and IMEP methods was proposed and investigated by Ku and Patterson [29]. Termed the *fixed sleeve* method their experiment was based on the replacement of the engine's cylinder liner with a sleeve supported on strain gages within a modified replica of the original

removable production liner. In this way the engine block remains largely unmodified. Likewise the cylinder head was modified only with the insertion of an in-cylinder pressure transducer. The sleeve is acted upon by both the friction of the piston assembly and the force which acts on the exposed upper ring of the sleeve. The latter may be calculated from the pressure trace and subtracted from the total, leaving only piston friction.

Another innovative method to measure piston assembly friction was proposed by Goto et al. [30]. Termed the 8-cycle method, four extra strokes were added to the regular 4-stroke cycle before exhausting the burnt gases, two extra compression and expansion strokes each, in order to essentially run a motoring test with gas pressure and temperature at firing levels. To accomplish this, custom camshafts were designed and driven at half the normal rate: one-fourth camshaft revolution per crankshaft revolution instead of one-half. The custom camshafts were created such that the cams for the number 1 cylinder opened the valves once per camshaft revolution, while the number 2-4 cylinder valves opened twice per camshaft revolution. The result was conventional engine operation in cylinders 2 to 4 (opening the valves once for every 2 revolutions of the crankshaft) but 8-cycle operation in cylinder 1 (opening the valves once for every 4 revolutions of the crankshaft). In this way cylinder 1 experiences regular operation during the first 3 cycles and then traps the products of combustion for the subsequent 4 cycles before exhausting the combustion gasses during cycle 8. During these 4 extra engine cycles friction measurements were taken with in-cylinder pressure transducers and strain gages on the connecting rods. Since the valves remain closed during these extra cycles, the gasses are

trapped at firing temperature and pressure so that measurements directly represent rubbing friction under gas pressure and temperature conditions comparable to those at the time of firing. Pumping losses are also completely eliminated from these cycles because the valves remain closed. While this method requires extensive modification to the valvetrain, it does not require any modifications to the piston, cylinder, or cylinder head which might otherwise alter the measured friction.

2.7 Independent Test Rigs

Focusing primarily on the piston assembly with hopes to reduce engine friction, several experimental setups have been developed to quickly quantify the effect of altering related parameters. Ting [31] built a reciprocating rig for tribological studies in the form of a slider-crank mechanism that caused relative motion between ring and liner specimens. Dearlove and Cheng [32] likewise used a reciprocating rig along with a laser fluorescence technique to investigate oil film thickness alongside ring friction. These studies have provided useful insight into the theory behind the friction characteristics between the piston rings and cylinder liner.

Chapter 3

3. Engine Modeling

This chapter discusses the general form of the Mean Value Engine Model (MVEM) used in this research. Depending on the objectives of the research for which a model is built mathematical models describing engines will have many different forms. The level of engine detail encompassed within these models varies greatly. Models can range from highly detailed cyclic models to phenomenological quasi-linear transfer function models. At the highest level of detail the goal is usually to improve engine design to increase power and efficiency while lowering emissions. Detailed data of cycle-to-cycle events must be therefore captured by these models. A simpler approach is often used for research related to control system design or vehicle modeling [33].

Due in part to the departmentalized nature of engine research, the literature contains many dynamic simulation models which have been presented for various subsystems of four-cycle spark ignition engines. These are specifically tailored to the applications with which they are presented. In this manner engine control or some aspect of the design of the particular subsystem can be improved. Few simulation models are presented for an entire engine which can claim a suitable level of accuracy for most engineering uses. The MVEM as described in the following sections is one such model.

3.1 Introduction to the MVEM

Proposed by Hendricks and Sorenson, the Mean Value Engine Model (MVEM) is a type of simple mathematical engine model which bridges the gap between large cyclic

simulation models and simplistic phenomenological transfer function models [34]. This type of model seeks to predict the mean values of the gross external and internal engine variables (such as crankshaft speed and volumetric efficiency) as they change with time. The time scale of these models is just sufficient to accurately describe the change in the mean value of the most dynamic engine variables. By selecting the correct physical variables as the model's backbone and ensuring that they are accurately represented the overall accuracy of the MVEM is maintained on the order of the experimental uncertainty of a typical dynamometer experiment (i.e. +/- 2-3%). Further the MVEM is mathematically compact with few adjustable parameters such that it may be adapted to a given engine without great difficulty. The following sections will describe the model and how it may be fitted to a given engine.

3.2 MVEM Basics

The MVEM was created to be easily adapted to differing engine designs. In order to discuss the basic design of the model a four-cycle S.I. engine using central fuel injection (CFI) as depicted schematically in figure 3-1 will be considered. In this scheme the fuel is injected into the intake manifold by a single centrally located fuel injector adjacent to the throttle body. This type of fuel injection is classically considered to be the most difficult to model as a result of the dynamics of the fuel flow in the intake manifold. The model handles both multi-point “batch” fuel injection (MPI) and sequential fuel injection (SEFI) equally well with proper fitting to the given engine. In an MPI engine multiple fuel injectors typically located much nearer to the intake valves inject the fuel together in one or more groups depending on design/number of cylinders. In a SEFI

engine the fuel injectors are located similarly to MPI but fire individually in sequence with the opening of the intake valves. It is important to note that the Ford engine used in this research employs direct injection of the fuel into the combustion chamber, and adjustment of the model to this feature will be treated in chapter 5 alongside the description of the model's fit to this engine. The basic idea of the MVEM is well represented schematically in figure 3-1. The basic systems to be modeled are depicted with abbreviated labels for both the physical components of the engine and the physical variables used to describe the engine dynamics. Specifically the physical components are labeled as the throttle body (Tb), fuel injector (Fi), throttle plate (Tp), intake manifold (Im), central engine (E), exhaust manifold (Em), engine internal frictional losses (F), engine load (L), area of the throttle body throat (A_t), and area of the intake valve ports (A_p). The physical variables are placed in their proper locations and are summarized in the nomenclature.

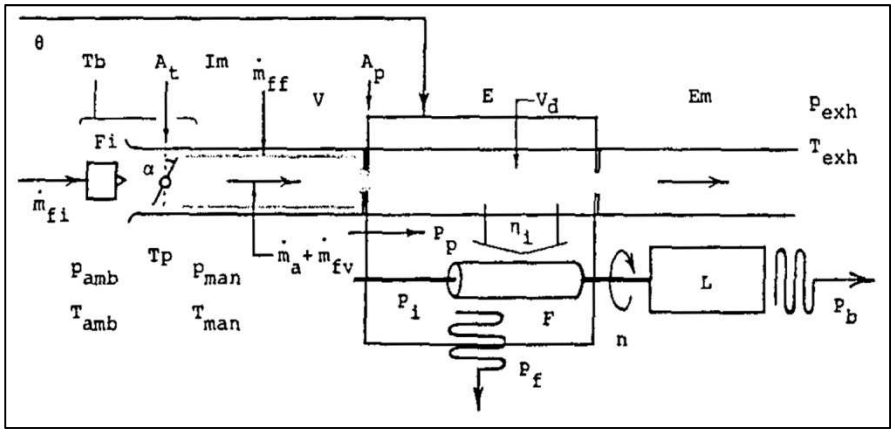

Figure 3-1: Schematic block diagram of a CFI engine, [34]

3.2.1 Time Scaling

The time scaling of the MVEM is designed to be faster than the fastest change in the mean value of any engine variable. Relationships between engine variables within the model can be broken down into two types: instantaneous and time developing. These two types of relationships evolve from the physical response of the engine subsystems. If the relevant subsystem responds to change by establishing equilibrium within only one or a few engine cycles it is considered instantaneous. Therefore for the purpose of the MVEM these relationships are represented by algebraic equations and truly occur instantly in the model. This is acceptable due to the time scale in which the model operates. Time developing relationships on the other hand may require anywhere from about 10 to 1000 engine cycles to reach equilibrium [34]. In the MVEM such relationships are described by differential equations.

3.2.2 Physical Overview of the MVEM

At this point some terminology to describe the various physical quantities that describe the engine is required to properly discuss the construction of the model. Engine *input variables* control the engine and are externally adjustable. In the case of the MVEM and other engine control schemes these are the throttle angle, the injected fuel flow, and the ignition timing. The load applied to the engine is also an input and is best described as a disturbance within the model that forces the engine away from its unloaded operating condition.

State variables are yielded by integrating the differential equations that form the basis for the model. The level of complication of these differential equations is largely

affected by the selection of the state variables. The state variables may also be considered *output variables* as they are in a sense the measurable result of the input variables. State variables for this model are chosen as the fuel film mass flow, the crankshaft speed, and the manifold pressure. Lastly, the *gross internal engine variables* may be determined as functions of the state variables and inputs. These include the thermal and volumetric efficiencies of the engine. These variables are summarized in figure 3-2 below:

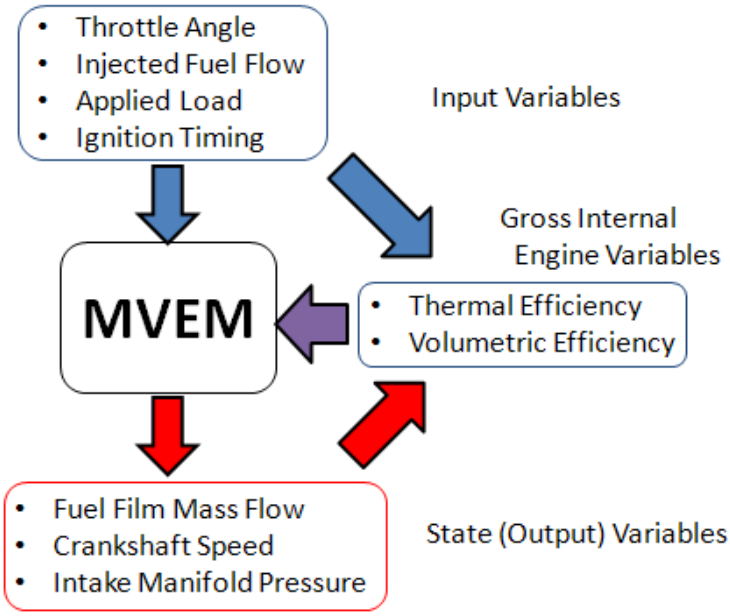

Figure 3-2: MVEM overview

In considering the input variables it is important to note that a system of control is implied but is not a feature of the MVEM. In the case of modern automobiles these values are regulated in concert based on current driving conditions and the position of the

accelerator pedal - the singular input from the (human) driver. This is accomplished within the vehicle's electronic control unit as the pedal position provides the degree of acceleration desired, feedback from other sensors provide current operating conditions, and the appropriate variables for engine control are selected to maintain efficient operation. Primarily this requires actuation of the throttle and fuel injectors to maintain a correct ratio of air to fuel as well as maintaining proper ignition timing (spark advance). The MVEM as presented here is a representation of the engine only and therefore depends on an external control scheme to properly select the values of input variables for simulation. In this way only realistic and matched values are input to the model. The selection of appropriate input variables for simulation will be discussed in chapter 5. For complete understanding of the MVEM it should be noted now that the throttle angle and the injected fuel flow may be directly related using the desired air/fuel ratio. For a given air/fuel ratio, selection of the throttle angle also determines the required injected fuel flow. The applied load (the required available torque to be produced by the engine) may be manually adjusted as an input to the model within the engine's reasonable output range. Through the construction of the model it is assumed that the air to fuel ratio and spark advance are maintained in such a way as to allow the engine to run properly. These parameters only enter into the model directly through the treatment of the thermal efficiency as will be seen in section 3.4.3 later in this chapter.

The chosen state variables provide a good physical representation of the engine. Crankshaft speed is a clear choice as a measured quantity to determine the operating condition of any engine, while intake manifold pressure is also a common measurement

and can be used to indicate engine loading conditions. An indication of fueling rate is also provided completing the physical picture of the engine. Overall the MVEM may be summarized as a tool to determine the engine speed and power output from a given engine when the common engine input variables are known and controlled.

3.3 Composing System State Equations

The creation of the MVEM begins with construction of the differential equations which describe the time developing relationships within the engine. Once the differential equations are established the algebraic equations describing the instantaneous engine processes are derived, completing the model. Selection of the state variables heavily impacts the overall quality and complexity of the resulting model. In selecting the state variables, Hendricks and Sorenson considered where the energy is concentrated within the engine to develop the model based on three dynamic subsystems. The input energy to the engine is delivered by the fuel and air flow while the output energy is present in the engine load and losses, considered to act upon the crankshaft. This suggests that the three major dynamic subsystems most involved in describing the engine are:

1) the fuel vapor and fuel film in the intake manifold,
2) the air mass flow in the intake manifold, and
3) the crankshaft loading.

These subsystems and their interactions in the model are depicted in figure 3-3. Applying conservation of mass or energy to these subsystems allows derivation of the state

equations [34]. Each of these systems and the related state equation will be presented in the following three sub-sections of this chapter.

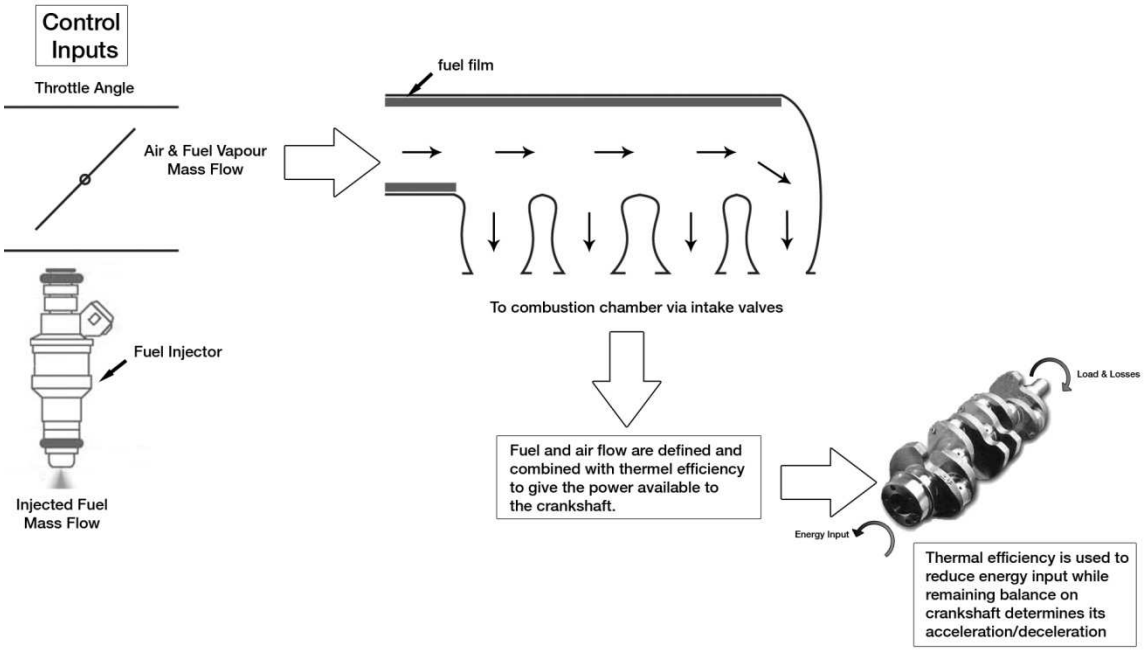

Figure 3-3: Depiction of MVEM subsystems and energy flow

3.3.1 Manifold Fuel Flow Equation

In conventional fuel injection one or more fuel injectors are used to spray a fine mist of fuel into the intake manifold. A simple sub-model for this fuel flow has been suggested by Rasmussen [34], [35] and later by Aquino [36], which considers two contributions to this total fuel flow: a fuel vapor flow and a fuel film (liquid) flow on the wall of the manifold. It is assumed that all of the injected fuel is vaporized and burned in the engine. In the MVEM the fuel vapor flow is considered an instantaneous variable as this portion of the fuel reaches the intake valves along with the intake air. The portion of the injected fuel which is initially deposited as a liquid film on the manifold wall

evaporates off the heated surface with a time constant such that a differential equation is needed for its expression. For convenience the fuel flow is considered per unit time rather than in relation to the engine cycle. The fuel flow subsystem is summarized in figure 3-4 below:

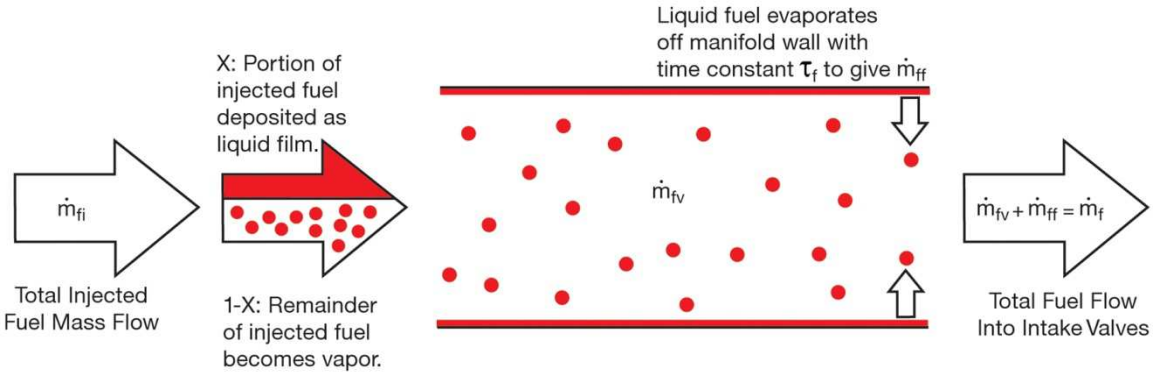

Figure 3-4: Physical depiction of MVEM fuel flow subsystem. Dynamics of the injected fuel are captured to yield the fuel flow rate into the cylinders.

Expressing the simplified fueling model in equation form and referring to the nomenclature as needed we have the following:

$$\dot{m}_{fv} = (1 - X)\dot{m}_{fi} \tag{3-1}$$

$$\ddot{m}_{ff} = (1/\tau_f)(-\dot{m}_{ff} + X\dot{m}_{fi}) \tag{3-2}$$

$$\dot{m}_f = \dot{m}_{fv} + \dot{m}_{ff}, \tag{3-3}$$

where $\dot{m}_{fv}$ is the portion of the total injected fuel flow $\dot{m}_{fi}$ that exists in the vapor phase and $\dot{m}_{ff}$ is the remaining portion which is deposited as a liquid film. The variable X defines this division while $\dot{m}_f$ is the total fuel flow into the cylinder port.

For a given manifold temperature and dependent on engine design, the variable X is either constant or a function of the throttle angle. The basic intent of this fueling sub-model is to account for the time delay experienced by a portion of the injected fuel before it reaches the cylinder port as fuel vapor. This delay occurs because the portion of the injected fuel that is deposited as a liquid film on the intake manifold requires time to evaporate. The total fuel flow into the cylinder port, $\dot{m}_f$, is therefore the delayed result of the total fuel injected, $\dot{m}_{fi}$. The engine control system is expected to compensate for this transient effect so that the correct amount of fuel is injected and an appropriate value of $\dot{m}_f$ results, nudging the engine's operating point in the correct direction. The above equations greatly simplify the true dynamics of fuel flow in the manifold however this representation has proven sufficiently accurate for use in the MVEM [34].

3.3.2 Manifold Air Flow Equation

The intake manifold is responsible for smoothly directing filtered air to the intake valves where it may be drawn into the combustion chambers. As such the functional volume of this component is that enclosed between the throttle plate and the intake valves. Applying conservation of mass to this volume according to figure 3-5 yields the necessary state equation for the manifold pressure. The rate of change of air mass flow in this volume, $\dot{m}_a$, is the difference between the flow entering the volume past the throttle plate, $\dot{m}_{at}$, and that exiting the volume through the engine intake valves, $\dot{m}_{ap}$, such that:

$$\dot{m}_a = \dot{m}_{at} - \dot{m}_{ap} \tag{3-4}$$

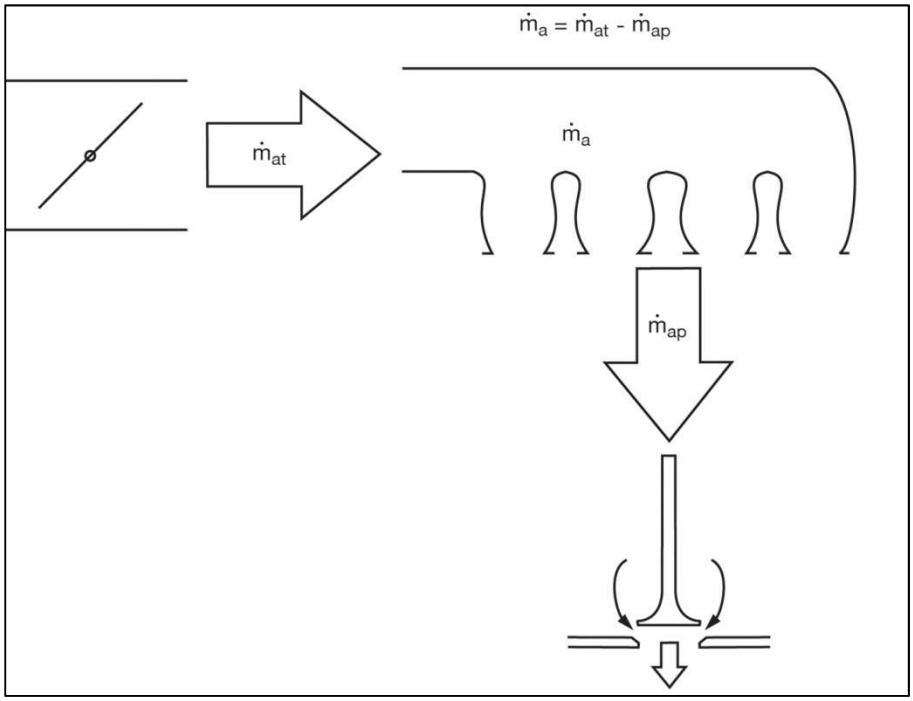

Figure 3-5: Physical depiction of MVEM air flow subsystem

The flow through the intake valves is obtained from the following equation specialized for four cycle engines and based on the speed density formula and ideal gas law [34]:

$$\dot{m}_{ap} = \frac{n}{120} V_d \rho \eta_{vol} = \frac{n}{120} \frac{V_d \eta_{vol}}{R T_{man}} p_{man} \quad (3\text{-}5)$$

where n is the crankshaft (engine) speed, V_d is the engine displacement volume, ρ is the air density, η_{vol} is the volumetric efficiency, R is the universal gas constant, and T_{man} and p_{man} are the temperature and pressure of air in the manifold. The manifold air pressure, p_{man}, appears in equation (3-5) and it is desirable to express this state equation in terms of this easily measured pressure instead of the less accessible mass air flow. This proves particularly convenient as this variable is often measured by stock engine

instrumentation or it can easily be added to any experimental setup. In order to express $\dot{m}_a$ in terms of $\dot{p}_{man}$ the ideal gas law may be applied to the volume V (the volume contained in the intake manifold between the throttle and the intake valves) such that:

$$\dot{m}_a = \frac{\dot{p}_{man}\, V}{R\, T_{man}} \tag{3-6}$$

Combining equations (3-4), (3-5), and (3-6) and rearranging in terms of $\dot{p}_{man}$ yields the manifold air flow state equation as:

$$\dot{p}_{man} = -\frac{n}{120}\frac{V_d}{V}\,\eta_{vol}\, p_{man} + \frac{R\, T_{man}}{V}\,\dot{m}_{at}(\alpha, p_{man}) \tag{3-7}$$

The mass flow of air past the throttle plate, $\dot{m}_{at}$, is shown here only as a function of throttle angle and manifold pressure as this relation is dependent on the geometry of the throttle. The relation is typically approximated by the usual expressions for a compressible flow through a converging nozzle and will be discussed in the next section of this chapter.

3.3.3 Crankshaft Equation

The crankshaft state equation is derived from the conservation of energy across it. The energy input to the crankshaft is considered to come from the fuel flow. While the injected fuel is assumed to be entirely consumed by the engine, in order to avoid complicated modeling of the cooling and exhaust systems the thermal efficiency of the engine is used instead as a multiplier of this fuel flow. In this way the fuel energy available to overcome engine losses and drive the load is used. This energy input is

balanced against the applied load as well as the pumping and frictional losses applied to the crankshaft in terms of its rotational inertia. The physical intent of this subsystem is summarized in figure 3-6. In equation form the energy balance may be expressed as follows:

$$\frac{d}{dt}\left(\frac{1}{2}\, I\, n^2\right) = I\, n\, \dot{n} = -\left(P_f + P_p + P_b\right) + H_u\, \eta_i\, \dot{m}_f(t - \tau_d) \tag{3-8}$$

where I is the total inertial load of the engine, n is the crankshaft speed, P_f, P_p, and P_b are the frictional, pumping, and load powers respectively, H_u is the lower heating value of the fuel, η_i is the indicated thermal efficiency of the engine, $\dot{m}_f$ is the rate of fuel mass flow into the cylinder, t is the time, and τ_d is a time delay inserted to describe the delay between the edge of a fuel flow step and the change in crankshaft speed.

Rearranged in terms of engine speed this becomes:

$$\dot{n} = -\frac{\left(P_f + P_p + P_b\right)}{I\, n} + \frac{H_u\, \eta_i\, \dot{m}_f(t - \tau_d)}{I\, n} \tag{3-9}$$

where the units of I have been chosen to provide a convenient equation in terms of RPM. It has been shown that approximating the time delay τ_d as the mean time between mixture ignitions is a sufficient treatment of the discrete nature of a reciprocating engine, [34]. For a four cycle engine:

$$\tau_d = \frac{4\pi}{n_{cyl}\,(2\pi\frac{n}{60})} = \frac{120}{n_{cyl}\, n} \tag{3-10}$$

where n_{cyl} is the number of engine cylinders, and n is the engine speed as before.

Figure 3-6: Physical depiction of crankshaft equation. Fuel flow into the cylinders is modified by the fuel heating value and engine thermal efficiency to give the energy input. This is then balanced against the load and losses to yield the state equation.

3.4 Composing Instantaneous Engine Variable Equations

In order to employ the differential equations described in the previous section additional algebraic equations are needed to express the instantaneous engine variables in terms of the state variables. Specifically equations are needed for X in equations (3-1) and (3-2), for η_{vol} and $\dot{m}_{at}$ in equation (3-7), and for P_f, P_p, P_b, and η_i in equation (3-9). Some of these variables, such as η_i, are purely phenomenological and must be fitted with specific data from the running engine. Hendricks and Sorenson [34] expended a great deal of effort to ensure that a minimal number of regression terms and parameters were utilized throughout the instantaneous variables such that the functional forms presented here are physically based and minimal in form. With brevity in mind the instantaneous variable equations will be presented in the following sections with a minimum of discussion of their derivation.

3.4.1 Fuel Film Variables and Parameters

It is not possible to obtain the values of X (the fraction of the fuel flow which becomes fuel film on the manifold) and the fuel film evaporation constant, τ_f, as used in equations (3-1) and (3-2) directly from steady state engine measurements for a CFI engine as presented by Hendricks and Sorenson [34] or for an MPI engine as presented by Hendricks et al. [37]. Instead the dynamic behavior of the engine must be mapped as it applies to fueling. For SEFI engines X and τ_f remain constant at constant temperature and so are not operating point dependent. For these engines the fueling submodel becomes linear and identification of the fueling parameters becomes somewhat more straightforward. In any case these parameters must be mapped for a given engine and operating temperature based on transient fired-engine testing. For the particular MPI engine studied by Hendricks et al. in [38] representative expressions may be given as [37]:

$$\tau_f(p_{man}, n) = 1.35(-0.672n + 1.68)(p_{man} - 0.825)^2 + (-0.06n + 0.15) + 0.56 \quad (3\text{-}11)$$

$$X_f(p_{man}, n) = -0.277p_{man} - 0.055n + 0.68 \quad (3\text{-}12)$$

where n is the engine speed and p_{man} is the intake manifold pressure as before.

3.4.2 Manifold Pressure Variables and Parameters

The two necessary instantaneous variables applying to the manifold filling dynamics are the volumetric efficiency, η_{vol}, and the air mass flow past the throttle plate, $\dot{m}_{at}$. As mentioned earlier the air mass flow past the throttle is often measured on production engines and is fully accessible for measurement in experimental setups. Approximating the throttle as a converging nozzle with the effective area of a

corresponding circle and considering the flow of a compressible fluid the following equation may be written [34]:

$$\dot{m}_{at}(\alpha, p_{man}) = C_t \frac{\pi}{4} D^2 \frac{p_{amb}\sqrt{\kappa'}}{\sqrt{R\,T_{amb}}} \beta_1(\alpha)\beta_2(p_{man}) + \dot{m}_{at0} \tag{3-13}$$

where C_t, D, p_{amb}, R, T_{amb}, and $\kappa' = 2\kappa/(\kappa - 1)$ are physical constants while $\dot{m}_{at0}$ is a fitting constant corresponding to the bypass air mass flow. The β functions are:

$$\beta_1(\alpha) = 1 - \cos(\alpha - \alpha_0) \tag{3-14}$$

$$\beta_2(p_{man}) = \sqrt{p_r^{\frac{2}{\kappa}} - p_r^{\frac{\kappa+1}{\kappa}}}, if\ p_r \geq \left(\frac{2}{\kappa+1}\right)^{\frac{\kappa}{\kappa-1}} = \sqrt{\left(\frac{1}{\kappa'}\right)\left(\frac{2}{\kappa+1}\right)^{\frac{\kappa+1}{\kappa-1}}}, otherwise \tag{3-15}$$

where $p_r = p_{man}/p_{amb}$ and α_0 is a constant.

The volumetric efficiency expression can be found by conducting a series of air flow measurements and calculating efficiency based on manifold conditions during fired-engine testing. The functional dependence of the volumetric efficiency for the MVEM is given as [34]:

$$\eta_{vol}(n, p_{man}) = \eta_{vn0} + \eta_{vn1} n + \eta_{vn2} n^2 + \eta_{vp1} p_{man} \tag{3-16}$$

where η_{vn0}, η_{vn1}, η_{vn2}, and η_{vp1} are physical constants.

3.4.3 Crankshaft Variables and Parameters

To solve the crankshaft state equation four expressions are needed; these are the power terms and the thermal efficiency. The load power, P_b, may be expressed as [38]:

$$P_b(n) = k_b n^3 \tag{3-17}$$

where k_b is the loading parameter and is adjusted to give the desired load at a given operating point.

The friction and pumping loss power terms may be expressed as polynomials in the engine speed and manifold pressure as [34]:

$$P_f + P_p = n(a_0 + a_1 n + a_2 n^2) + n(a_3 + a_4 n) p_{man} \tag{3-18}$$

where a_0 through a_4 are constants. These constant coefficients must be estimated via regression analysis on engine-specific test data.

Determining the expression for the engine's thermal efficiency (the proportion of the fuel's energy which is available to drive the load and overcome engine losses) is considerably more involved. However using this as an instantaneous variable in the MVEM is advantageous as it avoids modeling the thermal losses associated with the engine cooling system, radiation from all surfaces, and through the engine exhaust. The expression can be found from steady state engine mapping data prepared during fired-engine testing and may be split into dependencies on speed, manifold pressure, spark advance, and air/fuel ratio as shown in equation (3-19). It should be noted that this is the only location in the MVEM where either spark advance or air/fuel ratio appear directly. To ensure simulation of an efficiently running engine these variables must be controlled

as the model's inputs. The forms of the expressions for total thermal efficiency and for the individual dependencies of the total thermal efficiency are given as [34]:

$$\eta_i(\theta, \lambda, n, p_{man}) = \eta_i(\theta, n)\eta_i(\lambda, n)\eta_i(n)\eta_i(p_{man}) \quad (3\text{-}19)$$

$$\eta_i(n) = \eta_{i0} - \eta_{in}e^{-n/n_0} \quad (3\text{-}20)$$

$$\eta_i(p_{man}) = p_{m0} + p_{m1}p_{man} + p_{m2}p_{man} \quad (3\text{-}21)$$

$$\eta_i(\theta, n) = \Theta_0 + \Theta_1(\theta - [\Theta_2 n + \Theta_3])^2 \quad (3\text{-}22)$$

$$\eta_i(\lambda, n) = \Lambda_0 + \Lambda_1\lambda + \Lambda_2\lambda^2 + \Lambda_3 n \quad (3\text{-}23)$$

where η_i is the indicated thermal efficiency, θ is the spark advance, λ is the air/fuel equivalence ratio, n is the engine speed, and p_{man} is the intake manifold pressure while η_{i0}, η_{in}, and n_0 in equation (3-20), p_{m0}, p_{m1}, and p_{m2} in equation (3-21), the Θ's in equation (3-22), and the Λ's in equation (3-23) are all constants. When equation (3-19) is expanded with the expressions in equations (3-20) through (3-23) the full equation for engine thermal efficiency is obtained.

3.5 Detailed Engine Friction Modeling

While engine friction and pumping loss terms may be collapsed to simple polynomials in the engine speed and manifold pressure according to equation (3-18), this provides no insight into the nature of engine friction. Since rubbing friction terms are largely a function of known engine parameters and design it is possible to form a detailed physical model for the friction terms which represents the contributions of individual components. Such a model is of greater use for the characterization and potential reduction of internal friction. A component based model also makes it possible to verify some of the tested friction of the partially disassembled engine. A detailed friction model

is used to augment the MVEM according to work completed by Patton et. al. in the late 1980's [39] and updated by Sandoval and Heywood in the early 2000's [5]. This model as presented includes predictions of rubbing friction losses from the crankshaft, reciprocating assembly, valvetrain components, as well as auxiliary and pumping losses. The model is based on a combination of friction theory and empirical engine teardown/motoring and running engine data. Patton et. al. [39] describe the following three step process for relating the fmep at engine locations at which rubbing friction occurs to design and operating parameters. First, an assumption is made regarding which of the three lubrication regimes (as described in section 2.3) applies. This determines the relationship between the friction coefficient and a dimensionless duty parameter, $\mu V/P$, which was a function of viscosity (μ), velocity (V), and unit load (P). This general relation with respect to lubrication regime was depicted in figure 2-8. The first step relationships were assumed to be as follows for the three types of lubrication:

Boundary Lubrication – the friction coefficient is constant and independent of the design and operating parameters,

Mixed Lubrication – the friction coefficient varies approximately inversely with engine speed,

Hydrodynamic Lubrication – the friction coefficient varies with a term proportional to the duty parameter.

The second step of the process was to derive a term proportional to fmep based on the friction coefficient. This is accomplished by multiplying the friction coefficient by a

normal force to obtain a friction force. The friction force is then multiplied by a relevant velocity in order to obtain a term proportional to friction power loss. Lastly, this is divided by engine speed and displacement to become proportional to fmep. Bishop [40] had employed a similar process for the derivation of fmep relationships during his modeling efforts in the 1960's.

Lastly, the developed fmep terms were multiplied by constants to "calibrate" them based on empirical results. This three-step process provides insight into the formulation of this model. The work of Bishop [40] may be considered a starting point for the model, while the subsequent work of both Patton et. al. [39], and Sandoval and Heywood [5] have improved and updated the model over time.

The original work of Patton et. al. [39] was based on engine friction data collected prior to 1988 and required updating primarily due to improvements in lubricating oils, cylinder bore surface finishes, piston ring friction, and valvetrain mechanisms [5]. Lubricant viscosity scaling is also added to the model allowing the effects of changes in this critical operating parameter to be estimated. The updated version of the model gives reasonable estimates of component group and total engine friction mean effective pressures (measured in kPa) for current S.I. engine design and is presented in the following subsections [5].

3.5.1 Crankshaft Group

The first of three component groups into which the model divides rubbing friction is that of the crankshaft. This includes the main bearings and front and rear main oil seals. The first term in equation (3-24) gives the friction of the main bearing seals which are

assumed to operate in the boundary lubrication regime, the second term gives the hydrodynamic main bearing friction, while the final term represents the turbulent dissipation associated with transport of oil through the bearings. For the first two terms the three-step process described above is used to determine the design and operating parameter relation to fmep according to the relevant friction coefficient, friction force, and friction power. The third term is determined by assuming the fmep per bearing is proportional to the pressure drop through the bearing. For all three terms the constants are based on empirical fit.

$$cfmep = 1.22 \times 10^{5}\left(\frac{D_{bm}}{B^2 S n_{cyl}}\right) + 3.03 \times 10^{-4}\sqrt{\frac{\mu}{\mu_0}}\left(\frac{n {D_{bm}}^3 L_{bm} n_{bm}}{B^2 S n_c}\right) + 1.35 \times 10^{-10}\left(\frac{{D_{bm}}^2 n^2 n_{bm}}{n_{cyl}}\right) \quad (3\text{-}24)$$

where D_{bm} is the diameter of the main bearings, B is the bore, S is the stroke, n_{cyl} is the number of cylinders, μ is the oil viscosity for which predictions are being made, μ_0 is the oil viscosity for which the model was originally calibrated, n is the engine speed, L_{bm} is the length of the main bearings, and n_{bm} is the number of main bearings. Note that the $\sqrt{\frac{\mu}{\mu_0}}$ in the second term accounts for changes in lubricant viscosity that occur with changes in the type or temperature of the engine oil. This term is present throughout the model wherever hydrodynamic lubrication is assumed to occur.

3.5.2 Reciprocating Assembly Group

The reciprocating engine components group incorporates friction contributions from the connecting rod (journal) bearings, the piston skirt, and the piston rings. The model further divides the piston ring friction contribution into two terms: one for the rings without gas pressure loading, and one that predicts the increase in friction of the piston rings due to the gas pressure loading. Equation (3-25) gives the reciprocating friction without gas pressure loading while the additive loading term is found in equation (3-26). The first term of equation (3-25) represents the hydrodynamic lubrication friction of the piston, includes the $\sqrt{\frac{\mu}{\mu_0}}$ term as before, and its constant is again based on an empirical fit. The second term represents the friction of the piston rings without gas pressure loading, derived under the assumption of mixed lubrication. The primary design parameter is seen to be the diameter of the cylinder bore, while several terms are used to modify the constant which is again fit empirically. The F_t/F_{t0} term allows changes in the piston ring tension ratio, while the C_r term does the same for changes in the piston roughness constant. The $\left(1+\frac{500}{n}\right)$ term is added to cause the friction coefficient to decrease from low to high speed to account for the expected decrease in friction in the mixed lubrication regime. The third term is for the journal bearing hydrodynamic friction. Its relation is the same as for the crankshaft main bearings, including the same empirical constant.

$$rfmep = 2.94 \times 10^2 \sqrt{\frac{\mu}{\mu_0}}\left(\frac{S_p}{B}\right) + 4.06 \times 10^4 \left(\frac{F_t}{F_{t0}} C_r\right)\left(1 + \frac{500}{n}\right)\left(\frac{1}{B^2}\right) + 3.03 \times 10^{-4} \sqrt{\frac{\mu}{\mu_0}}\left(\frac{n {D_{bj}}^3 L_{bj} n_{bj}}{B^2 S n_{cyl}}\right) \quad (3\text{-}25)$$

where S_p is the mean piston speed, $\frac{F_t}{F_{t0}}$ is the piston ring tension ratio, C_r is the piston roughness constant, D_{bj} is the diameter of the journal bearings, L_{bj} is the length of the journal bearings, and n_{bj} is the number of journal bearings.

$$rfmep_{gas} = 6.89 \frac{p_{man}}{p_{amb}} \left[0.088 \sqrt{\frac{\mu}{\mu_0}} r_c + 0.182 \left(\frac{F_t}{F_{t0}}\right) {r_c}^{(1.33 - K S_p)}\right] \quad (3\text{-}26)$$

where p_{man} is the intake manifold pressure, p_{amb} is the atmospheric pressure, r_c is the compression ratio, and K is a constant equal to 2.38×10^{-2}.

The reciprocating friction due to gas pressure loading, $rfmep_{gas}$, is related to the physics of the combustion process and is based on an expression developed by Bishop from firing friction data [40]. Here the constant factor of 6.89 is used to convert from units of psi to kPa. Bishop's term used the product of intake pressure and a factor which included the compression ratio raised to an exponent that decreased as mean piston speed increased. This accounts for the relationship between the friction coefficient and duty parameter within the mixed lubrication regime in which the rings operate. The expression

is used with the addition of the previously described $\sqrt{\frac{\mu}{\mu_0}}$ and $\frac{F_t}{F_{t0}}$ terms, and the constant K is due to Bishop.

3.5.3 Valvetrain

The valvetrain friction group accounts for the camshafts, cam followers, and valve actuation mechanisms. Constants corresponding to the type of valvetrain design are used as weighting terms to allow the model to work for various engines. In order to maintain flexibility within the model these constants were adjusted so that their sum can represent a variety of valvetrain configurations and still be based on the individual component contributions to friction. The equation's first term accounts for camshaft bearing hydrodynamic friction derived similarly to the other bearings as has been described. The second and fifth terms predict the camshaft follower friction for flat followers, and oscillating components for mixed lubrication friction. They include the $\left(1+\frac{500}{n}\right)$ terms to account for the same behavior as described for the mixed lubrication term of the reciprocating friction. The third term predicts rolling contact (boundary) friction for the roller followers, while the fourth term predicts the contributions of oscillating components in the hydrodynamic regime. Finally, the constant term of 4.12 kPa represents the boundary-lubricated friction of the camshaft bearing seals and was fit from calibration engine data that indicated this portion of the valvetrain friction was independent of piston speed [5]. Collectively, the valvetrain friction terms are expressed as:

$$vfmep = 244\sqrt{\frac{\mu}{\mu_0}}\frac{nn_{bc}}{B^2Sn_{cyl}} + C_{ff}\left(1+\frac{500}{n}\right)\frac{n_v}{Sn_{cyl}} + C_{rf}\left(\frac{nn_v}{Sn_{cyl}}\right) + C_{oh}\sqrt{\frac{\mu}{\mu_0}}\left(\frac{{L_v}^{1.5}n^{0.5}n_v}{BSn_{cyl}}\right) + C_{om}\left(1+\frac{500}{n}\right)\frac{L_v n_v}{Sn_{cyl}} + 4.12 \quad (3\text{-}27)$$

where n_{bc} is the number of camshaft bearings, n_v is the total number of valves, L_v is the maximum valve lift, and C_{ff}, C_{rf}, C_{oh}, and C_{om} are constants dependent on valvetrain configuration as shown in table 3-1. For each type of valvetrain configuration commonly used in engines there is a corresponding set of constants for use in equation (3-27). Most of the constant coefficients shown in table 3-1 were first suggested in the original model by Patton et. al. [39] based on testing data of the various valvetrain configurations. The row for the DOHC finger follower configuration was added by Sandoval and Heywood by matching the model to the newer valvetrain friction data [5].

Table 3-1: Constants for valvetrain mechanism terms [5]

Valvetrain Mechanism Type	Cam Flat Follower Constant, C_{ff}	Cam Roller Follower Constant, C_{rf}	Oscillating Hydrodynamic Constant, C_{oh}	Oscillating Mixed Constant, C_{om}
SOHC finger follower	600	0.0227	0.2	42.8
SOHC rocker arm	400	0.0151	0.5	21.4
SOHC direct acting	200	0.0076	0.5	10.7
DOHC finger follower	600	0.0227	0.2	25.8
DOHC direct acting	133	0.0050	0.5	10.7
OHV	400	0	0.5	32.1

3.5.4 Auxiliary Friction

Auxiliary friction suggested by the model is an empirical match to the sum of oil pump, water pump, and non-charging alternator friction calibrated from two S.I. engines and given by [5]:

$$afmep = 8.32 + 1.86 \times 10^{-3} n + 7.45 \times 10^{-7} n^2 \quad (3\text{-}28)$$

3.5.5 Air Pumping Losses

Pumping losses are predicted separately (though similarly) for the intake and exhaust systems, calculated as the difference between cylinder pressure and atmospheric pressure integrated over the volume of the stroke, given by [5]:

$$pmep_{intake} = (p_{amb} - p_{man}) + 3.0 \times 10^{-3} \left(\frac{p_{man}}{p_{amb}}\right)^2 \left(\frac{{S_p}^2}{{n_{vi}}^2 {r_i}^4}\right) \quad (3\text{-}29)$$

where n_{vi} and r_i are the number and diameter of the intake valves respectively, and,

$$pmep_{exhaust} = 0.178 \left(\frac{p_{man}}{p_{amb}} S_p\right)^2 + 3.0 \times 10^{-3} \left(\frac{p_{man}}{p_{amb}}\right)^2 \left(\frac{{S_p}^2}{{n_{ve}}^2 {r_e}^4}\right) \quad (3\text{-}30)$$

where n_{ve} and r_e are the number and diameter of the exhaust valves respectively.

As can be seen the pressure differences are both dependent on the manifold pressure, piston speed, and the flow area as seen in the rightmost terms corresponding to valve pressure drop. The constant is fit to appropriate data as usual. The first term in the intake pmep equation is simply the intake manifold (vacuum) pressure. The first term in the exhaust pmep equation is the steady state exhaust system pressure, assumed to scale with the square of piston speed and empirically fit.

3.5.6 Total Engine fmep

The total power losses of the engine due to friction, accessories, and pumping may be found by summing the individual fmep terms from equations (3-24) to (3-30). For comparison to mechanical friction alone the predictions for the accessory and pumping losses are simply omitted.

The application and adaptation of the MVEM and physical friction model described above to the Ford engine used in this research is discussed in Chapter 5 alongside simulation results. The next chapter describes the design of the experimental setup and the collection of motored engine data.

Chapter 4

4. Experimental Setup of Motoring Test Stand

Engine friction is one of the most difficult effects to characterize and has a substantial impact on both fuel efficiency and performance. Reduction of frictional losses can universally benefit nearly any engine including those used to power current conventional and hybrid vehicles. Detailed characterization of friction is a necessary first step in the pursuit of friction reduction or the development of condition or fault monitoring strategies. Dynamometers are typically used for the characterization of engine friction, while motoring tests (in which the engine is not fired) can provide sufficient information. Such testing requires a *motoring* or *driving* dynamometer capable of rotating the engine over a range of speeds while measuring the torque required to do so. This chapter describes the experimental setup created for this purpose. It details the complete design and build of the test stand used to conduct engine motoring tests in order to characterize internal friction. This includes everything from the physical mounting and alignment of the electric motor and the engine to the design of the electrical cabinet that houses the motor controller and all power and data acquisition wiring. This is followed by a description of the sequence of experiments and the resulting engine friction measurements. The mathematical characterization of friction and the total engine model are presented alongside simulation results in chapter 5.

4.1 Experimental Requirements

In order to experimentally characterize engine friction a motoring test stand was constructed. This stand had to be capable of driving the engine over a range of speeds while measuring the inline torque. Heating the engine oil to more closely approximate running conditions as they apply to rubbing friction was a further requirement. Lastly, monitoring the engine's crankshaft position sensor for rotational speed and logging several engine temperatures completes the simple list of testing requirements. Considering the research objectives it was clear that the test stand required the capacity to:

- securely mount the drive motor and engine with allowance for misalignment;
- motor the engine from idle to a mid-level cruising speed of at least 3000RPM;
- heat the engine motor oil to a target temperature of 90˚C;
- measure torque needed to drive the engine, the engine speed, and the temperatures of the intake air and the motor oil;
- monitor and control the experiment; and
- safely enclose all rotating equipment and heated fluids.

These requirements were satisfied by designing and constructing a dedicated dynamometer for friction characterization as described in the following section.

4.2 Experimental Components and Specifications

The dynamometer primarily consists of the following major components: drive motor and motor controller, crankshaft angle sensor, torque sensor, misalignment couplers,

coolant heater and circulation pump, thermocouples, and a safety enclosure. These components are shown in figure 4-1. The following subsections describe these components in detail.

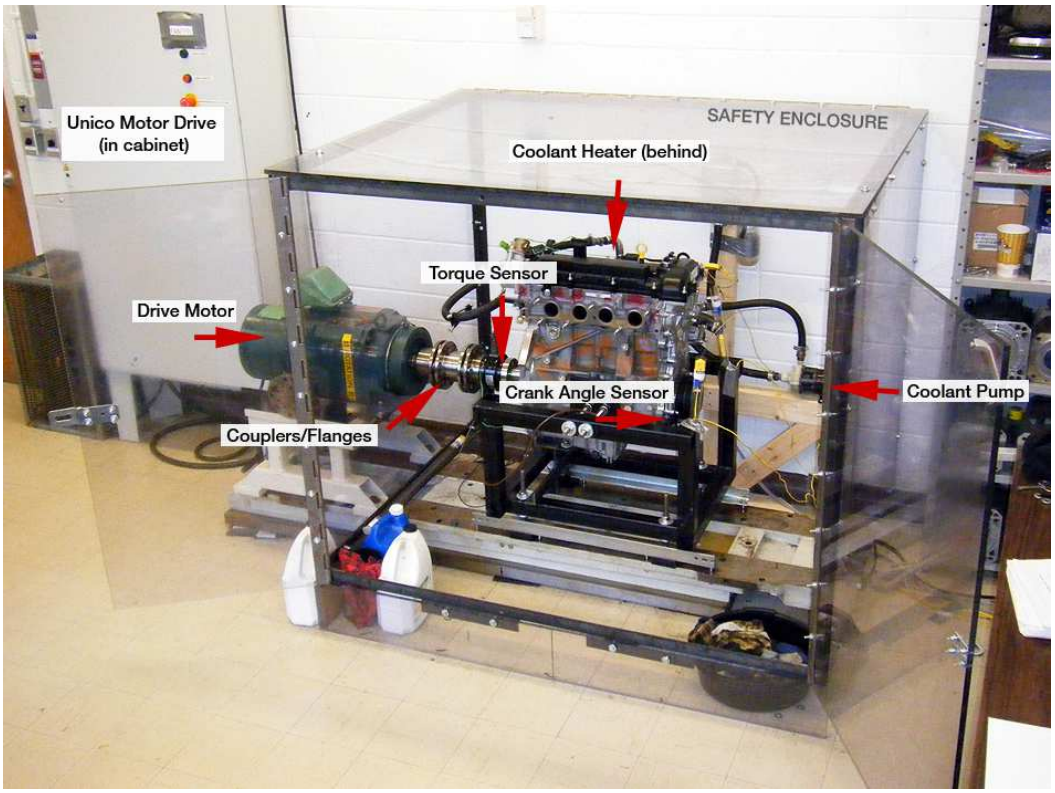

Figure 4-1: Primary components of the experimental setup

4.2.1 Drive Motor

An electric drive motor was provided to the project by The Ford Motor Company of Canada, and is the main element of the motoring test stand. It is a 3-phase, 15HP AC induction electric motor made by Reliance Electric (now Baldor Electric Company). The motor is a member of the *RPM AC* line of inverter duty motors and its speed is controlled by using pulse-width modulation (PWM). The motor has a small frame size, reducing

rotor inertia and overall weight. Operating at a drive frequency of 120 Hz the motor is capable of continuous duty and speeds up to 3530 RPM. The drive motor is shown in figure 4-2.

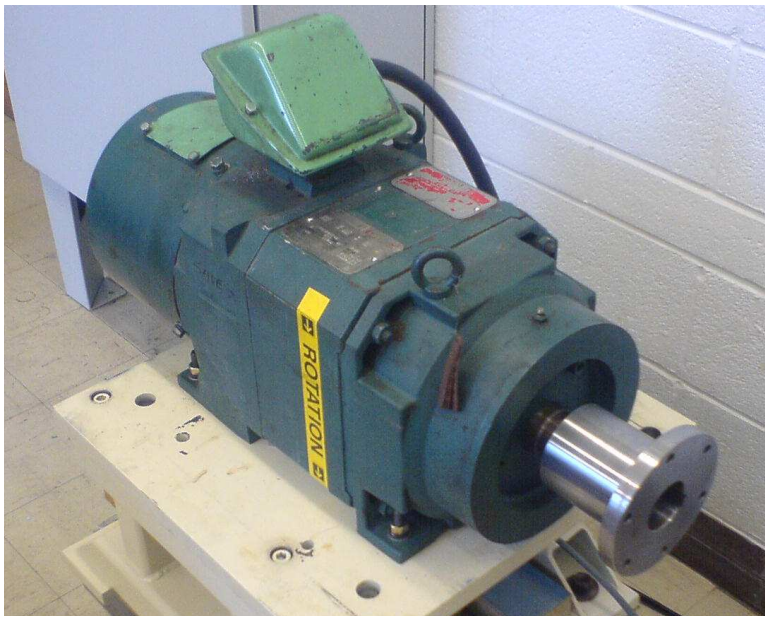

Figure 4-2: Reliance RPM AC electric drive motor

4.2.2 Unico Motor Drive

A Unico 2400 digital AC flux vector drive powers and controls the electric motor. The Unico 2000 series motor drives provide modular and motor-independent solutions for many industrial applications and the 2400 unit as used was proven to be an excellent match for the Reliance motor in previous use by Ford. Its auto-tuning feature automatically adjusts virtually all motor and load dependent parameters to easily control any brushless DC, standard, or inverter-duty AC induction motor to which it is attached and configured. It is possible to configure the drive for either torque or velocity control modes and several options are available for command and feedback interfaces. When the

drive is set to the torque control mode the drive generates a torque command which is proportional to velocity error of the motor. When the drive is set to the velocity control mode the torque command is a function of both position and velocity errors of the motor. In either mode further options allow selection between a critical or a slightly underdamped response. This equipment is shown in figure 4-3.

Figure 4-3: Unico 2400 motor controller and charging unit

Since the characterization of friction requires only steady-state motoring tests the electric motor needs to be controlled through the simple voltage control option of the Unico 2400 drive. In this mode the controller is configured to follow a +/- 10 V DC analog signal from the PC such that the speed of the motor is linearly controlled. Parameters pertaining to the rate of acceleration or deceleration of the motor while under this mode of control may be configured within the drive, however maintaining the correct speed is all that is required. This is accomplished by the controller via a built in feedback

loop using an incremental encoder attached to the motor shaft. For most tests, the drive is configured for velocity control with a slightly underdamped response characteristic.

All electrical equipment needed to support the drive motor and other powered components is contained within a large free-standing electrical cabinet. This allows for easy mounting of components and common grounding on the steel back plate of the cabinet while properly housing the high-voltage equipment contained within. All wiring connections are made according to the electrical diagram given in figure A-1 of Appendix A.

4.2.3 Crank Angle Sensor

Engine speed is monitored in two ways:

1) An incremental optical encoder affixed to the rear end of the electric drive motor's output shaft measures the speed of the drive motor. This encoder is manufactured by BEI Sensors as a member of their E25 series and has a disc resolution of 1024 cycles per turn. Output from this sensor in the 2-channels-in-quadrature format is read by the Unico motor controller and is used as feedback to control the motor speed. A +/- 10V analog output signal linearly scaled over the range of motor speeds is provided by the controller for external monitoring.

2) The original equipment engine crank angle sensor affixed to the front of the crankshaft measures the speed of the engine. This is a digital transducer known as a Hall Effect sensor and operates in conjunction with a toothed wheel fitted behind the crankshaft pulley as shown in figure 4-4. As the teeth pass by a magnetic field in the

sensor a voltage is induced. The output takes the form of a square wave with frequency corresponding to engine speed. The specific wheel used is known as a 60-2 wheel because with even spacing, it would have sixty teeth. However, two are missing to provide a position reference to the internal engine geometry. This provides critical engine timing information which enables control of the engine. The gap corresponds to a specific position of the engine cylinders. For testing purposes, it is desirable to locate the crankshaft angle that corresponds to top dead center (TDC) position of cylinder #1, which is commonly used as a starting point for the engine cycle. For this engine, the crankshaft angle corresponding to cylinder #1 TDC position is 120˚ behind the point where the gap passes the sensor. In all testing circumstances the engine's crank angle sensor is used for measuring the engine speed.

Figure 4-4: Crankshaft position sensor and wheel on Ford 2.0L engine

4.2.4 Torque Sensor

With the engine driven and its speed known, the measurement of torque is the next requirement of the test stand. This is accomplished with a rotary slip-ring style torque sensor. Essentially this allows a Wheatstone bridge strain gauge to be installed in the driveline between the electric motor and the engine. A slip-ring allows the signal from the strain gauge to pass from the rotating shaft to the stationary housing of the torque sensor. This signal is then conditioned and amplified by a powered signal conditioner, converting it to a +/- 10V signal that can be read into the PC data acquisition system. The Model 1228 flange drive torque sensor from Honeywell (formerly made by Lebow) allows easy mounting of the sensor with bolted flange connections on both sides. The DMD-465 Bridgesensor signal conditioner from Omega allows easy linearization of the torque sensor and provides a stable and accurate output. Selected key specifications for the torque sensor and signal conditioner can be found in Appendix B, table b-1 and table b-2 respectively. The torque sensor is shown in figure 4-5.

It is important to note that the specified dynamic response of the signal conditioner is DC to -3dB = 3Hz. This hardware low-pass filter helps to eliminate noise in the measurement of average torque values in the steady state. Measurement of the torque profile as it varies throughout the engine cycle is not possible with this signal conditioner as the stated gain of this filter will have reduced the measured torque values by half at only 3Hz.

Figure 4-5: Honeywell Model 1228-2k torque sensor

In order to employ the torque sensor as intended, the +/- 10 V output of the signal conditioner must be fitted to a known range of torque values. The torque range for this purpose was chosen to be approximately 0-60 lb-ft (0-81 N m). This range was selected within the total 0-166 lb-ft (0-225 N m) range of the sensor in order to improve resolution while still providing significant overhead above the maximum anticipated torque values. With this target in mind, the gain of the signal conditioner was set as needed and calibration weights were used to apply a series of known torque values to the sensor. This resulted in the system gain characteristic shown in figure 4-6. Simple linear regression is applied to the data to generate the equation and coefficient of determination, R^2, as shown. Note that an R^2 value of 1 represents a perfect fit, so the given equation is seen to fit the torque sensor calibration data quite well.

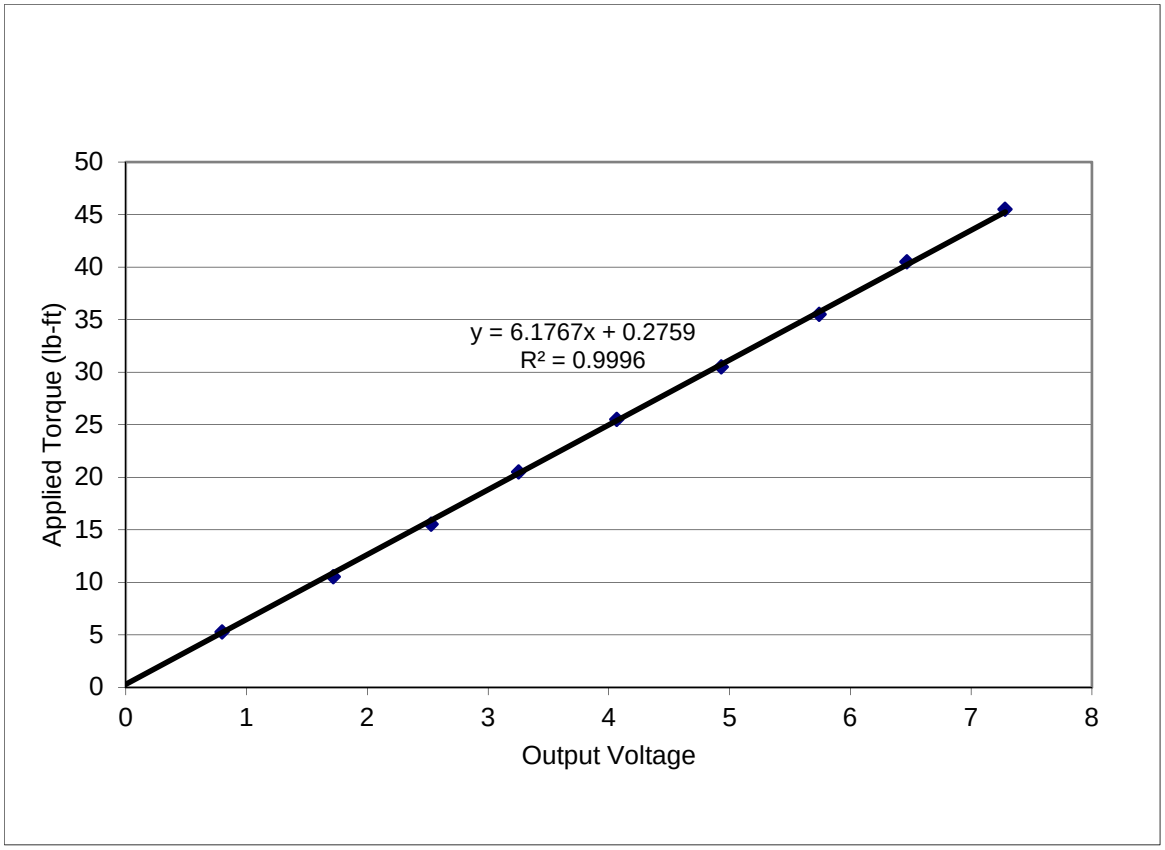

Figure 4-6: Honeywell Model 1228-2k torque sensor characteristic

4.2.5 Mechanical Alignment & Couplers

Due to the finished nature and limited size of the lab space in which this experiment was to take place a large piece of steel, formerly part of a heavy industrial machining operation, was repurposed as a base for the motoring test stand. Heavy enough to stay in place without the need for floor anchors, this available piece provided a convenient foundation with straight machined surfaces and existing holes for mounting the motor and engine (or other driven equipment). The steel base was positioned in place and a custom stand previously built for the motor was bolted to it. Made primarily of square structural steel tubing, a rendering of this simple stand is shown in figure 4-7. The

electric motor was then bolted on top of the stand in its fixed position. This fixed the output shaft of the electric motor directly over center on the base and at a convenient height of 18 inches (46cm). This mounting also determines the height of the engine and the selected height allows easy access for service such as changing the oil.

A similarly constructed stand was designed and built to support the engine. This stand required adjustability to allow alignment to the motor's shaft. As such it meets the base with individual steel feet attached via threaded rod. These feet allow individual height adjustment at the four corners of the stand to set engine height and finely adjust inclination of the stand. Threaded rod is also used for the engine supports which are located on either side of the engine block. These allow fine adjustment of the engine side-to-side while a final threaded rod located beneath the rear of the engine adjusts tilt of the engine relative to the stand. Figure 4-8 provides a quick rendering of the steel base, mounted electric drive motor, and engine support stand.

In order to execute motoring tests the engine's crankshaft must be driven by the motor. The most convenient location to couple to the crankshaft occurs at the back of the engine where the flywheel normally attaches. With the flywheel removed a simple flanged connection may be made directly to the crankshaft at this location. By adjusting the threaded connections of the engine stand the engine can be located such that this flange approximately lines up with the motor's output shaft. All that remains is to create appropriate couplers to complete the driveline.

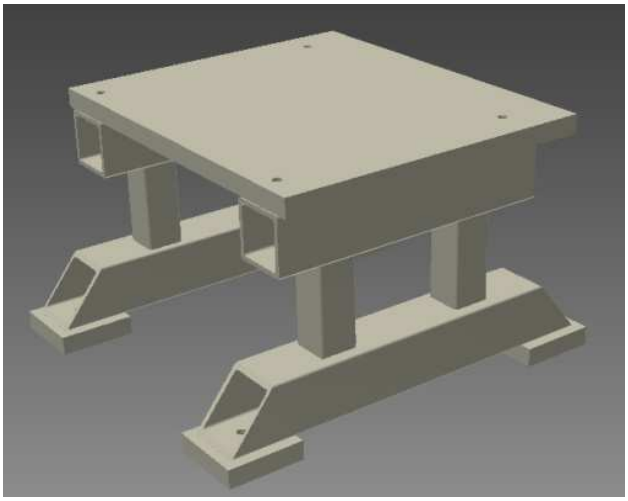

Figure 4-7: Electric drive motor support stand

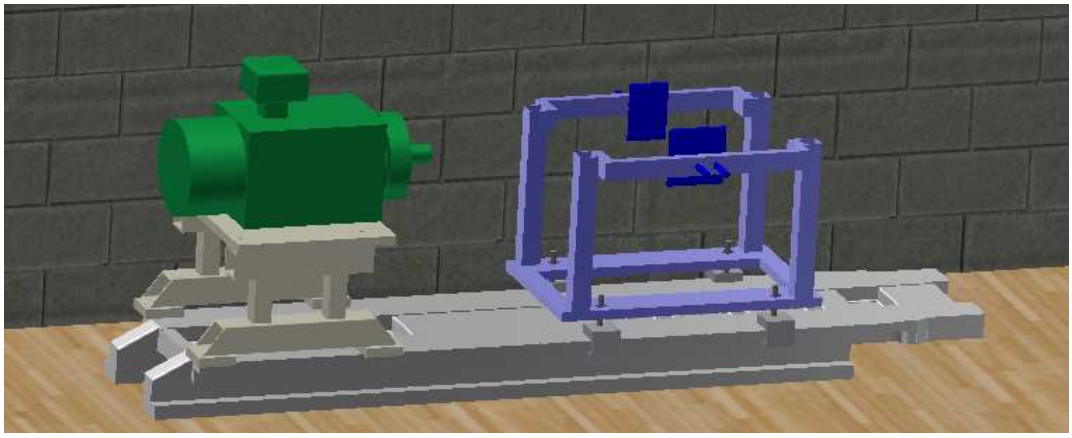

Figure 4-8: Supporting base with mounted electric drive motor and engine support cradle

In order to allow for the imperfect alignment between motor and engine, flexible couplings were added inline. Specifically model SX-6 disc type industrial couplings made by Lovejoy were selected. This style of coupling includes two unitized disc packs that are mounted between flanges as depicted in figure 4-9. This allows the coupling to accommodate all three types of misalignment as defined in figure 4-10 and quantified in

table 4-1. For convenience these couplings are maintenance free and remain torsionally rigid without any backlash. The disc packs, two end flanges, and the center spacer that installs between the disc packs are supplied by Lovejoy. In order to utilize the coupling, one Lovejoy end flange was modified to fit the electric motor's keyed output shaft while the other was modified to bolt to the torque sensor's flange. In this way the two-disc coupling is installed between the drive motor and the torque sensor such that the driveline is kept as short as possible. The final driveline component connects the torque sensor to the engine with appropriate flanges on either end. All flanges have machined recesses for center alignment on available bosses to ensure minimal run-out throughout the driveline.

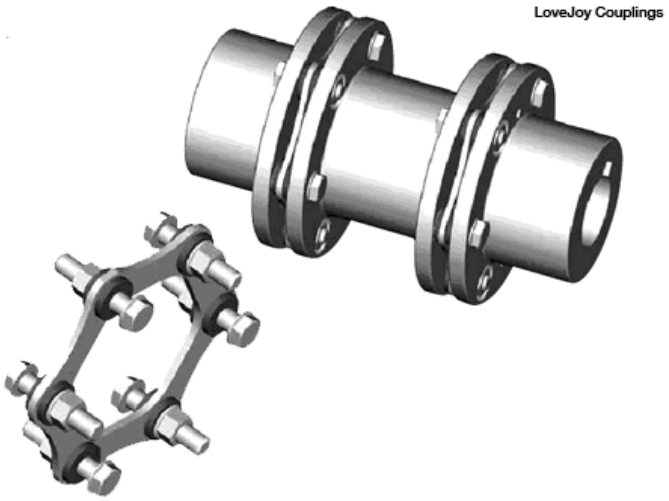

Figure 4-9: Lovejoy SX-6 disc couplings

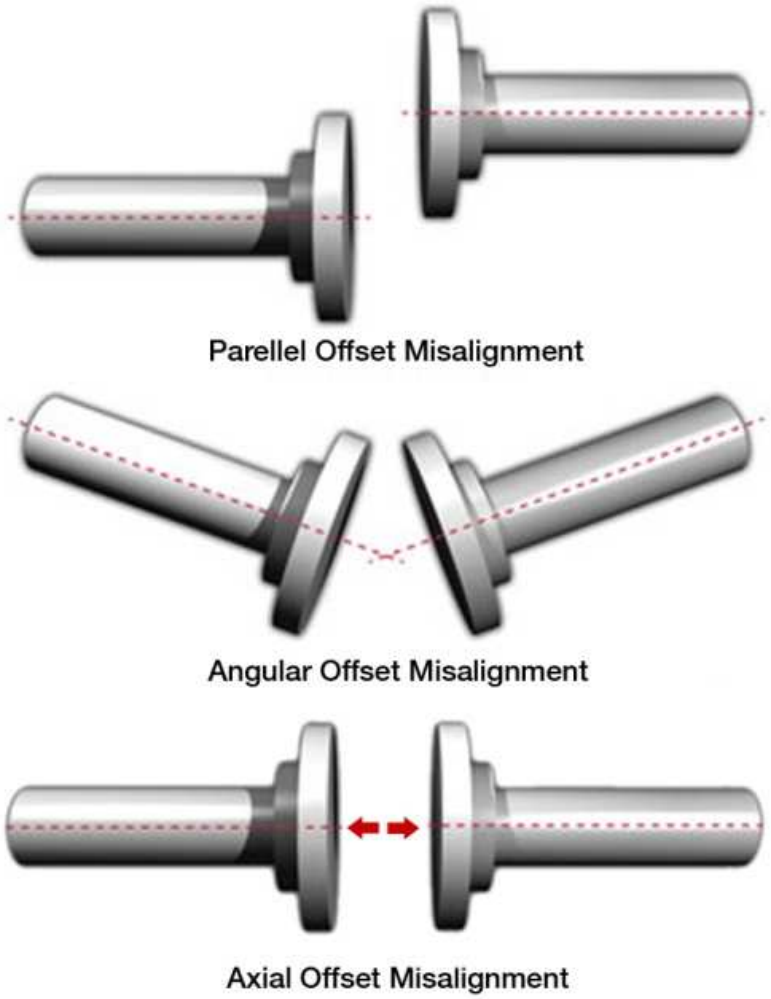

Figure 4-10: Types of shaft misalignment

Table 4-1: Acceptable maximum misalignment of Lovejoy SX-6 coupling

Misalignment Type	Acceptable Maximum
Parallel Offset	defined by angular offset allowance
Angular Offset	1.5˚ (each disc pack)
Axial Offset	3.1 mm

Installation of the driveline components and engine are fairly straightforward. Adapters are mounted to both the electric motor and the engine and are verified for run-out. The torque flange is then attached to the flange on the engine side and again verified for run-out as the engine is rotated. The remaining modified Lovejoy adapter is mounted on the motor side of the torque sensor and checked for run-out a final time. The engine is then leveled and positioned such that the Lovejoy coupler flanges line up and are parallel to each other. The distance between them is then measured at all points around the circumference of the flanges and the engine is positioned so that this measurement is within 11.2 +/- 0.16mm as specified by Lovejoy to ensure the allowable misalignment of table 4-1 is not exceeded. The engine is then securely clamped down to the steel base by bolting a bracket on top of the feet of the engine cradle. Lastly, the Lovejoy disc packs and spacer are installed, completing the physical mounting of the engine and driveline as shown in figure 4-11.

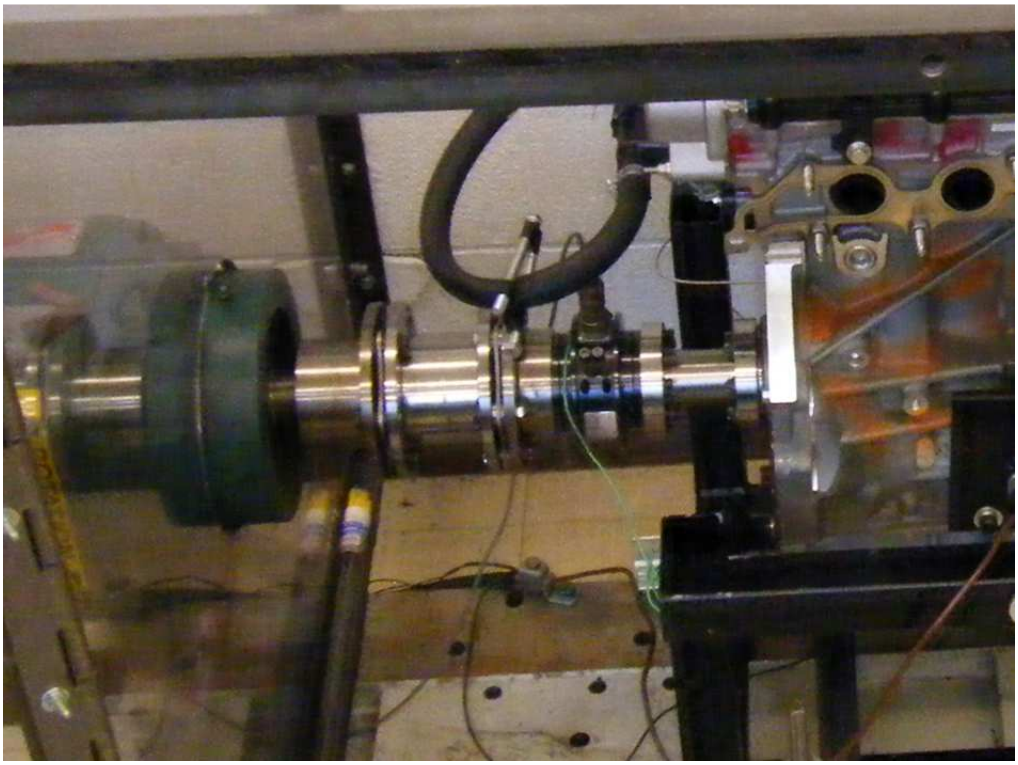

Figure 4-11: Flexible couplings and torque sensor mounted between drive motor and engine

4.2.6 Engine Heating & Temperature Measurement

Heating of the engine oil to operating temperatures is critical to ensure proper oil viscosity and lubrication is encountered throughout the test. Heat is injected into the engine block by way of the engine coolant passages. A thermocouple is placed in the oil passage to monitor the temperature of the oil. This is in principal the reverse of the regular operation of the engine where heat is removed from the oil by the coolant. Heating of the oil by this indirect method eliminates the possibility of altering the lubrication system from its original operation. Functionally it is a fairly straightforward matter to heat the coolant as several open connections to the coolant passages are readily

available on the engine. Inlet and outlet connections usually servicing the vehicles heater are instead connected to an external 1500W heater and $\frac{1}{15}$ HP (0.05kW) circulating pump. All other open connections are blocked off. The pump and heater can then be manipulated as needed to heat the engine coolant as desired. Expansion and overflow tanks are plumbed in at the highest point, and a thermocouple is added downstream of the heater to measure the maximum temperature in the circuit. The components of this system are depicted in figure 4-12.

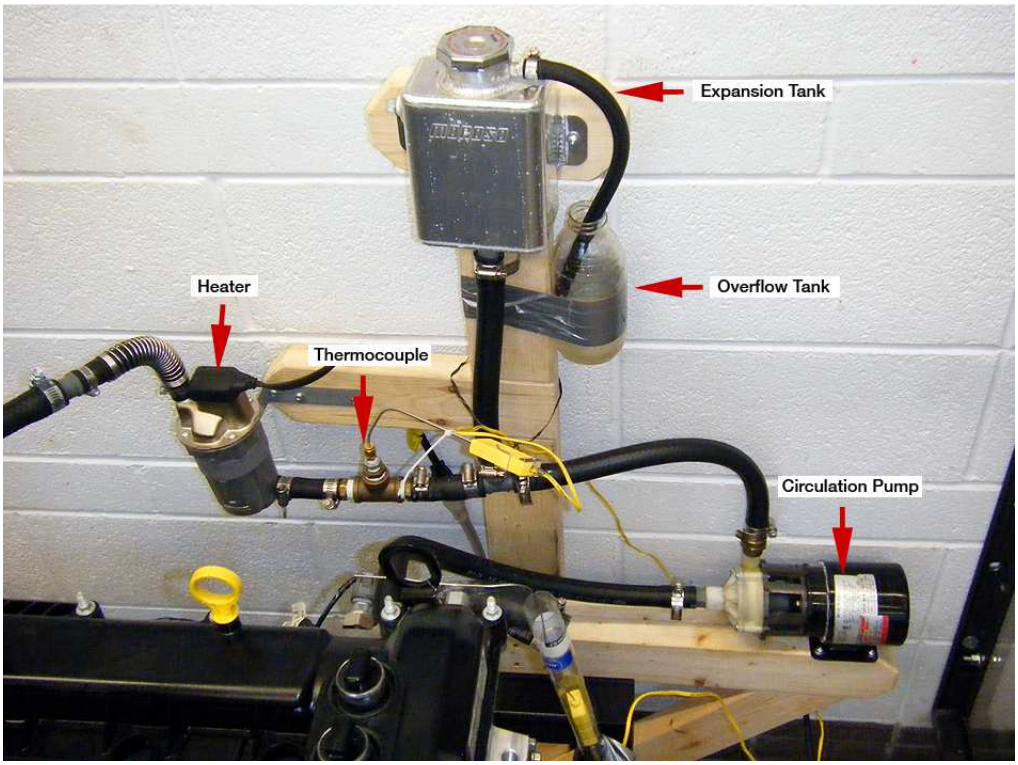

Figure 4-12: Engine coolant heating system used to bring the engine/oil temperature to operating conditions

Further heating of the oil also occurs from motoring the engine due to flow through the restrictions in the system. This effect is significant at higher speeds. This

direct heating of the oil prevents precise control of oil temperature during motoring testing on the test stand, but is beneficial in achieving operating temperatures. Care must be exercised in monitoring the current oil temperature while collecting data to ensure it is within the chosen acceptable range of 90 +/- 5˚C.

4.2.7 Mechanical Considerations of the Engine

With the exception of the oil pump, no auxiliary losses should be present on the engine. An external electric pump is used to circulate the coolant without the use of the engine's coolant pump, while no other front end accessories (alternator, power steering pump, air conditioning compressor, etc.) are present. The Ford 2.0L engine does however employ a high-pressure fuel pump that is mechanically driven by one of the camshafts. This pump is disabled throughout testing as no fuel is used and power requirements of this pump are not of interest in this work.

4.2.8 Physical Enclosure

In order to safely contain the rotating equipment and heated fluids, the entire experimental setup is enclosed in ½" (13mm) thick polycarbonate. This highly impact-resistant plastic provides protection for users as well as an unrestricted view of the experiment. Hinged lid and hinged split-front doors are included for easy access to the test equipment.

4.2.9 Data Acquisition

Collection of data for the experiment is handled by a National Instruments PCI-6229 data acquisition (DAQ) card. Sold as a low-cost multifunction board optimized for cost-sensitive applications, the PCI-6229 provides more than sufficient treatment for a

standard motoring test rig. General specifications include 16-bit analog input/output (I/O) channels at a maximum sampling rate of 250kS/s accompanied by many bidirectional digital I/O channels and a pair of 32-bit counters. Connected to the card are two National Instruments SCC-68 connecting blocks that provide conveniently laid out screw terminal connections for all channels. Further, two National Instruments SCC-TC02 modules are used to connect the critical oil and coolant temperature thermocouples. These modules are designed to easily interface with the software and precisely filter and condition these signals. This card performs well for this experiment and is expected to have sufficient additional channels for any future testing. The usage and expansion availability of this card is depicted in figure 4-13.

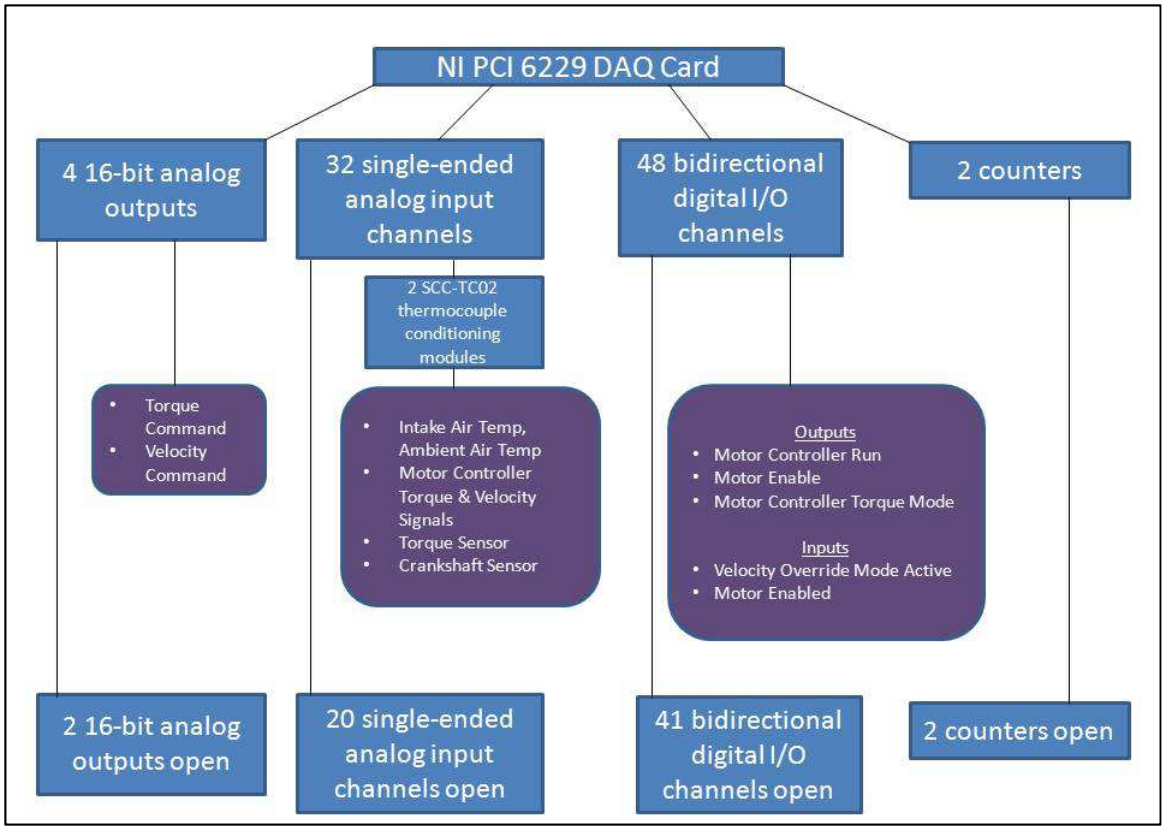

Figure 4-13: National Instruments PCI-6229 DAQ card usage and availability

4.3 Software Environment

The DAQ card works in conjunction with PC software to control the electric drive motor and collect all sensor data. Either Matlab/Simulink or Labview software may be used to control the test stand and acquire data. For the majority of testing in this work Labview is chosen for the convenience and accessibility of its graphical programming and customizable *virtual instrument (VI)* user interface. This allows all control, monitoring, and data acquisition to be carried out with a highly visible and familiar set of controls (such as dials and switches) and indicators (such as gauges and plots). The operating state of the engine is thus clearly visible while collecting data. Since only steady-state

measurements are necessary this manual control is perfectly adequate to bring the engine to the required operating point before writing data to file for later post-processing in Matlab.

4.4 Data Collection

During data collection the primary intent is to measure the torque required to motor the engine at a given rotational speed. This corresponds directly to the frictional losses experienced by the engine at the conditions of the test. For all data collection runs, the engine is first brought to steady state conditions at the desired speed and oil temperature. Data is then logged at a rate of at least 10 000 samples per second for a period of time such that no less than one hundred engine revolutions are recorded. The 10kHz sample rate may be compared to the frequency of passing teeth on the crankshaft speed sensor. For the maximum rated motor speed of 3530 RPM the 60-2 crankshaft sensor wheel's teeth will pass by the sensor at a rate of 3.53 kHz. The frequency of the torque measurement must also be considered but is seen to be much slower. For each rotation of the crankshaft each of the 4 pistons travels through 2 strokes. These overlap such that for every revolution of the crankshaft 2 power strokes occur at the same crank angle positions each revolution. In this way the production of torque occurs with a frequency twice that of the engine speed. The maximum rated test stand motor speed of 3530 RPM results in a rate of only 118Hz for torque production at this speed. While no power is actually produced while motoring the engine, the chosen sampling rate is clearly more than sufficient to capture the torque due to engine friction.

Collected data includes the torque signal from the torque transducer, engine speed signal from the crankshaft sensor, and coolant and oil temperatures from the thermocouples. The data files used are simple comma-delimited text files which can be easily viewed as-is or imported into Matlab or a spreadsheet for plotting. Temperatures corresponding to the ambient air and intake manifold air temperatures are also noted for each data file.

4.5 Data Processing

All data processing is conducted offline by first importing data text files into Matlab. The analog crankshaft speed sensor signal is first digitized and then adjusted to locate the timing of rising edges on the crankshaft sensor wheel's teeth. At the same time the location of the missing tooth is located and the timing of individual cycles is determined. This can then be used to determine the actual rotational speed of the engine by calculating the time to complete each cycle. The per-cycle speed is a useful way to eliminate some of the cycle-to-cycle variation from the analysis by allowing cycles to be sorted to within a given tolerance range around the target speed. The known timing of individual engine cycles also allows conversion from the time-domain into the crank-angle domain. This involves resampling the data with respect to the engine's angular position from a given point on the crankshaft sensor wheel such that the data points correspond with engine position from 0 to 360 degrees. The top dead center (TDC) position of cylinder 1 is chosen as the 0 degree point for this resampling. This need only be conducted for the torque data and with the chosen length of the data files the resampling results in torque curves for at least 100 engine revolutions.

Conducting the data analysis offline in Matlab allows any noise present in the torque data to be removed easily through digital filtering. Specifically zero-phase digital filtering is employed via Matlab's *filtfilt* command, which filters the data in both the forward and reverse directions in order to prevent any phase distortion. This is critically important for resampling into the crank angle domain, as the relation between time and torque cannot be skewed. Matlab is used to design a low-pass finite impulse response filter that produces clean torque profiles for individual engine cycles. Specifically the chosen filter is 15^{th} order with a cut off frequency of 150Hz. It must again be noted that these torque values have already been filtered by the sensor's signal conditioner and thus have been attenuated at or above 3Hz. They can only be used to calculate mean torque at a given engine speed. Representative data before and after this filtering is applied are shown in figure 4-14. This figure depicts the raw and filtered torque measurements from 100 complete engine revolutions at a speed of 2200RPM. The spread of this data is typical and may be attributed to the cyclic variation of parameters within the engine itself, as well as slight variations in motored speed. In determining the torque at a given speed the mean torque for all recorded cycles is found.

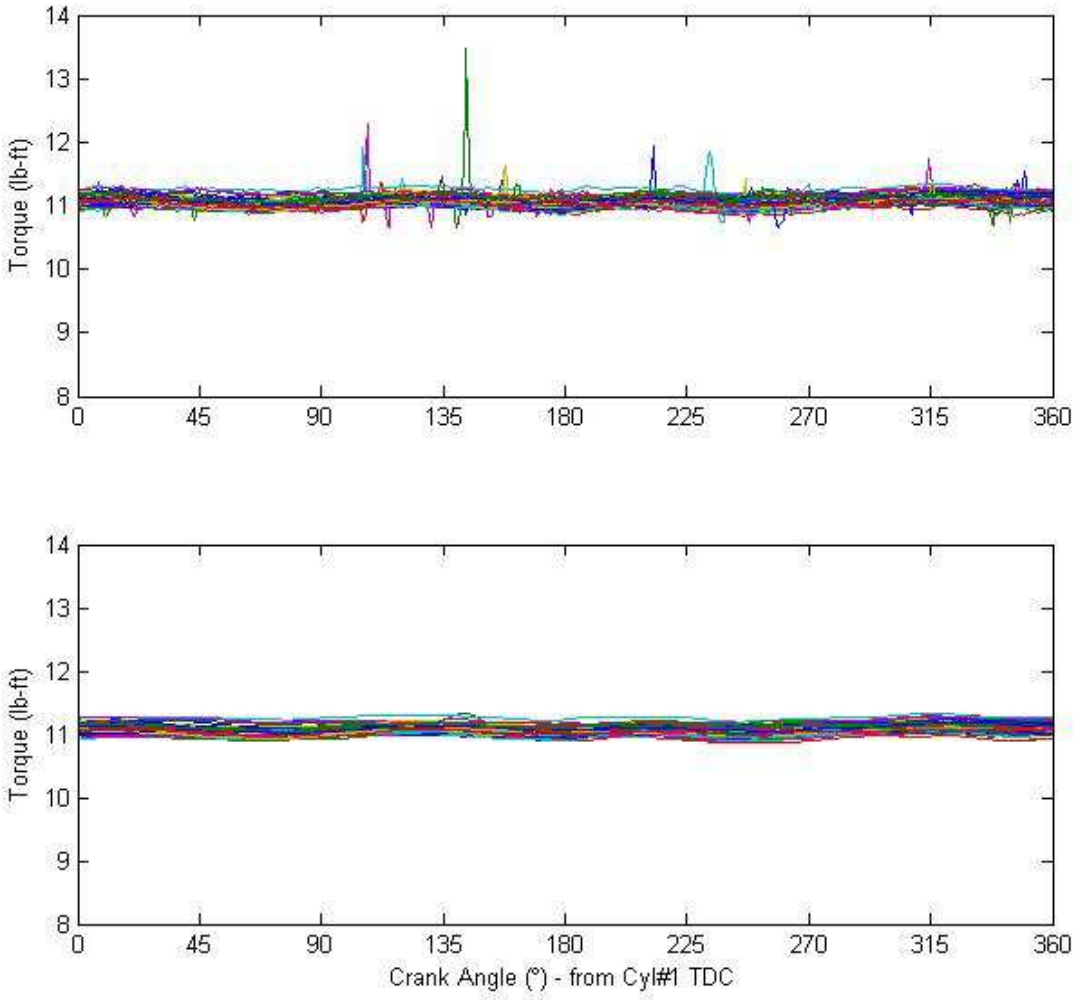

Figure 4-14: Sample cyclic torque data before (top) and after zero-phase digital FIR filtering (bottom)

4.6 Test Data

While the crank angle domain analysis could have been used to determine the torque profile of individual engine cycles using alternate signal conditioning of the torque sensor, it is the average torque at a range of speeds that is of primary interest. This quantity reflects the frictional losses experienced by the engine at that speed and can be directly compared to the useable torque the engine may produce. Analysis in the crank

angle domain is still used to ensure the averaged torque corresponds to the speed for which it is plotted. Using these post-processing techniques on 10 datasets collected during 5 identical motoring tests conducted on the Ford 2.0L engine with intake and exhaust manifolds removed, figure 4-15 was produced. Note that two subsequent datasets are collected and processed for each of the 5 tests. The datasets are therefore numbered Test 1-1, Test 1-2, Test 2-1, Test 2-2, and so on. As such, Test 1-1 and Test 1-2 are acquired as consecutive blocks of time twice the length of the recording for a single dataset (representing an average of at least 100 engine cycles for each datapoint). The 5 tests represent complete repetition of the experiment at different times. The mean value of these datasets is presented in figure 4-16 with error bars corresponding to +/- 1 standard deviation as an indication of variability in the data.

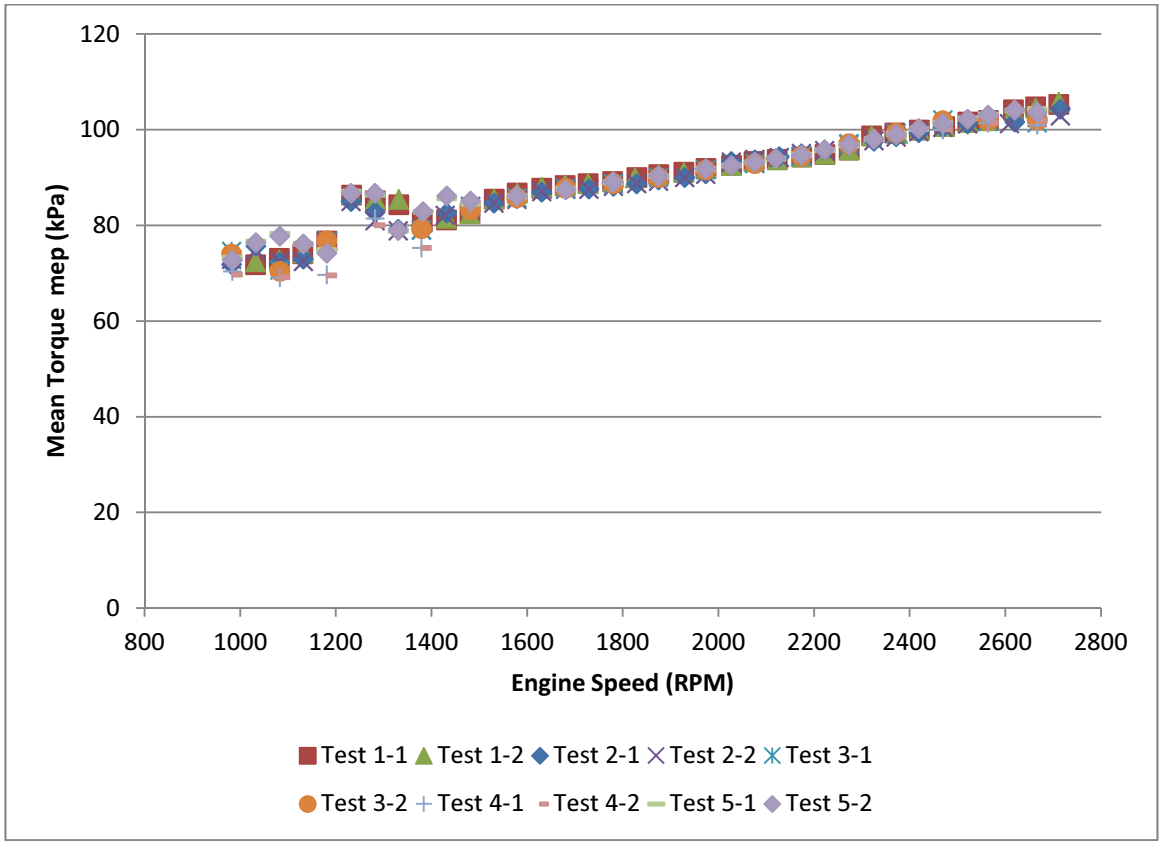

Figure 4-15: Motoring test data from 10 datasets for Ford 2.0L engine with manifolds removed

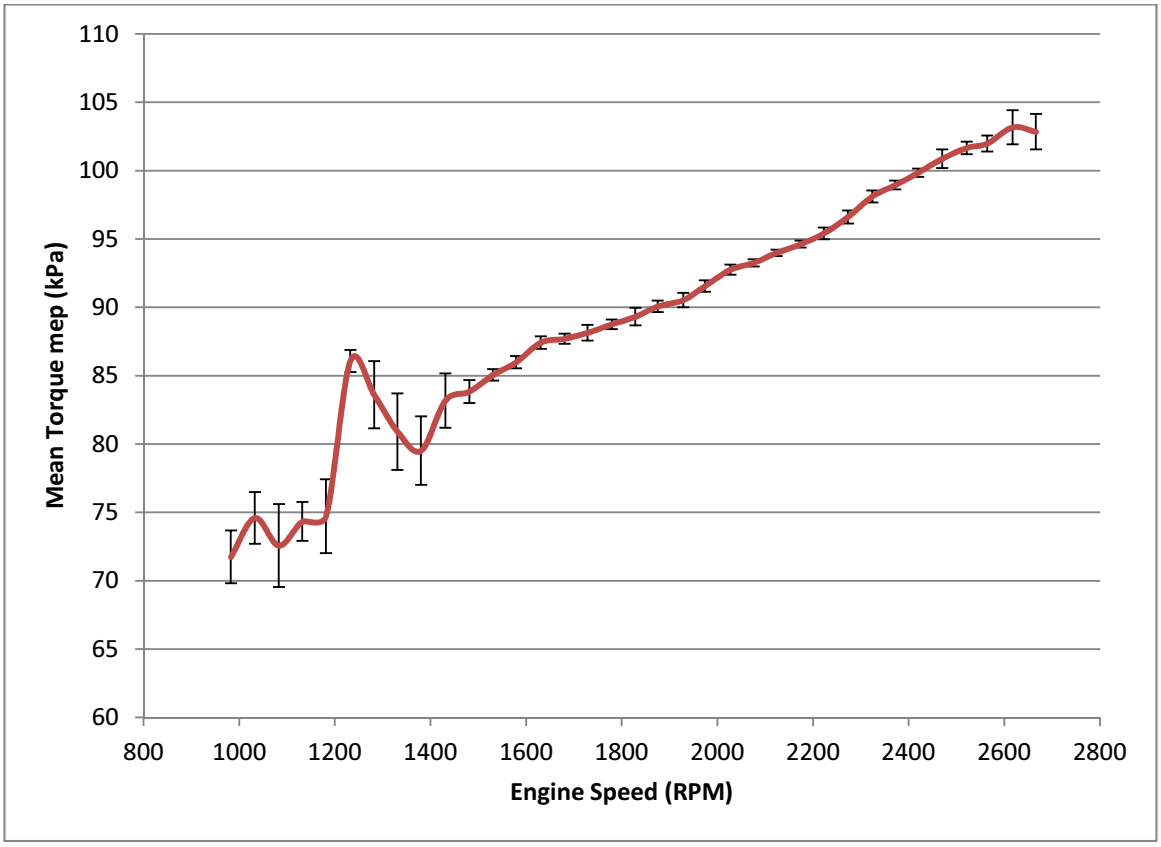

Figure 4-16: Mean vale motoring test data from 10 datasets for Ford 2.0L engine with manifolds removed - error bars correspond to +/- 1 standard deviation

Note that the plot is presented with mean effective pressures, the work per cycle per unit displaced volume, on the ordinate. This treatment is merely a scaling of the directly measured torque values but is a common representation and thus allows easier comparison to existing data. This data represents the total frictional losses with pumping losses reduced to their minimum and auxiliary losses present only in the oil pump. Testing the engine in this state provides the main data for modeling its total friction.

Repeating this test with manifolds in place restores some of the pumping losses, specifically those associated with directing air out of the intake and into the exhaust

systems. For this test, two consecutive datasets are recorded as before; they are denoted as Test 6-1 and Test 6-2. This test varies from tests 1 through 5 only through the removal of the manifolds. Data from this test is shown in figure 4-17.

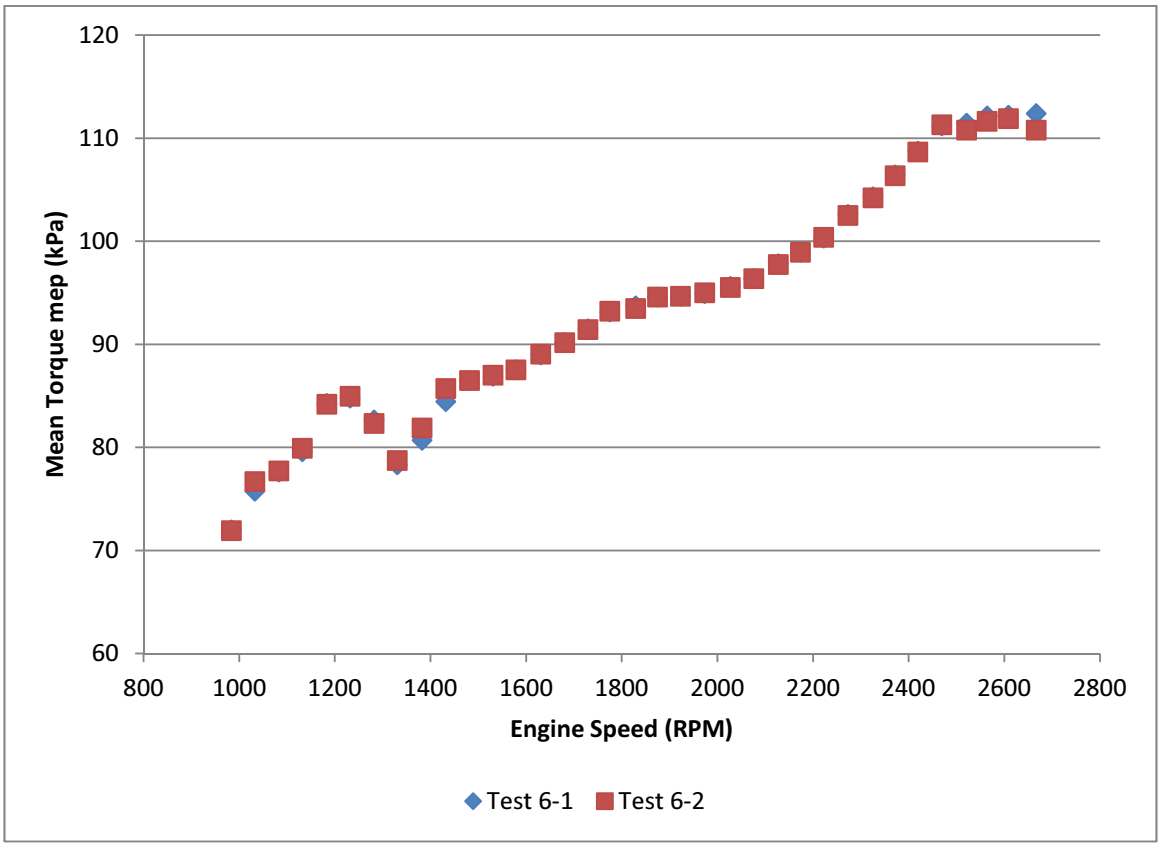

Figure 4-17: Motoring test data from 2 consecutive datasets for Ford 2.0L engine with manifolds in place

Subtracting the losses of figure 4-15 from those of figure 4-17 yields the loss attributable to the manifolds alone as shown at the bottom of figure 4-18. The reduced temperatures of gasses passing through the manifolds, especially on the exhaust side,

limit the application of this data to the motoring state, but the increased losses at higher engine speeds show the experiment's sensitivity to relatively minor changes.

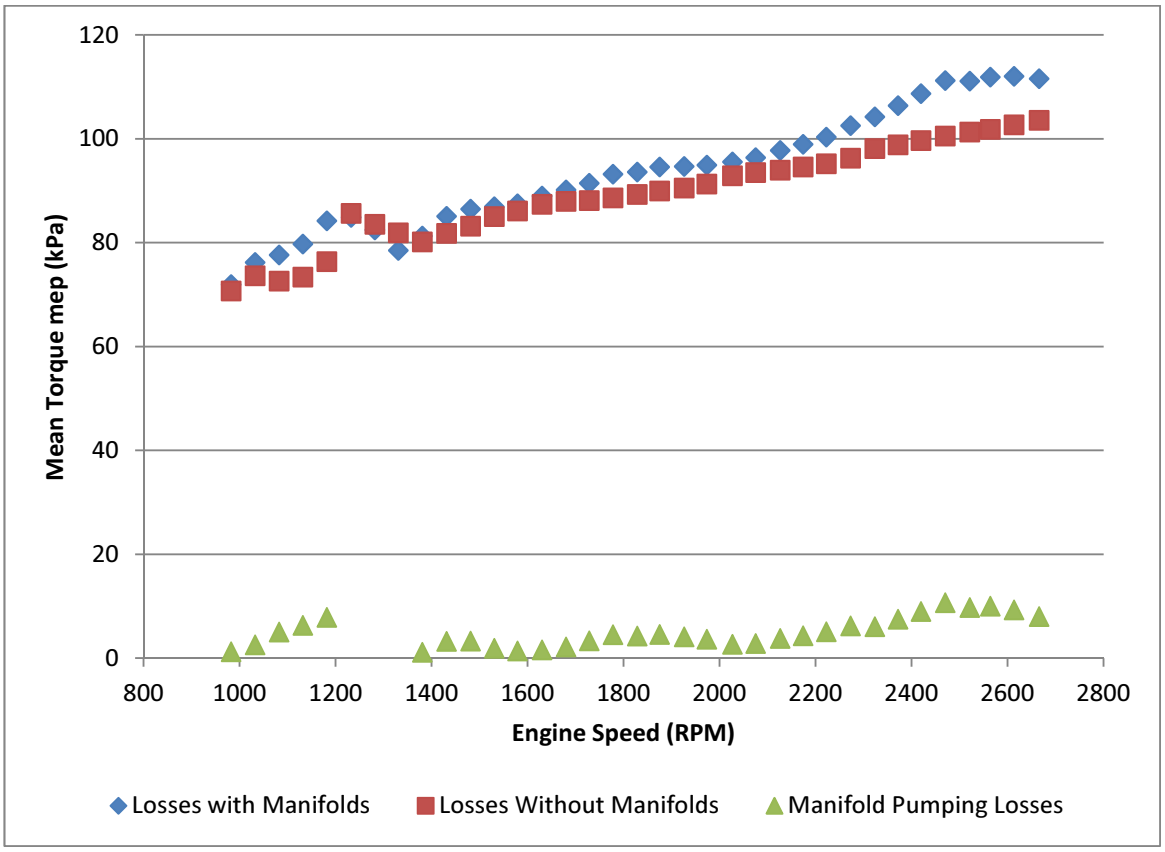

Figure 4-18: Motoring test comparison with and without manifolds

4.6.1 Data Collection Limitations

The motoring data presented above includes three limitations of the experimental setup which must be called to attention. The first is seen as the lack of collected data below 1000RPM. At lower speeds the control of the drive motor reacts to the varying load imposed by the engine due to changes in compression over the cycle such that a

constant speed cannot be maintained. For this reason, no data below 1000RPM is collected.

The second occurs between approximately 1200 to 1400 RPM and is mostly visible as an uncharacteristic increase in the measured friction. During experimentation this speed range was noted to contain a resonant frequency of the system. The vibration and noise level of the experiment increased significantly within this range, and this increased vibration is believed to dissipate the extra energy that appears in the increased torque measurement. The location of this apparent natural frequency of the system is inconvenient, but is perhaps difficult to avoid with rigid mounting of the engine. Due to time constraints, the design and construction of a new stand to support the engine in hopes to improve data collection within this range was not viable. Instead data from this range is omitted from the analysis.

The third limitation appears as the upper limit of the data. Data beyond 2700 RPM is not presented above, although the motor is able to turn the Ford 2.0L engine up to approximately 3400 RPM. Beyond 2700 RPM the measured torque values become increasingly noisy and quickly drop to less than 1/3 of the value corresponding to 2700 RPM. The full range of the data presented earlier in figure 4-15 can be seen in figure 4-19 depicting the erroneous drop in torque values. This drop is not present in the calculated torque signal from the motor controller, further verifying what is already known: this is not representative of any physical phenomenon. It is thus apparent this data is not useable, although the cause for the limitation of this signal with speed is not precisely known. The torque sensor itself is believed to be at the center of the issue,

although it is rated to 5000 RPM and was in new condition prior to this experiment. Since the measured friction trend is expected to continue largely unchanged between 2700 RPM and 3400 RPM the reduced range is deemed sufficient.

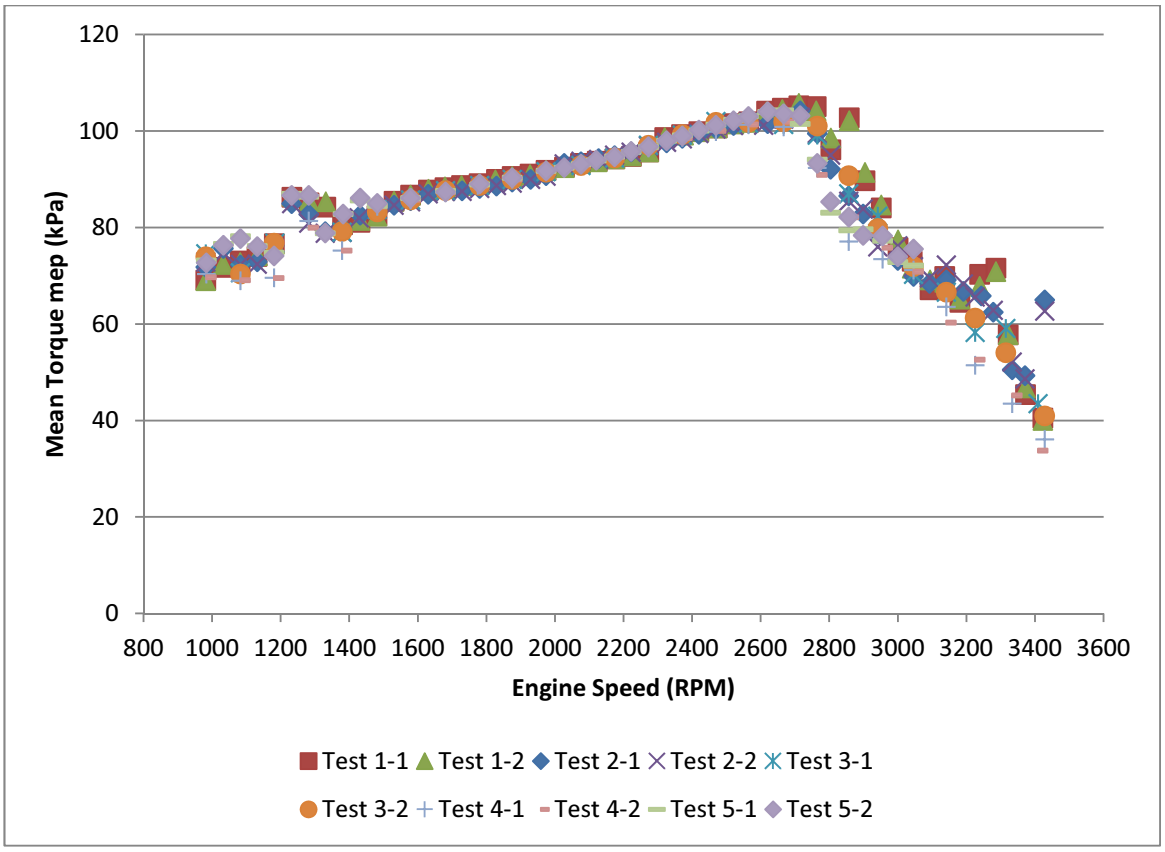

Figure 4-19: Full range of motoring test data depicting erroneous drop in measured torque signal above 2700 RPM; from 10 datasets for Ford 2.0L engine with manifolds removed

4.6.2 Selected Data Range

Calculating the standard deviation and variance of the test data presented in figure 4-19 confirms the limitations discussed in the previous subsection. In fact, this simple analysis suggests the torque measurements become inconsistent above 2600 RPM rather than 2700 RPM. The mean value of the measured data is shown for the full speed range

in figure 4-20 with error bars corresponding to +/- 1 standard deviation. The standard deviation is noted to more than double when moving from either the data point corresponding to 1500RPM to the preceding point or from the data point corresponding to 2600RPM to the following data point.

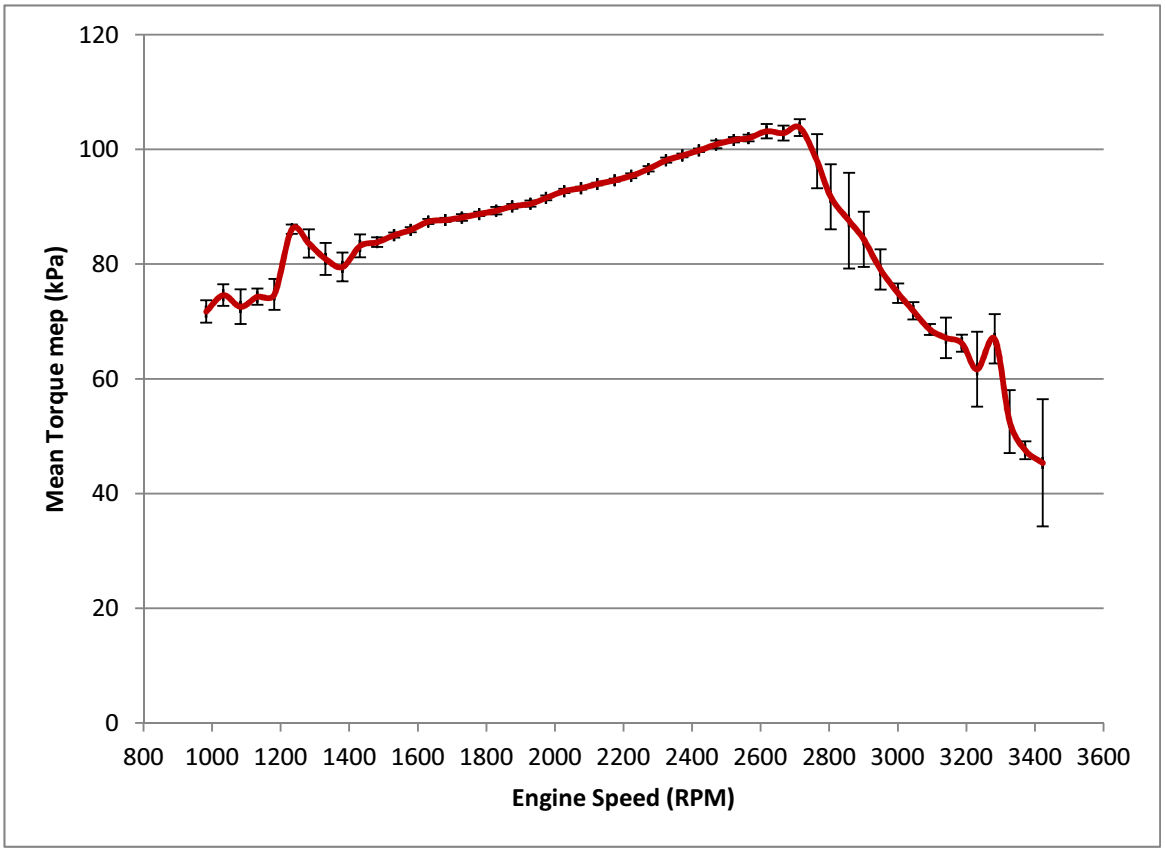

Figure 4-20: Full range of mean value motoring test data for the Ford 2.0L engine demonstrating increased variability below 1500 RPM and above 2600 RPM - the average of 10 datasets is shown with error bars corresponding to +/- 1 standard deviation

Collected data from 1000-1200 RPM and 1500-2600 RPM is selected for fitment of the model in the next chapter. The data below 1200 RPM varies slightly between the

ten datasets, and these points have standard deviation up to 3kPa. Between 1500 and 2600 RPM the data is very repeatable across the ten datasets. Standard deviation within this range reaches a maximum of 0.7 kPa with variance under 0.5 kPa^2. A closer look at the data points for the ten datasets within this range is provided in figure 4-21.

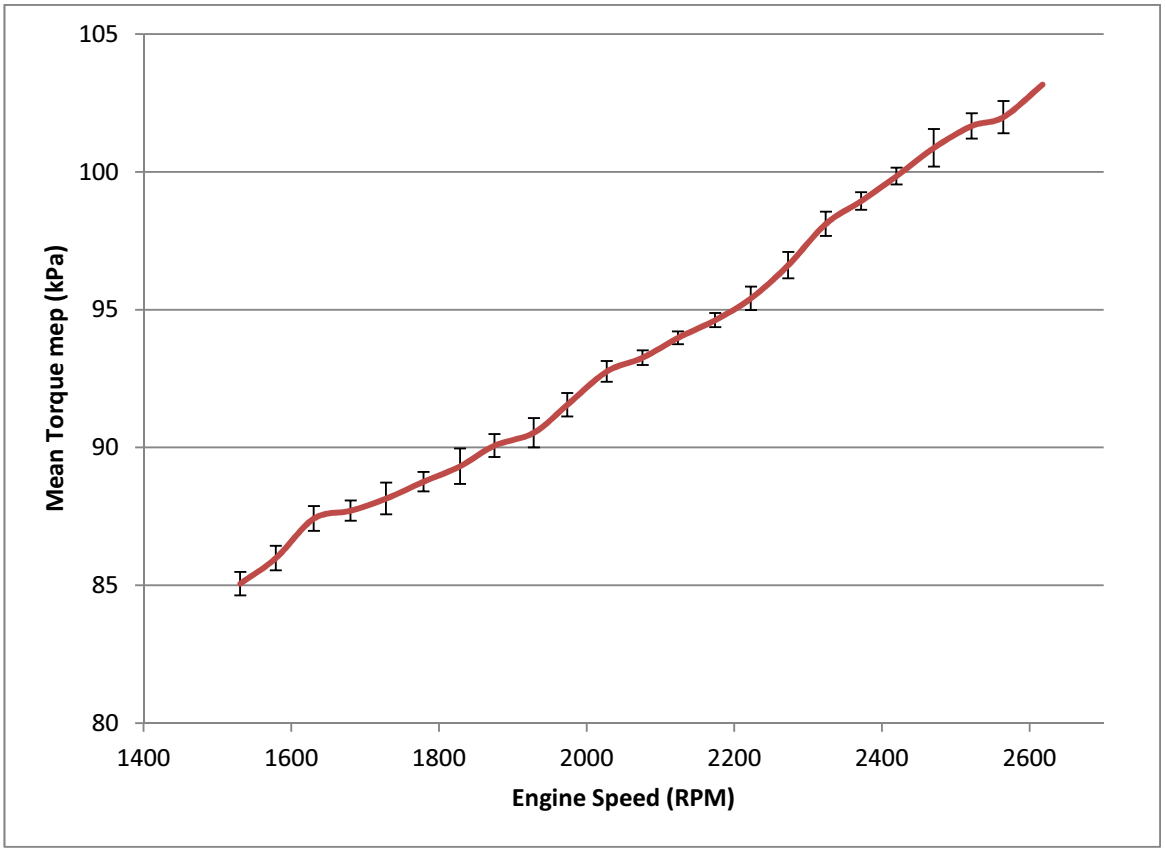

Figure 4-21: A closer look at the mean value motoring test data for the Ford 2.0L engine demonstrating repeatability over this speed range - the average of 10 datasets is shown with error bars corresponding to +/- 1 standard deviation

4.6.3 Engine Disassembly Data

While total engine friction can be characterized based on motoring tests conducted on the assembled engine, the friction model as presented in Section 3.5 predicts the

friction attributable to individual component groups. It is therefore desirable to collect data for the partially disassembled engine in order to improve the fit of certain portions of the model. Specifically, the primary division of components within the model are those related to the crankshaft, the reciprocating assembly (comprised of the pistons and connecting rods), and the valvetrain. Losses attributable to the pumping of air and driving the auxiliary components complete the model. In order to collect useful data for the partially disassembled engine it is important to ensure that the air pumping losses are either maintained, or eliminated in a meaningful manner. This means that if a given piston is in place and pumping, its corresponding valves must either remain closed throughout the cycle or be actuated as per usual. Any other alternatives would allow air to flow incorrectly, altering the pumping losses. Alternatively, custom components may be machined to circumvent this issue. In the case of all valves remaining closed throughout the engine cycle, pumping losses are eliminated. Naturally this is not possible without also eliminating the valvetrain group losses, as the valvetrain will not be operating. Testing of this case was attempted on the Ford 2.0L engine by removing both camshafts. Testing in this state of assembly appeared to be viable; however unnoticed damage to the torque sensor ultimately rendered the collected data unusable. Time constraints prevented repeat testing from appearing in this research.

Since disassembly of individual valvetrain components will alter the air pumping losses away from the regular mode of operation as previously discussed, further opportunity for disassembly data lies in separating the reciprocating component group friction from that of the crankshaft. In an attempt to collect this data, pistons 1 and 3

were removed from the engine. With the engine's firing order, this arrangement maintains the overall rotating balance of the engine since the pistons are removed from opposite sides of the crankshaft. However, each piston is counter balanced by a counter-weight. With pistons removed, these counter-weights effectively cause the shaft to become eccentrically loaded along its length. Not surprisingly, this arrangement caused excessive vibration levels in the motored engine, and no useable data could be collected.

The data presented in this chapter portrays the frictional losses encountered within the Ford 2.0L engine. In the next chapter a detailed physical friction model will be compared to this data and adjusted accordingly to fit it. A complete running engine model including the verified frictional losses will then be suggested.

Chapter 5

5. Simulations and Results

This chapter provides the details of fitting the friction model given in section 3.5 to the 2.0L Ford engine. Simulation results follow and the model is compared to the measured friction of chapter 4. The fit of the running-engine MVEM to the 2.0L Ford engine is then discussed along with the insertion of the friction model and final simulation details.

5.1 Fitting the Friction Model

The 2.0L Ford engine used in this research is thoroughly modern in design. Reduction of internal engine friction and reduction of total mass are evident key strategies. This includes advanced surface treatments to the valvetrain and specialized coating of the piston skirts. While the mass reduction accomplished by exclusive use of aluminum for the engine block, cylinder heads, and oil pan has little impact on this research, the pistons are also cast aluminum which helps to reduce the engine's reciprocating mass. This continuing effort to reduce frictional losses presents a reason to anticipate the Sandoval & Heywood model [5] as presented in section 3.5 may over-estimate certain losses. With this in mind, the model is adjusted to the 2.0L parameters so that its predictions may be compared to the motoring data. This is accomplished by applying equations (3-24) to (3-30), which estimate the friction attributable to the component groups shown in figure 5-1. The frictional losses of the engine are then easily simulated over the engine's range of operating speed and can be plotted for total engine friction, or for the friction of individual component groups.

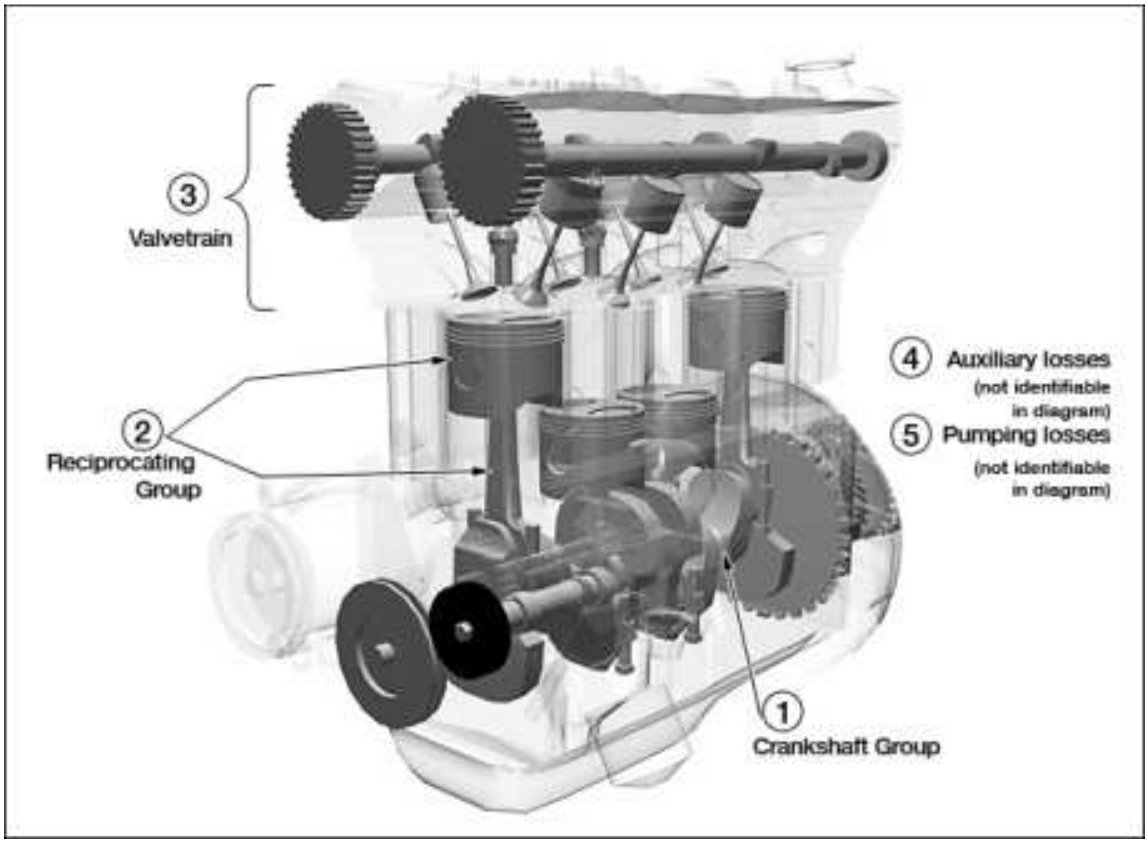

Figure 5-1: Simple cutaway of a generic 4-cylinder engine depicting the main components responsible for engine friction as modeled, **[41]** (image only)

The equations of the friction model may be repeated according to the component groups shown in figure 5-1 as follows, with detailed explanations of these equations presented earlier in section 3.5:

(1) Crankshaft group:

$$cfmep = 1.22 \times 10^{5}\left(\frac{D_{bm}}{B^2 S n_{cyl}}\right) + 3.03 \times 10^{-4}\sqrt{\frac{\mu}{\mu_0}}\left(\frac{n {D_{bm}}^3 L_{bm} n_{bm}}{B^2 S n_{cyl}}\right) + 1.35 \times 10^{-10}\left(\frac{{D_{bm}}^2 n^2 n_{bm}}{n_{cyl}}\right) \quad (3\text{-}24)$$

(2) **Reciprocating assembly group, including piston gas pressure loading:**

$$rfmep + rfmep_{gas} = 2.94 \times 10^{2} \sqrt{\frac{\mu}{\mu_0}} \left(\frac{S_p}{B}\right) + 4.06 \times 10^{4} \left(\frac{F_t}{F_{t0}} C_r\right) \left(1 + \frac{500}{n}\right) \left(\frac{1}{B^2}\right) + 3.03 \times 10^{-4} \sqrt{\frac{\mu}{\mu_0}} \left(\frac{n {D_{bj}}^3 L_{bj} n_{bj}}{B^2 S n_{cyl}}\right) + 6.89 \frac{p_{man}}{p_{amb}} \left[0.088 \sqrt{\frac{\mu}{\mu_0}} r_c + 0.182 \left(\frac{F_t}{F_{t0}}\right) {r_c}^{(1.33 - K S_p)}\right] \quad (3\text{-}25) + (3\text{-}26)$$

(3) **Valvetrain:**

$$vfmep = 244 \sqrt{\frac{\mu}{\mu_0}} \frac{n n_{bc}}{B^2 S n_{cyl}} + C_{ff} \left(1 + \frac{500}{n}\right) \frac{n_v}{S n_{cyl}} + C_{rf} \left(\frac{n n_v}{S n_{cyl}}\right) + C_{oh} \sqrt{\frac{\mu}{\mu_0}} \left(\frac{{L_v}^{1.5} n^{0.5} n_v}{B S n_{cyl}}\right) + C_{om} \left(1 + \frac{500}{n}\right) \frac{L_v n_v}{S n_{cyl}} + 4.12 \quad (3\text{-}27)$$

(4) **Auxiliary components:**

$$afmep = 8.32 + 1.86 \times 10^{-3} n + 7.45 \times 10^{-7} n^2 \quad (3\text{-}28)$$

(5) **Air pumping losses:**

$$pmep_{intake} + pmep_{exhaust} = (p_{amb} - p_{man}) + 3.0 \times 10^{-3} \left(\frac{p_{man}}{p_{amb}}\right)^2 \left(\frac{{S_p}^2}{{n_{vi}}^2 {r_i}^4}\right) + 0.178 \left(\frac{p_{man}}{p_{amb}} S_p\right)^2 + 3.0 \times 10^{-3} \left(\frac{p_{man}}{p_{amb}}\right)^2 \left(\frac{{S_p}^2}{{n_{ve}}^2 {r_e}^4}\right) \quad (3\text{-}29) + (3\text{-}30)$$

Applying appropriate engine parameters to this base model gives the predicted losses for individual component groups as shown in figure 5-2. All plots are shown in terms of mean effective pressures. These initial estimates mainly involve known engine parameters for the Ford 2.0L engine, with remaining values suggested by Sandoval & Heywood [5]. All parameters used within the model to yield these preliminary results are listed in table 5-1.

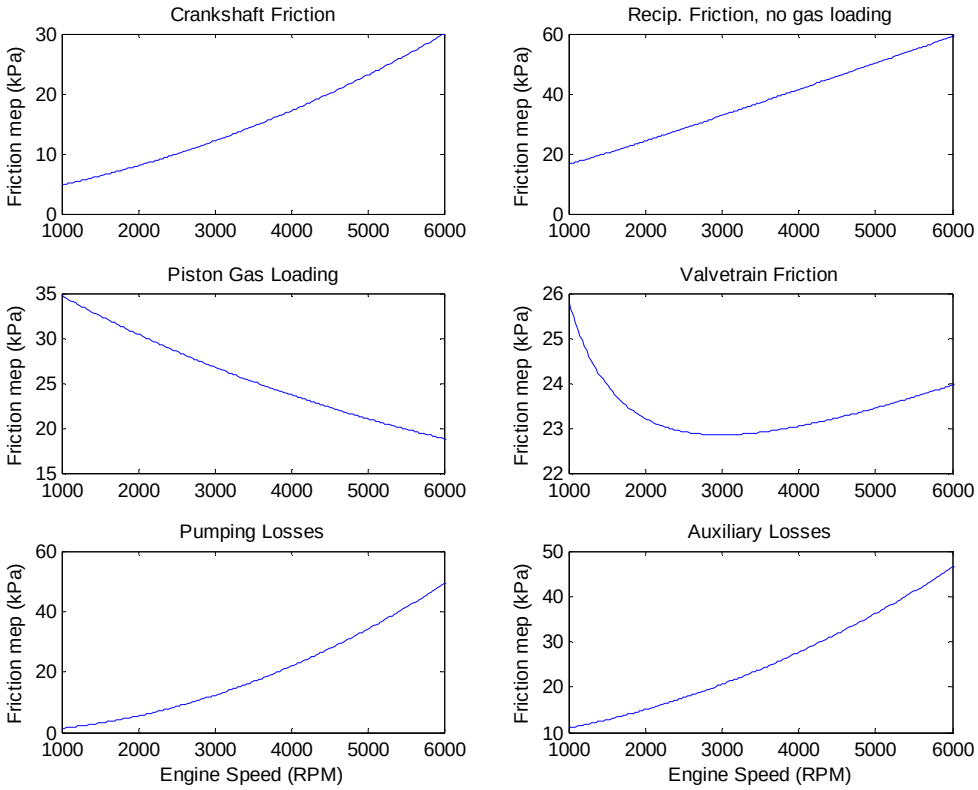

Figure 5-2: Individual component group losses for the motored Ford 2.0L engine as predicted by the uncalibrated model

Table 5-1: Initial parameter values used to apply friction model to the 2.0L engine, according to known and suggested values as shown

Symbol	Description (units)	Value
D_{bm}	main bearing diameter (mm)	52
D_{bj}	journal bearing diameter (mm)	47
B	bore (mm)	87.5
S	stroke (mm)	83.1
n_{cyl}	number of cylinders	4
μ	oil viscosity (cSt)	9.7
μ_0	reference oil viscosity (cSt)	13
n	engine speed (RPM)	
L_{bm}	main bearing length (mm)	25.4
L_{bj}	journal bearing length (mm)	20.64
n_{bm}	number of main bearings	5
n_{bj}	number of journal bearings	4
n_{bc}	number of camshaft bearings	5
S_p	mean piston speed (m/s)	
F_t/F_{t0}	piston ring tension ratio	0.98
C_r	piston roughness constant	0.98
p_{man}	intake manifold pressure (kPa)	101.3
p_{amb}	atmospheric pressure (kPa)	101.3
r_c	compression ratio	12:1
K	constant	2.38×10^{-2}
C_{ff}	constants based on valvetrain mechanism	133
C_{rf}		0.005
C_{oh}		0.5
C_{om}		10.7
n_v	number of valves (intake and exhaust)	16
L_v	maximum valve lift (mm)	14.3
r_i	intake valve diameter/bore	35mm
r_e	exhaust valve diameter/bore	30mm
	Known or selected values for the Ford 2.0L Engine	
	Values used as suggested by Sandoval & Heywood	
	Unknown scaling parameters, to be used for model fit	

A summation of these losses as shown in figure 5-3 predicts the total internal friction of the Ford 2.0L engine and may be expressed mathematically by summing equations (3-24) to (3-30) as:

$$fmep = 1.22 \times 10^{5}\left(\frac{D_{bm}}{B^{2}Sn_{cyl}}\right) + 3.03 \times 10^{-4}\sqrt{\frac{\mu}{\mu_0}}\left(\frac{n{D_{bm}}^{3}L_{bm}n_{bm}}{B^{2}Sn_{cyl}}\right) + 1.35 \times 10^{-10}\left(\frac{{D_{bm}}^{2}n^{2}n_{bm}}{n_{cyl}}\right) + 2.94 \times 10^{2}\sqrt{\frac{\mu}{\mu_0}}\left(\frac{S_p}{B}\right) + 4.06 \times 10^{4}\left(\frac{F_t}{F_{t0}}C_r\right)\left(1 + \frac{500}{n}\right)\left(\frac{1}{B^{2}}\right) + 3.03 \times 10^{-4}\sqrt{\frac{\mu}{\mu_0}}\left(\frac{n{D_{bj}}^{3}L_{bj}n_{bj}}{B^{2}Sn_{cyl}}\right) + 6.89\frac{p_{man}}{p_{amb}}\left[0.088\sqrt{\frac{\mu}{\mu_0}}r_c + 0.182\left(\frac{F_t}{F_{t0}}\right){r_c}^{(1.33-KS_p)}\right] + 244\sqrt{\frac{\mu}{\mu_0}}\frac{nn_{bc}}{B^{2}Sn_{cyl}} + C_{ff}\left(1 + \frac{500}{n}\right)\frac{n_v}{Sn_{cyl}} + C_{rf}\left(\frac{nn_v}{Sn_{cyl}}\right) + C_{oh}\sqrt{\frac{\mu}{\mu_0}}\left(\frac{{L_v}^{1.5}n^{0.5}n_v}{BSn_{cyl}}\right) + C_{om}\left(1 + \frac{500}{n}\right)\frac{L_v n_v}{Sn_{cyl}} + 4.12 + 8.32 + 1.86 \times 10^{-3}n + 7.45 \times 10^{-7}n^{2} + (p_{amb} - p_{man}) + 3.0 \times 10^{-3}\left(\frac{p_{man}}{p_{amb}}\right)^{2}\left(\frac{{S_p}^{2}}{{n_{vi}}^{2}{r_i}^{4}}\right) + 0.178\left(\frac{p_{man}}{p_{amb}}S_p\right)^{2} + 3.0 \times 10^{-3}\left(\frac{p_{man}}{p_{amb}}\right)^{2}\left(\frac{{S_p}^{2}}{{n_{ve}}^{2}{r_e}^{4}}\right), \quad (5.1)$$

where the terms are as described previously.

As seen in table 5-1 the intake manifold pressure is held constant and equal to the atmospheric pressure for this prediction. This would approximate an engine running at wide open throttle, or with manifolds removed as in the primary motoring test sequences.

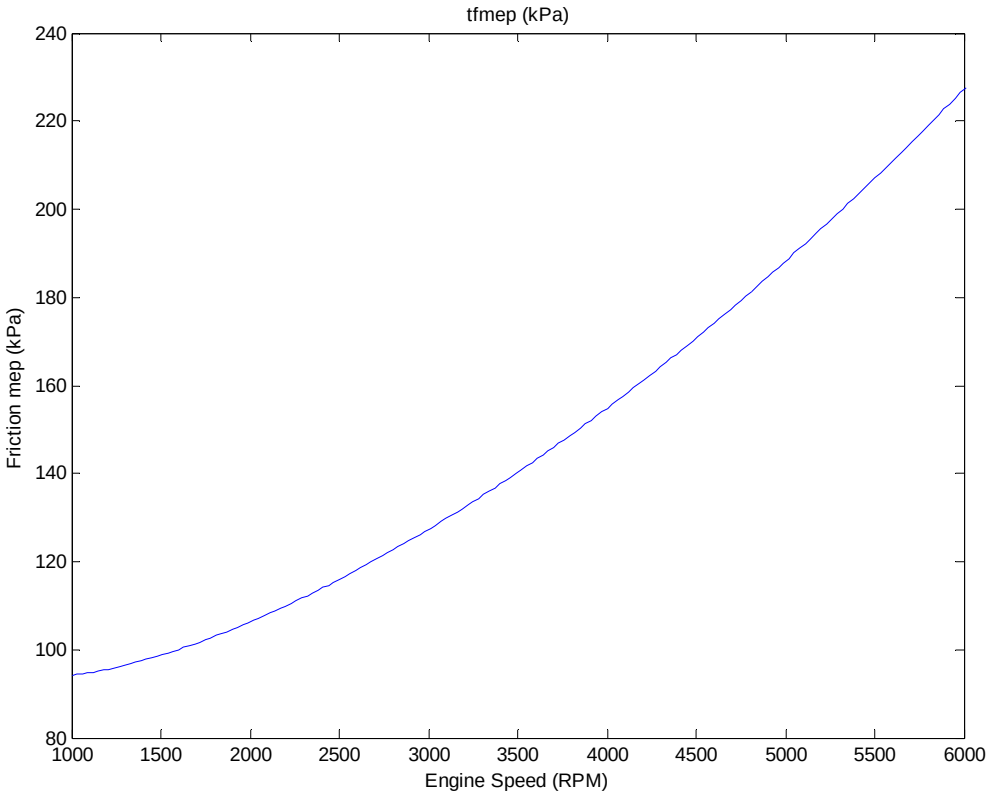

Figure 5-3: Total friction losses for the motored Ford 2.0L engine as predicted by the uncalibrated model

5.1.1 Friction Model Adjustments

It is expected that recent advancements in engine design will require alteration of the friction model in order for it to better align with the measured data of the Ford 2.0L engine. One such adjustment is required to the modeled auxiliary losses before any comparison to the data can be made. This is because the auxiliary losses suggested in the original model include an empirical fit to the losses of the oil pump, water pump, and non-charging alternator, for two current S.I. engines (with displacements of 3.0L and 5.4L), [5]. The engine under test employs an externally powered water pump, and has no

alternator. Only the oil pump remains as an auxiliary loss. Ideally, an accurate empirical fit of the Ford 2.0L engine's oil pump would be known. As neither this information nor the testing facilities to establish it are readily available, the losses due to the oil pump must be estimated. In order to do so, the auxiliary loss trend suggested by Sandoval and Heywood [5] is assumed to apply in some percentage to the oil pump alone. The approximate fraction of the auxiliary losses due to the oil pump can be determined from figure 5-4. As seen from this motored friction breakdown data collected on a four-cylinder S.I. engine, the measured relative contributions of the oil pump versus the water pump and non-charging alternator were approximately 30% and 70% respectively. However, this breakdown is specific to the equipment for which it was determined and auxiliary losses are known to vary significantly with design details [2]. The design details of the specific oil pump used on the Ford 2.0L engine are not known to the author. At low to moderate speeds it is generally accepted that the fmep due to oil pump losses will be in the approximate range of 4-10kPa [2], [42], [43]. Since the auxiliary friction equation is a function of engine speed only it is easy to verify that maintaining 30% of the auxiliary losses as suggested by figure 5-4 will cause the oil pump fmep to fall near the upper end of this range. Noting the probable use of a slightly smaller oil pump and the known usage of a lighter grade of oil on the Ford 2.0L engine compared to the engines for which the empirical auxiliary loss fit was calibrated, an additional reduction is assumed to be needed. A degree of justification for this assumption may be found in the following public statement from Ford Motor Company, "…the oil pump and its drive ratio are sized for the exact capacity requirements of the new 2.0L engine". In light of these

considerations, the auxiliary losses in the model are reduced by 75%. This represents an additional 1/6 reduction versus the assumed oil pump losses within the original model's fit, such that 25% of these losses are maintained to represent the losses attributable to the oil pump in the Ford 2.0L engine. This approximate value is selected to force the pump fmep away from the upper end of the typical range, as the Ford 2.0L engine's oil pump is assumed to be smaller and of a more efficient design. Unavoidably, the assumptions made regarding the oil pump losses will introduce some error in the representation of the Ford 2.0L engine's oil pump. Due to the relatively small portion of the overall engine friction that is attributable to the oil pump (approximately 4-6% dependent on engine speed, see figure 5-11) this error is not considered significant. The auxiliary friction, equation (3-28), becomes:

$$afmep = 0.25(8.32 + 1.86 \times 10^{-3}n + 7.45 \times 10^{-7}n^2) \quad (5.2)$$

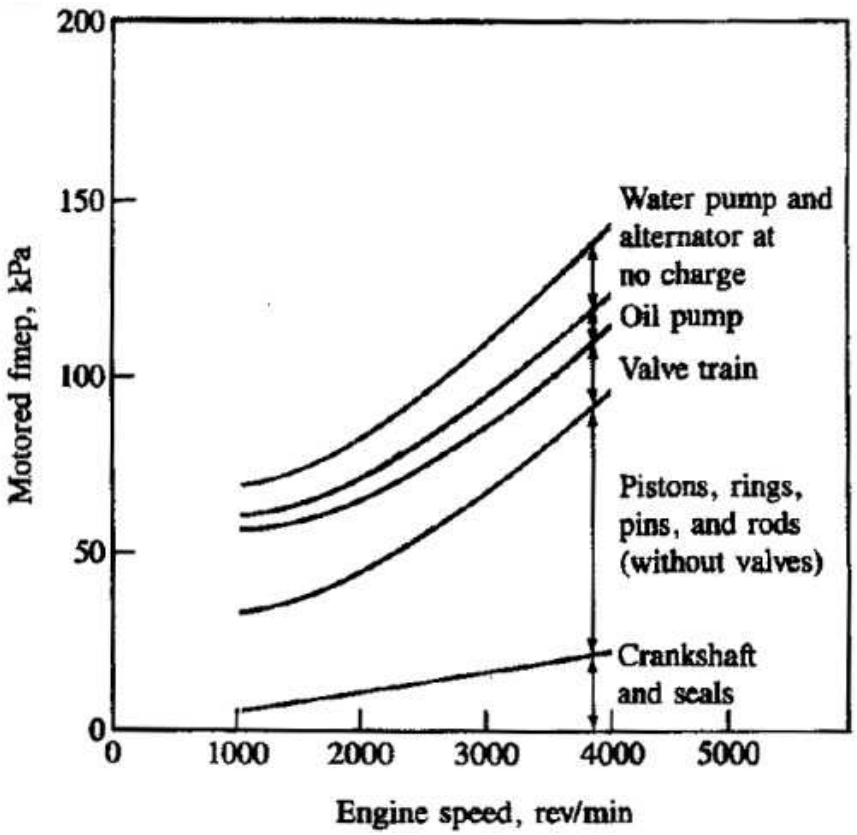

Figure 5-4: Motored friction mean effective pressure vs engine speed for engine breakdown tests on a four-cylinder S.I. engine, [2]

This initial adjustment combined with zooming in on the range for which data is available produces figure 5-5. This presents the first opportunity for comparison between modeled and measured friction for the complete engine. Adding the corresponding test data to figure 5-5 yields this comparison in figure 5-6.

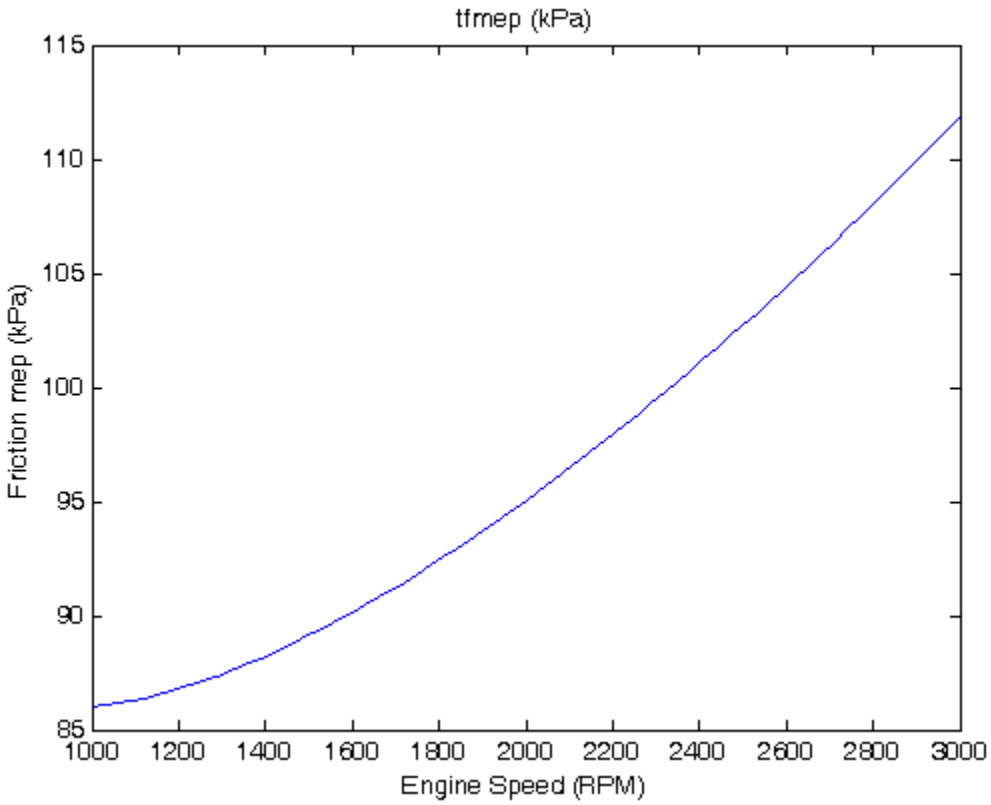

Figure 5-5: Total friction losses with reduced auxiliary friction for the motored Ford 2.0L engine as predicted by the uncalibrated model

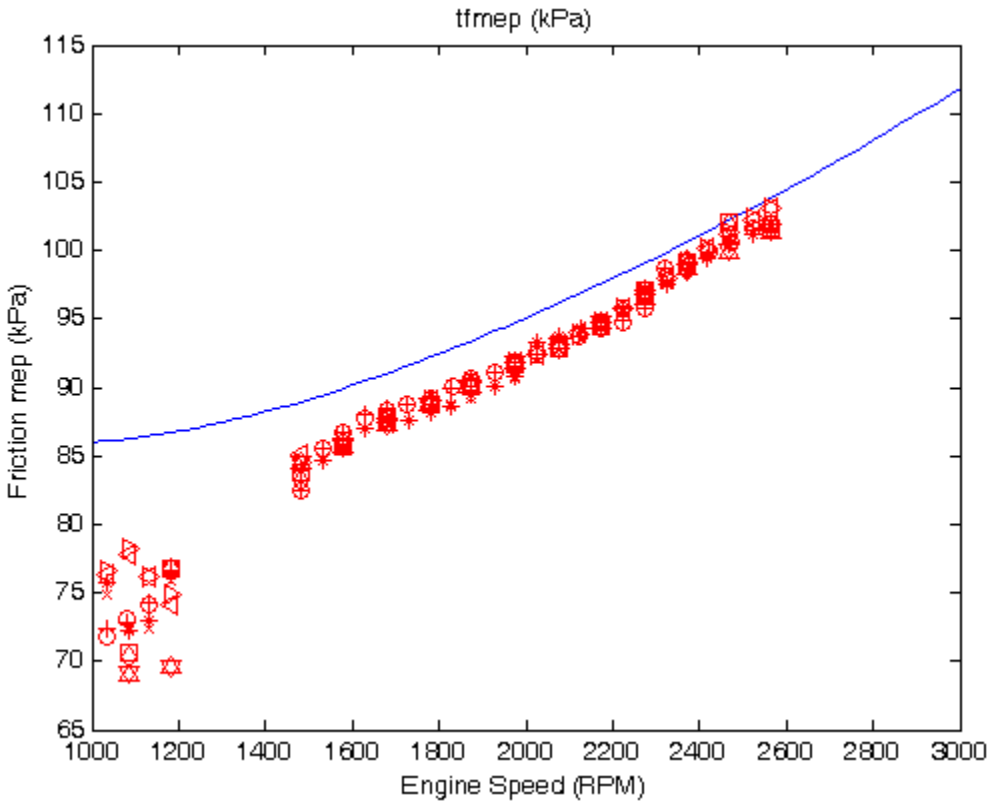

Figure 5-6: Comparison of total friction losses predicted by the uncalibrated model (solid line) to the motored engine loss data

As seen above in figure 5-6 the model slightly over-predicts the measured friction data. This is especially true in the low range of speed between 1000 and 1500 RPM. Referring back to figure 5-2, it can be seen that this apparent error is likely due to the friction estimates for the valvetrain component group, which are uniquely high at low speeds. This group is therefore the initial area of concern within the model. Review of available data presented by Sandoval and Heywood [5] suggested a flatter profile for the valvetrain group is expected. Viewing the individual terms of the valvetrain component group equations separately, it was determined that the higher-than-expected values at low

speeds were attributable to the flat follower and oscillating mixed lubrication terms, or the 2nd and 5th terms in equation (3-27), restated below for convenience. Since the Ford 2.0L engine employs direct acting mechanical buckets with flat followers it is reasonable to focus on these terms.

$$\begin{aligned} vfmep = 244 &\sqrt{\frac{\mu}{\mu_0}}\frac{nn_{bc}}{B^2Sn_{cyl}} + C_{ff}\left(1+\frac{500}{n}\right)\frac{n_v}{Sn_{cyl}} \\ &+ C_{rf}\left(\frac{nn_v}{Sn_{cyl}}\right) + C_{oh}\sqrt{\frac{\mu}{\mu_0}}\left(\frac{{L_v}^{1.5}n^{0.5}n_v}{BSn_{cyl}}\right) \\ &+ C_{om}\left(1+\frac{500}{n}\right)\frac{L_v n_v}{Sn_{cyl}} + 4.12 \end{aligned} \tag{3-27}$$

To lower these values, the $\left(1+\frac{500}{n}\right)$ terms, which are used to make the friction coefficients related to these terms decrease by a factor of about 1.8 from low to high speeds, were reduced. To maintain physical significance in the friction coefficient reduction, the same adjustment was applied within the reciprocating friction group for the single $\left(1+\frac{500}{n}\right)$ term. In order to investigate the sensitivity of the model to changes in these coefficients, the total fmep was plotted for subsequent reductions of the coefficients from $\left(1+\frac{500}{n}\right)$ to $\left(1+\frac{150}{n}\right)$ in $\left(1+\frac{50}{n}\right)$ increments. This analysis is shown in figure 5-7 and shows that a decrease of $\left(1+\frac{50}{n}\right)$ causes approximately a 1kPa drop in the total fmep at 1000RPM. The effect diminishes with increasing speed such that it accounts for approximately a 0.4kPa drop at 3000RPM and is negligible by 6000RPM. Matching the shape of the model curves to the data shown in figure 5-7, a final value of $\left(1+\frac{250}{n}\right)$ is

selected. This lowers the friction coefficients, especially at low speeds, while causing them to decrease by a factor of about 1.35 from low to high speeds. The slight reduction in friction coefficient for these terms may likely be attributed to the modern surface finishes of related valvetrain and reciprocating friction components. The adjusted valvetrain group expression becomes:

$$\begin{aligned} vfmep = {} & 244\sqrt{\frac{\mu}{\mu_0}}\frac{nn_{bc}}{B^2Sn_{cyl}} + C_{ff}\left(1+\frac{250}{n}\right)\frac{n_v}{Sn_{cyl}} \\ & + C_{rf}\left(\frac{nn_v}{Sn_{cyl}}\right) + C_{oh}\sqrt{\frac{\mu}{\mu_0}}\left(\frac{{L_v}^{1.5}n^{0.5}n_v}{BSn_{cyl}}\right) \\ & + C_{om}\left(1+\frac{250}{n}\right)\frac{L_v n_v}{Sn_{cyl}} + 4.12 \end{aligned} \tag{5.3}$$

While the reciprocating friction equation becomes:

$$\begin{aligned} rfmep = {} & 2.94\times10^{2}\sqrt{\frac{\mu}{\mu_0}}\left(\frac{S_p}{B}\right) \\ & + 4.06\times10^{4}\left(\frac{F_t}{F_{t0}}C_r\right)\left(1+\frac{250}{n}\right)\left(\frac{1}{B^2}\right) \\ & + 3.03\times10^{-4}\sqrt{\frac{\mu}{\mu_0}}\left(\frac{n{D_{bj}}^{3}L_{bj}n_{bj}}{B^2Sn_{cyl}}\right) \end{aligned} \tag{2.1}$$

This adjustment greatly improved the shape of the model's prediction when compared to the measured data.

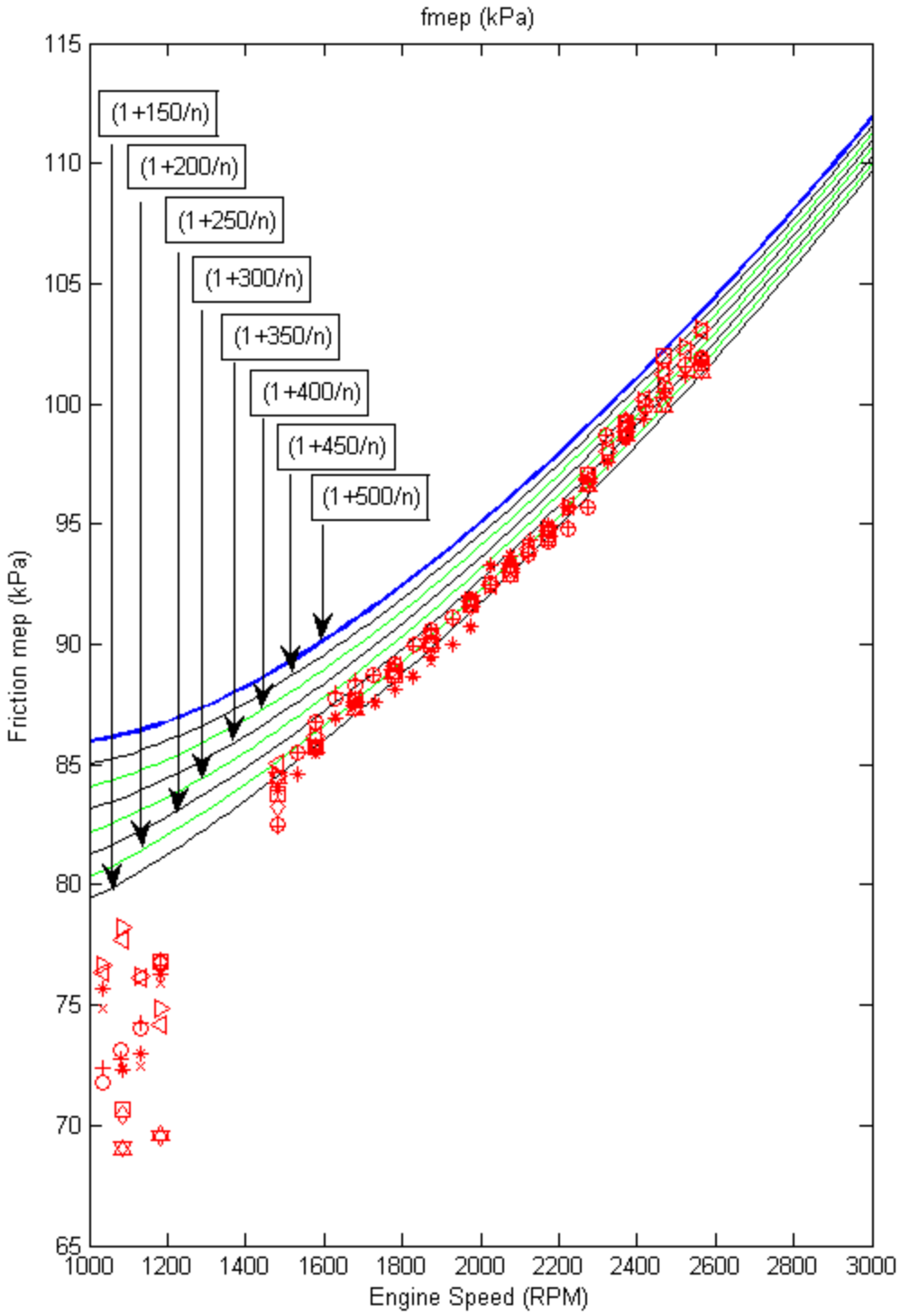

Figure 5-7: Model sensitivity to changes in the friction coefficient found within the reciprocating friction and valvetrain flat-follower and oscillating mixed groups

The only other adjustments made were to the piston ring tension ratio, F_t/F_{t0}, and the piston roughness constant, C_r. The piston ring tension ratio accounts for potential differences in the combined effect of the radial pressure exerted on the cylinder walls by the piston rings, as compared to the engines for which the model was originally suggested. The piston roughness constant addresses the surface finishes between the piston and cylinder walls. Setting these parameters to a value of 1 assumes no related changes from the original 1980's model, while values lower than 1 account for improvements. Final values for these parameters were both reduced from 0.98 to 0.95, as selected in accordance with the analysis shown in figure 5-8 and figure 5-9, in order to lower their respective portions of the total friction predicted by the model and to better fit the motored friction data. As seen in figure 5-8, reducing F_t/F_{t0} by 1% results in an approximate 0.4kPa reduction in total fmep at 1000RPM, with diminishing effect to approximately 0.25kPa at 6000RPM. Figure 5-9 shows the model is considerably less sensitive to changes in the piston roughness constant, C_r, with a 1% reduction causing less than a 0.1kPa drop in total fmep with negligible dependence on speed. With the final values selected, the small reduction to the losses predicted by these terms for the Ford 2.0L engine is in line with ongoing efforts to improve fuel efficiency.

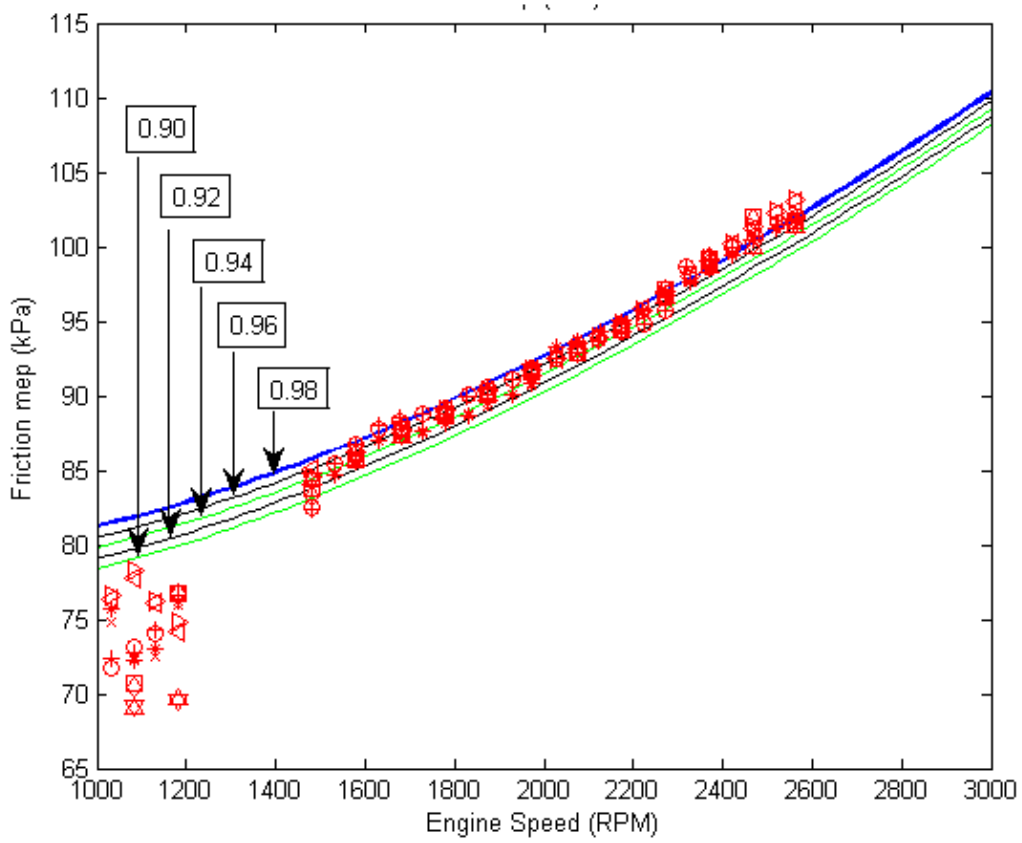

Figure 5-8: Model sensitivity to changes in the piston ring tension ratio, $F_t/F_{t0,}$ found within the reciprocating friction and piston gas pressure loading groups

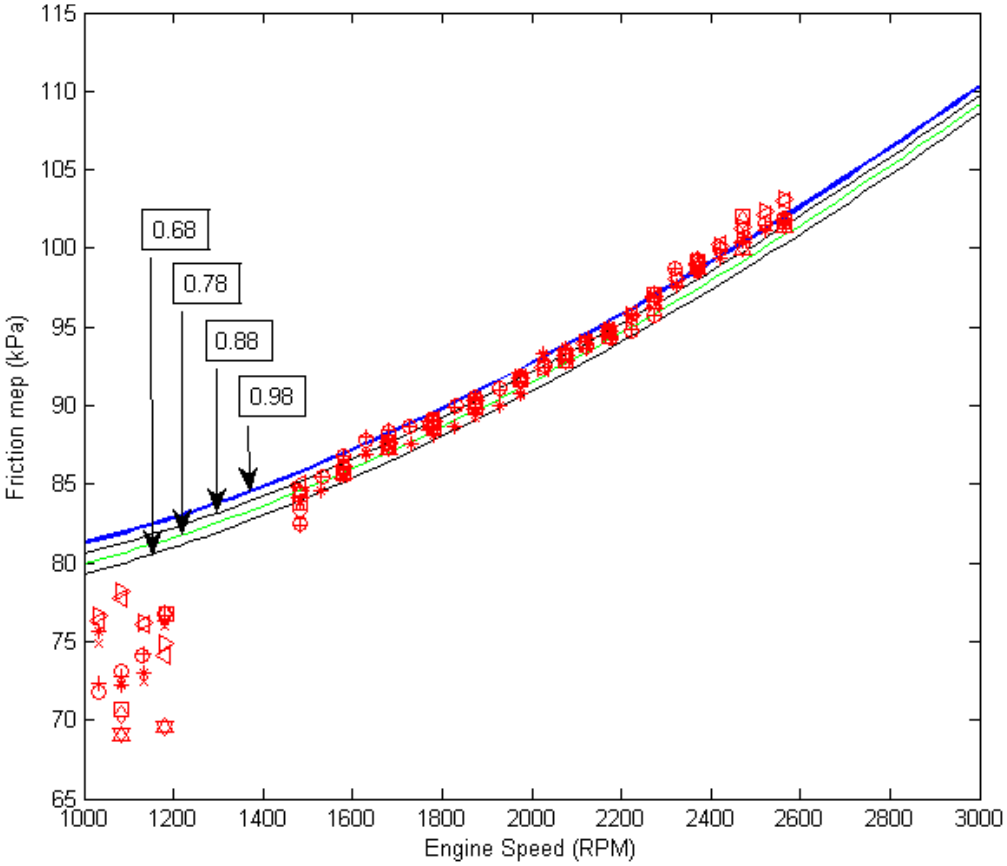

Figure 5-9: Model sensitivity to changes in the piston roughness constant, $C_{r,}$ found within the reciprocating friction group

5.1.2 Demonstration of Friction Model Fit

The results of all adjustments made are depicted for the individual component groups in figure 5-10. Note that no changes are made to the crankshaft friction, pumping losses, or auxiliary friction component groups. Slight overall reductions are seen in the plots of the reciprocating friction and piston gas loading terms. The more significant adjustments made to the low speed range of the valvetrain friction are also easily observed. Recall that these changes relate to the friction coefficients for the flat follower and oscillating mixed lubrication valvetrain terms, and reflect improvements to valvetrain

components. To better assess the relative contributions of the component groups and the effects of changes to the model, figure 5-11 re-plots the individual component groups on a single set of axes. The area between plotlines in this figure shows the added impact of each component group as labeled. The updated prediction of total friction is plotted against the test data in figure 5-12.

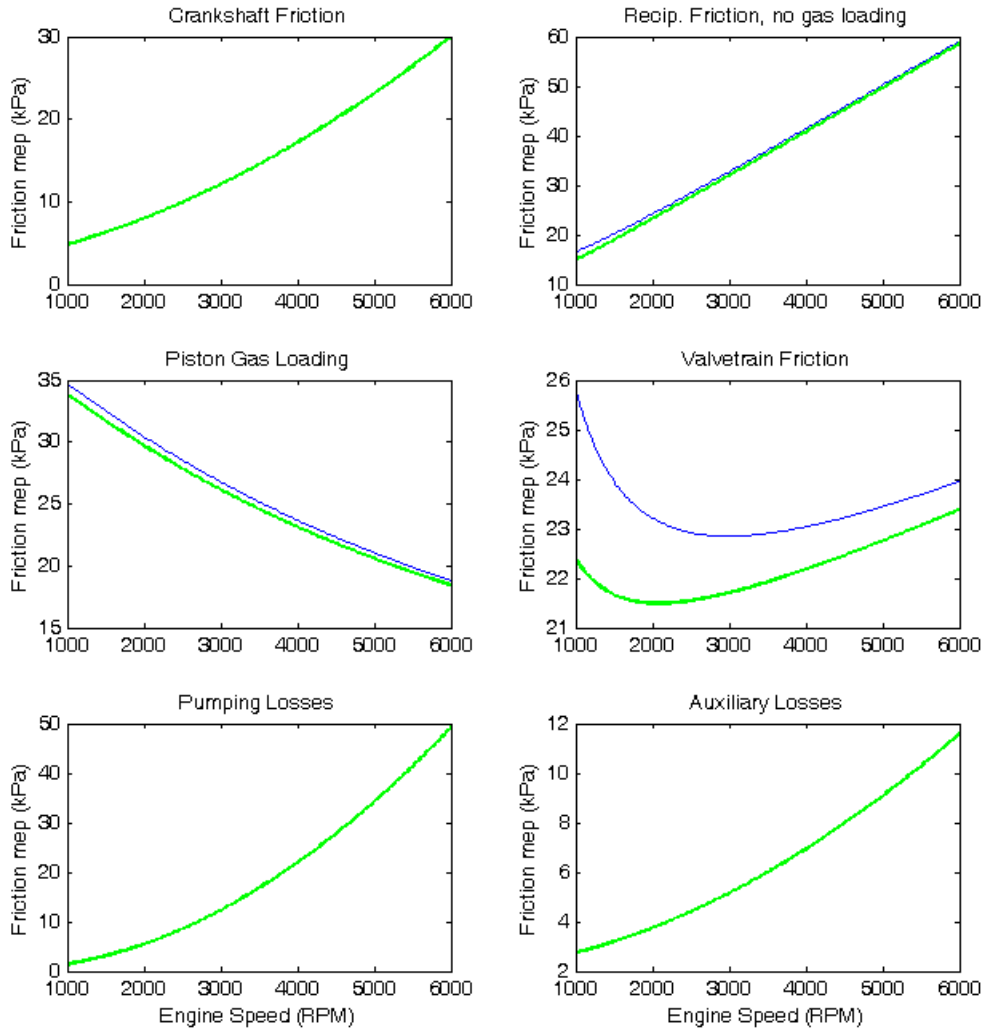

Figure 5-10: Individual component group losses for the motored Ford 2.0L engine as predicted by the uncalibrated (blue) and calibrated model (heavy green)

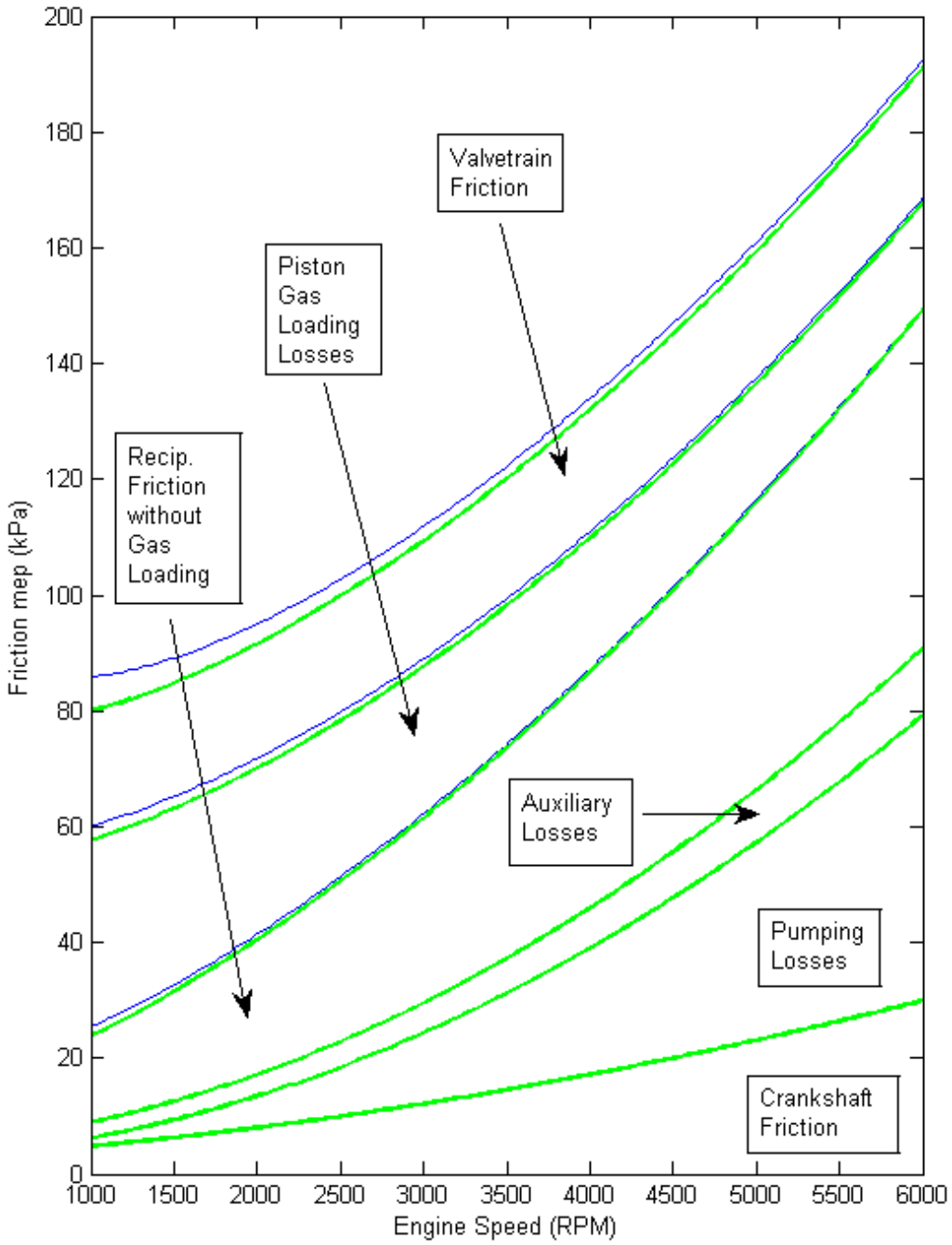

Figure 5-11: Stacked individual component group losses for the motored Ford 2.0L engines as predicted by the uncalibrated (blue) and calibrated model (heavy green)

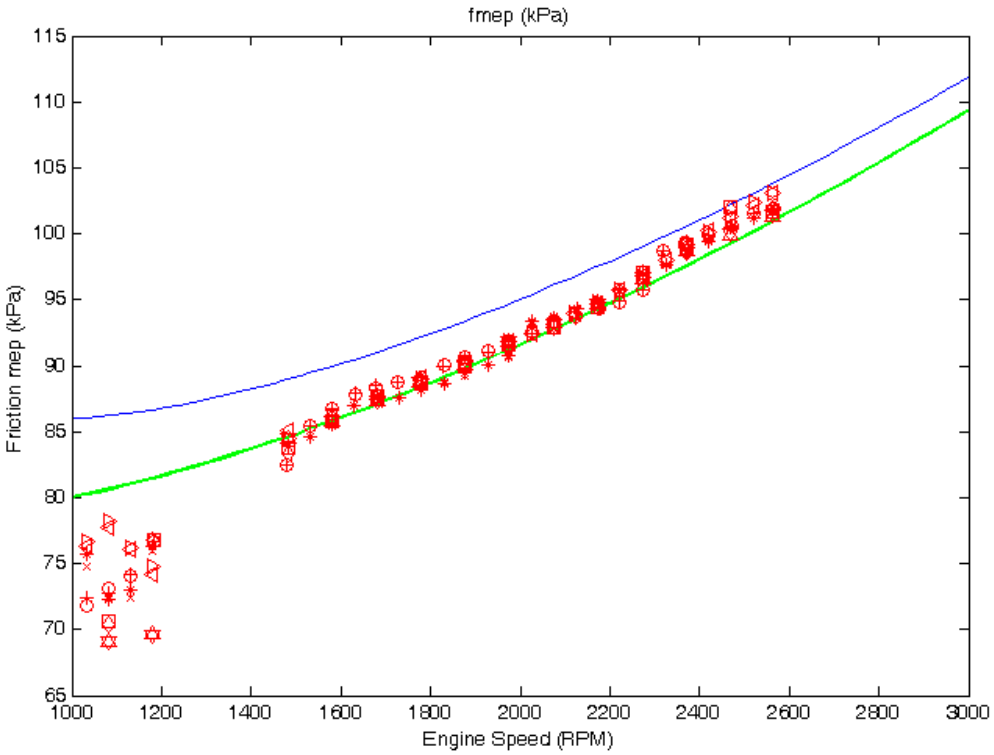

Figure 5-12: Comparison of total friction losses predicted by the uncalibrated model (blue), calibrated model (heavy green), and the motored engine loss data (red)

It is seen that the measured data from 1000 – 1200 RPM does not align with the model's prediction. The relative noisiness of this data compared to the data above 1500 RPM suggests the possibility of inaccuracy. Another possibility is that without combustion pressure from a firing engine, the compression within the engine alone is not adequate at low speeds to ensure sealing and consistent behavior of the piston rings. This possibility is supported by the relatively high contribution to total friction at low speeds predicted by the piston gas loading term, as seen in figure 5-10. Beyond this range the model is seen to fit fairly well overall before it begins to slightly under-predict the

measured values at higher speeds. No resulting changes to the model are justified without additional data at higher engine speeds. Extending the plot to the full engine speed range produces figure 5-13, where it can be seen that the calibrated model approaches the original model at the engine's top speed.

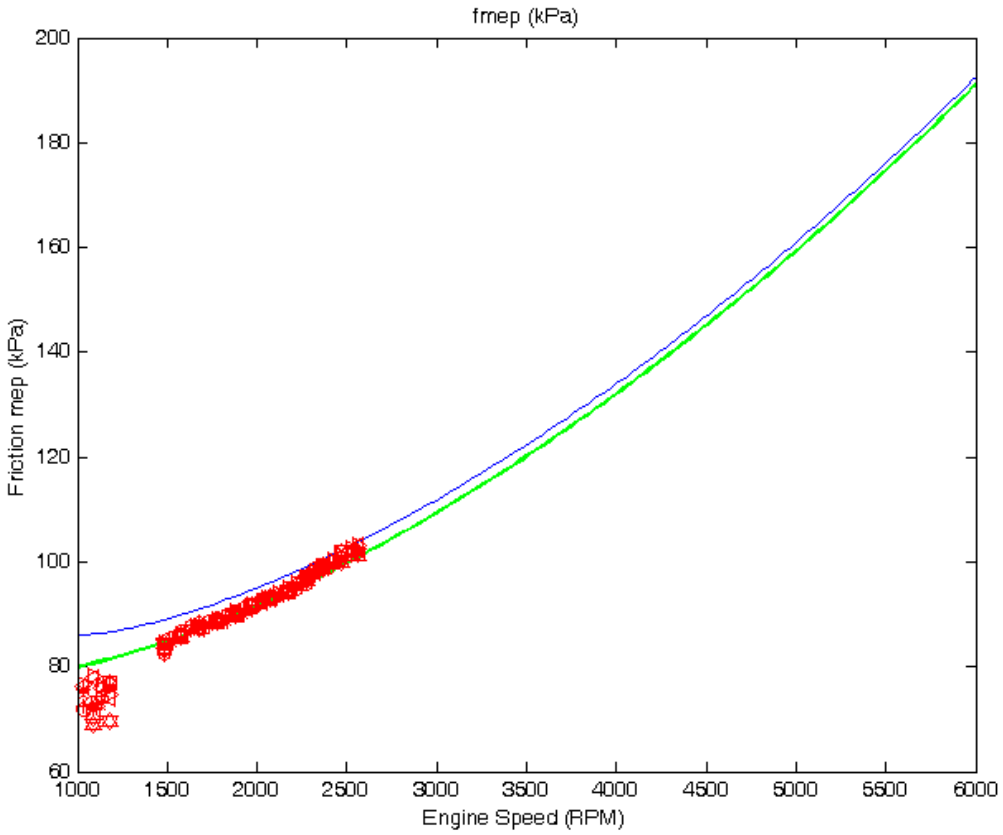

Figure 5-13: Comparison of total friction losses predicted by the uncalibrated model (blue), calibrated model (heavy green), and the motored engine loss data (red) over the full speed range

The final friction model recommended for the Ford 2.0L engine is given in equation (2.2) below, while its parameter values are listed in table 5-2.

$$
\begin{aligned}
fmep = {} & 1.22\times10^{5}\left(\frac{D_{bm}}{B^{2}Sn_{cyl}}\right)+3.03\times10^{-4}\sqrt{\frac{\mu}{\mu_0}}\left(\frac{n{D_{bm}}^{3}L_{bm}n_{bm}}{B^{2}Sn_{cyl}}\right)\\
& +1.35\times10^{-10}\left(\frac{{D_{bm}}^{2}n^{2}n_{bm}}{n_{cyl}}\right)+\ 2.94\times10^{2}\sqrt{\frac{\mu}{\mu_0}}\left(\frac{S_p}{B}\right)\\
& +4.06\times10^{4}\left(\frac{F_t}{F_{t0}}C_r\right)\left(1+\frac{250}{n}\right)\left(\frac{1}{B^{2}}\right)\\
& +3.03\times10^{-4}\sqrt{\frac{\mu}{\mu_0}}\left(\frac{n{D_{bj}}^{3}L_{bj}n_{bj}}{B^{2}Sn_{cyl}}\right)+\ 6.89\frac{p_{man}}{p_{amb}}\left[0.088\sqrt{\frac{\mu}{\mu_0}}r_c+0.182\left(\frac{F_t}{F_{t0}}\right){r_c}^{(1.33-KS_p)}\right]\\
& \qquad +\ 244\sqrt{\frac{\mu}{\mu_0}}\frac{nn_{bc}}{B^{2}Sn_{cyl}}+C_{ff}\left(1+\frac{250}{n}\right)\frac{n_v}{Sn_{cyl}}\\
& +C_{rf}\left(\frac{nn_v}{Sn_{cyl}}\right)+C_{oh}\sqrt{\frac{\mu}{\mu_0}}\left(\frac{{L_v}^{1.5}n^{0.5}n_v}{BSn_{cyl}}\right)\\
& +C_{om}\left(1+\frac{250}{n}\right)\frac{L_vn_v}{Sn_{cyl}}+4.12+\ 0.25(8.32+1.86\times10^{-3}n+7.45\times10^{-7}n^{2})\\
& \qquad +\ (p_{amb}-p_{man})+3.0\times10^{-3}\left(\frac{p_{man}}{p_{amb}}\right)^{2}\left(\frac{{S_p}^{2}}{{n_{vi}}^{2}{r_i}^{4}}\right)+0.178\left(\frac{p_{man}}{p_{amb}}S_p\right)^{2}\\
& \qquad +3.0\times10^{-3}\left(\frac{p_{man}}{p_{amb}}\right)^{2}\left(\frac{{S_p}^{2}}{{n_{ve}}^{2}{r_e}^{4}}\right)
\end{aligned}
\tag{2.2}
$$

Table 5-2: Parameter values used to apply final suggested friction model to the 2.0L engine

Symbol	Description (units)	Value
D_{bm}	main bearing diameter (mm)	52
D_{bj}	journal bearing diameter (mm)	47
B	bore (mm)	87.5
S	stroke (mm)	83.1
n_{cyl}	number of cylinders	4
μ	oil viscosity (cSt)	9.7
μ_0	reference oil viscosity (cSt)	13
n	engine speed (RPM)	
L_{bm}	main bearing length (mm)	25.4
L_{bj}	journal bearing length (mm)	20.64
n_{bm}	number of main bearings	5
n_{bj}	number of journal bearings	4
n_{bc}	number of camshaft bearings	5
S_p	mean piston speed (m/s)	
F_t/F_{t0}	piston ring tension ratio	0.95
C_r	piston roughness constant	0.95
p_{man}	intake manifold pressure (kPa)	101.3
p_{amb}	atmospheric pressure (kPa)	101.3
r_c	compression ratio	12:1
K	constant	2.38×10^{-2}
C_{ff}	constants based on valvetrain mechanism	133
C_{rf}		0.005
C_{oh}		0.5
C_{om}		10.7
n_v	number of valves (intake and exhaust)	16
L_v	maximum valve lift (mm)	14.3
r_i	intake valve diameter/bore	35mm
r_e	exhaust valve diameter/bore	30mm
	Known or selected values for the Ford 2.0L Engine	
	Values used as suggested by Sandoval & Heywood	
	Scaling parameters used for model fit	

5.2 Fitting the MVEM

With a detailed physical model of engine friction fit to the motoring test data an inclusive model of the engine for overall simulation is desired. The MVEM as presented in chapter 3 is used for this purpose. The following subsections describe the processes of fitting the MVEM and simulating the engine.

5.2.1 Fired Engine Test Data

The MVEM as presented in chapter 3 is a versatile model which may be fit to a variety of engines in order to simulate the basic behavior of the engine itself. It does not include any operational controls and requires dynamometer testing of the running engine in order to complete the model. It was not possible to conduct such testing for inclusion within this research so the MVEM must be simplified for use with available data. Specifically, data was made available from Ford of Canada from standardized dynamometer testing used to verify the engine's power output. This data is not sufficient to fully fit the MVEM to the engine for simulation of all operating conditions. Instead it is used to ensure the MVEM can properly predict the engine's response to the general conditions of the Ford test data. The functions of the dynamometer test thus define the control needed in the engine simulations. This power test is conducted at wide open throttle with the dynamometer applying a varying load to hold the engine at a series of steady speeds at which measurements are taken. This is done over the full range of engine operation, with torque measured by the dynamometer at each speed. In this way the maximum torque and power curves of the engine are recorded.

The MVEM simulation is simplified as needed and set up to mimic this test according to the schematic shown in figure 5-14. The following subsections will refer back to this figure as the MVEM simulation is described in detail. Instead of the dynamometer holding the engine to a set of given speeds and measuring the load at these points, the load points are input to the MVEM and the engine speed is determined. This reversal is a result of the original construction of the MVEM, which uses engine speed as a state and applied load as a variable. To simulate the power test, the MVEM is run for each of the steady-state speeds for which data is available. At each point, the corresponding engine load from the data supplied by Ford is entered as an input to the model, as shown at the top of figure 5-14. Other required inputs include setting of the throttle angle, which for the power-test remains wide-open throughout, and expressions for the volumetric and thermal efficiencies. These expressions are also taken from the Ford data, and are discussed momentarily. First, the required adjustments made to the MVEM system state equations are discussed.

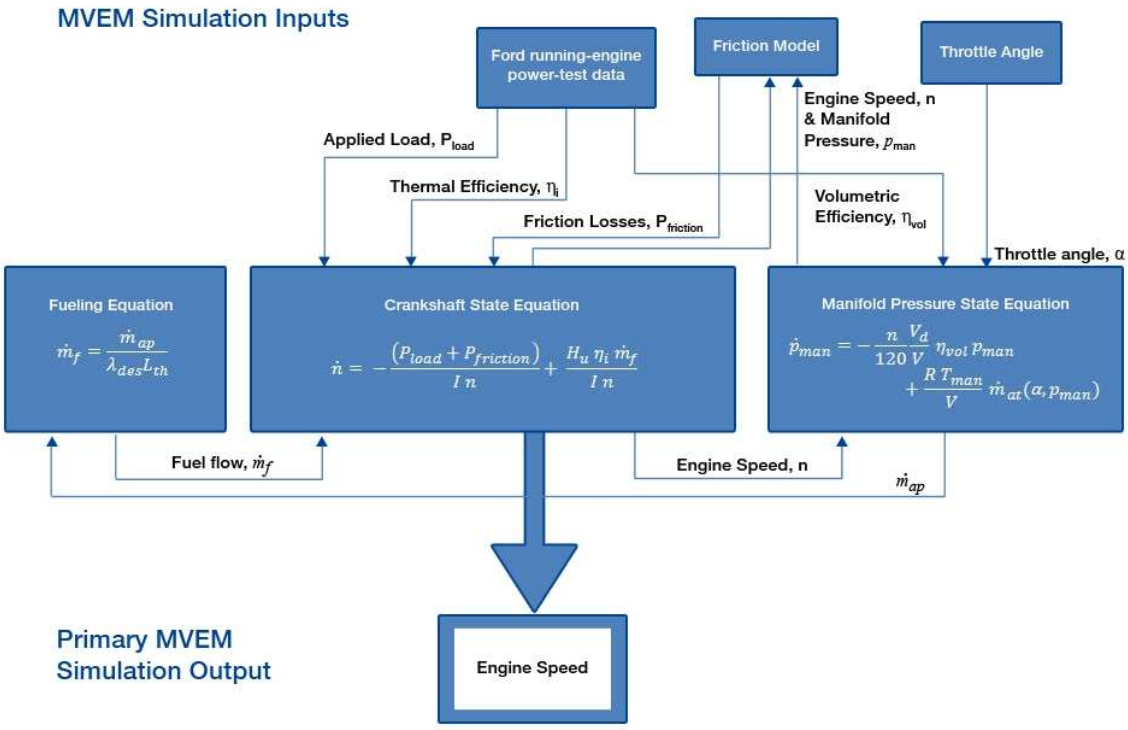

Figure 5-14: Schematic of modified MVEM for power-test simulation

5.2.2 Modified Fuel Flow Equation

Recall the general form of the MVEM manifold fuel flow equation was given as follows:

$$\dot{m}_f = \dot{m}_{fv} + \dot{m}_{ff}, \tag{3-3}$$

where $\dot{m}_f$ is the total fuel flow into the cylinder port, $\dot{m}_{fv}$ is the portion of the total injected fuel flow that exists in the vapor phase, and $\dot{m}_{ff}$ is the remaining portion of the fuel in the form of a liquid film on the manifold wall.

Since the Ford engine employs direct fuel injection into the combustion chamber, the fueling dynamics modeled by this original form do not apply. Testing of the fired engine would be required to determine the actual fueling dynamics required to be modeled in order to complete this area of the MVEM for general simulation of the Ford 2.0L engine. Since limited fired engine data was available only for steady operation at wide open throttle, detailed modeling of fueling is clearly not possible, but also not needed. Since the model will only consider operation under these conditions, only the *amount* of injected fuel need be determined. For the purposes of comparing the MVEM to the power test it is reasonable to reduce the fueling controls to simple maintenance of the stoichiometric air/fuel ratio. This is accomplished by replacing equation (3-3) with this simple calculation of fuel flow based on the manifold pressure:

$$\dot{m}_f = \frac{\dot{m}_{ap}}{\lambda_{des} L_{th}}, \tag{2.3}$$

where $\dot{m}_f$ is the fuel mass flow rate, $\dot{m}_{ap}$ is the air mass flow rate into the combustion chamber, λ_{des} is the desired ratio of the actual air/fuel ratio to the stoichiometric air/fuel ratio, and L_{th} is stoichiometric air/fuel ratio.

5.2.3 Modified Air Flow Equation

Recall the general form of the MVEM manifold air flow equation was given as follows:

$$\dot{p}_{man} = -\frac{n}{120}\frac{V_d}{V}\,\eta_{vol}\,p_{man} + \frac{R\,T_{man}}{V}\,\dot{m}_{at}(\alpha, p_{man}) \tag{3-7}$$

where n is the crankshaft (engine) speed, V_d is the engine displacement volume, V is the volume contained in the manifold between the throttle plate and the intake valves, η_{vol} is the volumetric efficiency, R is the universal gas constant, T_{man} and p_{man} are the temperature and pressure of air in the manifold, and, $\dot{m}_{at}$ is the mass flow of air past the throttle plate.

Since the throttle remains fully open throughout the power test, the expression used for the mass flow of air past the throttle plate, $\dot{m}_{at}$, is less critical than it would otherwise be. At wide open throttle, the throttle plate presents no restriction to the airflow and the pressure within the intake manifold, p_{man}, will in theory be equal to the atmospheric pressure. Therefore, the air flow state equation is used in the modified form of the MVEM unchanged. Only the treatment of the volumetric efficiency, discussed shortly, is adjusted.

5.2.4 Modified Crankshaft Equation

Recall the general form of the MVEM crankshaft equation was given as follows:

$$\dot{n} = -\frac{\left(P_f + P_p + P_b\right)}{I\,n} + \frac{H_u\,\eta_i\,\dot{m}_f(t-\tau_d)}{I\,n}, \tag{3-9}$$

where I is the total inertial load of the engine, n is the crankshaft speed, P_f, P_p, and P_b are the frictional, pumping, and load powers respectively, H_u is the lower heating value of the fuel, η_i is the indicated thermal efficiency of the engine, $\dot{m}_f$ is the rate of fuel mass flow into the cylinder, t is the time, and τ_d is a time delay inserted to describe the delay between the edge of a fuel flow step and the change in crankshaft speed.

Since the modified MVEM is used only for simulation of steady-state data the time delay described above is not needed. This is because at steady operating conditions the calculated fuel flow within the model should not change. The time delay is therefore removed. Aside from grouping the frictional and pumping powers together as $P_{friction}$, this is the only modification. The equation becomes,

$$\dot{n} = -\frac{\left(P_{friction} + P_b\right)}{I\,n} + \frac{H_u\,\eta_i\,\dot{m}_f}{I\,n}. \tag{2.4}$$

5.2.5 Volumetric and Thermal Efficiencies

The preferred forms for the volumetric and thermal efficiencies within the MVEM were given in chapter 3 as follows:

$$\eta_{vol}(n, p_{man}) = \eta_{vn0} + \eta_{vn1} n + \eta_{vn2} n^2 + \eta_{vp1} p_{man} \quad (3\text{-}16)$$

where η_{vn0}, η_{vn1}, η_{vn2}, and η_{vp1} are physical constants, and

$$\eta_i(\theta, \lambda, n, p_{man}) = \eta_i(\theta, n)\eta_i(\lambda, n)\eta_i(n)\eta_i(p_{man}) \quad (3\text{-}19)$$

where η_i is the indicated thermal efficiency expressed as individual functions of θ the spark advance, λ the air/fuel equivalence ratio, n the engine speed, and p_{man} the intake manifold pressure.

As the testing required to fit these expressions to the engine could not be completed within the scope of this research an alternate approach is needed. Functions in terms of engine speed were instead fit to the running engine data provided by Ford of Canada. While this further limits the model to simulations of the standard power test, it is the only available way to proceed. Second order polynomials in terms of engine speed were fit to the provided measured Ford data as depicted in figure 5-15 and given in equations (2.5) and (2.6) below.

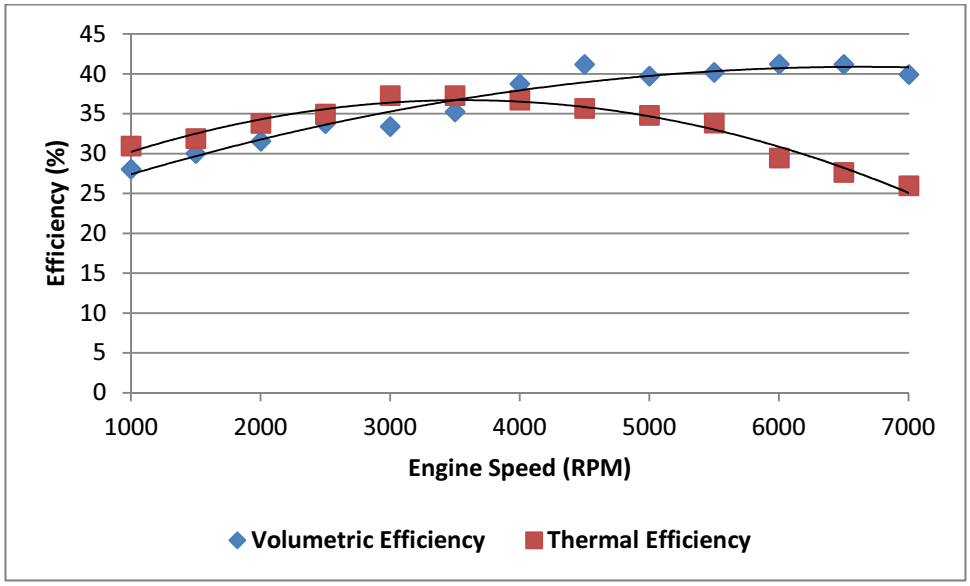

Figure 5-15: Volumetric and thermal efficiency trends as fit to data provided by Ford for the fired engine power test data

The trends shown in figure 5-15 required scaling for use in the MVEM, but the engine's behavior as it relates to both efficiencies are captured according to the following expressions for volumetric and thermal efficiency.

$$\eta_{vol} = [-0.4239\left(\frac{n}{1000}\right)^2 + 5.6273(\frac{n}{1000}) + 22.212]/41, \quad (2.5)$$

$$\eta_i = [-0.9855\left(\frac{n}{1000}\right)^2 + 7.025(\frac{n}{1000}) + 24.194]/70, \quad (2.6)$$

where n is the engine speed in RPM.

In general, volumetric efficiency refers to the percentage of air/fuel that enters the cylinder compared to the capacity of the cylinder under static conditions. At wide open throttle the volumetric efficiency of an engine like the Ford 2.0L engine should be near 100%. Clearly the data provided by Ford in figure 5-15 does not depict this, and is

defined differently. The volumetric efficiency from the Ford data is scaled for use in the MVEM such that it approaches 100%. However, the modified model is particularly sensitive to the volumetric efficiency, and this expression is problematic at low speeds as the volumetric efficiency dips too low. To address this issue, the action of the volumetric efficiency from the data is reduced by a factor of 2 by replacing η_{vol} in the model with the following expression: $1 - \left[\frac{(1-\eta_{vol})}{2}\right]$. This allows the model to operate closer to 100% volumetric efficiency as needed to better fit the overall power-test data, while maintaining some of the behavior demonstrated by the volumetric efficiency trend given in the Ford data. While this treatment of the volumetric efficiency is uncertain it is preferable to assuming a constant value for η_{vol}.

5.3 Power Test Simulation

With the detailed engine friction model fit to the motored engine data and the MVEM adjusted according to figure 5-14, the standard power test may be simulated for comparison to the available fired engine data. The Matlab/Simulink environment is used to acquire steady-state values corresponding to each point for which data was available. A fixed step size of 1ms is used for all simulations, as is the fourth-order Runge-Kutta integration technique. It is believed that this treatment is more than sufficient for simulation of the course nature of the power test data. Repeating the simulation yields no significant change in the results. The flow and interdependency of data within the simulation is depicted in figure 5-14. The resulting simulation is compared to the test

data and presented in terms of brake power in figure 5-16, and in terms of brake torque in figure 5-17. In the case of both figures, the total friction losses which first had to be overcome, as calculated by the friction model, are also plotted.

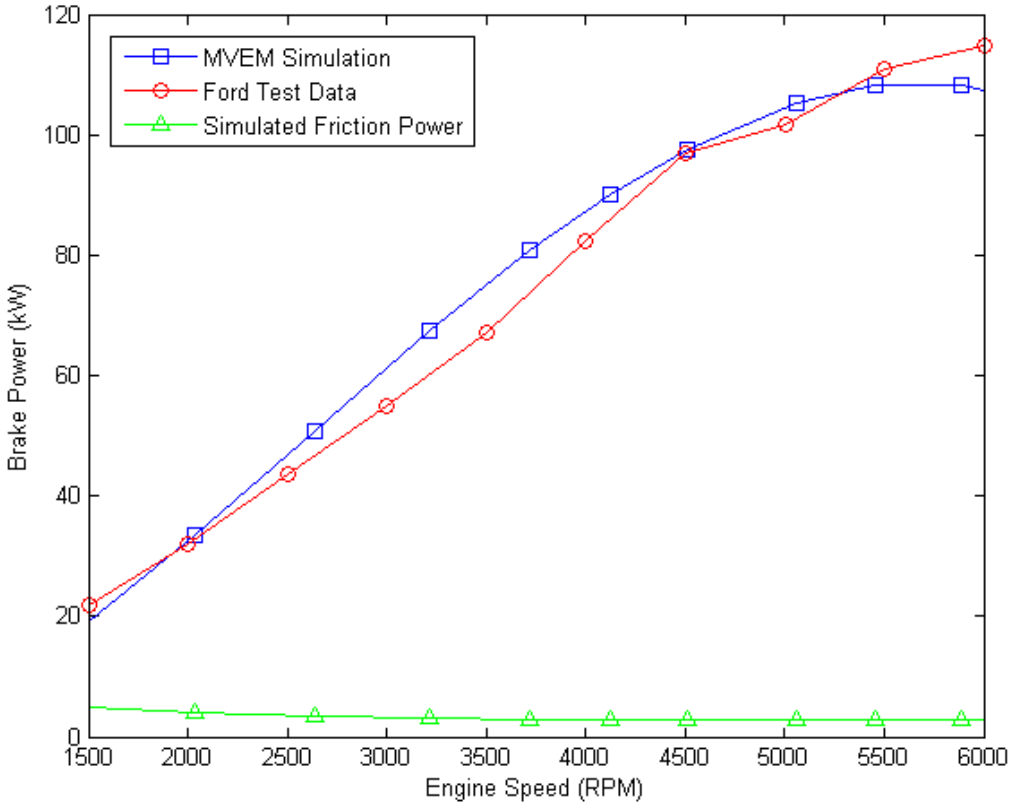

Figure 5-16: MVEM simulated and actual brake power

As seen above, the models fit reasonably well at low and high speeds, but over-predict the engine's power in the mid-range between approximately 2500 and 4500RPM. This error is more apparent when the same data is viewed in terms of brake torque as shown in figure 5-17.

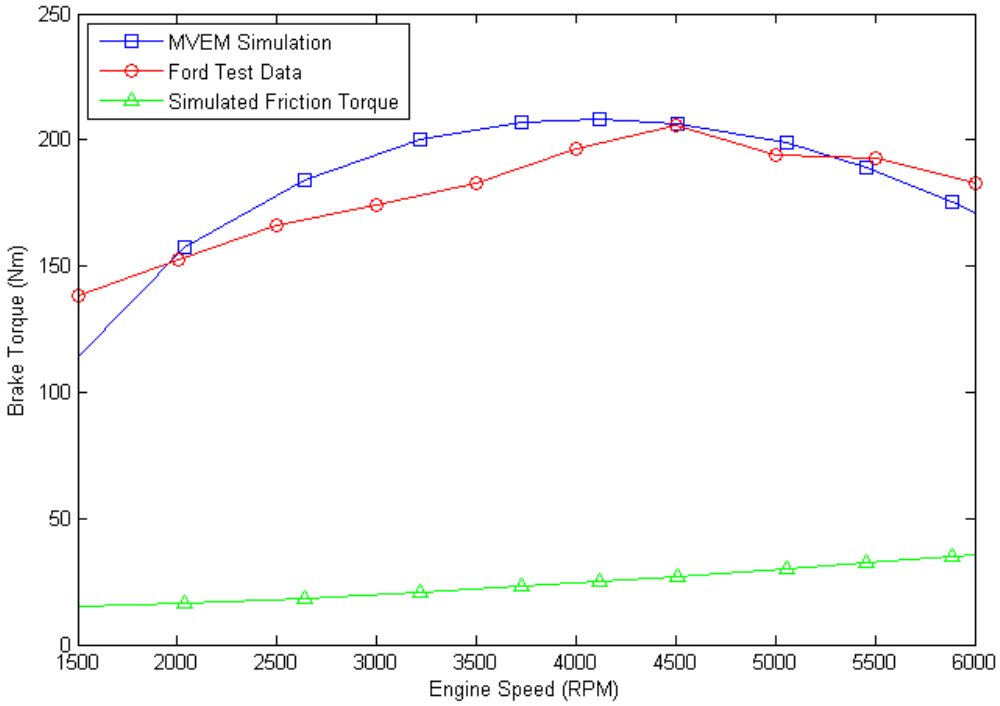

Figure 5-17: MVEM simulated and actual brake torque

It is apparent that despite efforts to tailor the model to the available data, it is not a particularly good approximation of the actual power test. Overall, the shape of the power curves suggested by the model are seen to be smoother and more gradual than the actual data, demonstrating that certain changes over the engine's operating window are being missed. The MVEM as presented in chapter 3 is expected to have the capacity to accurately model the Ford 2.0L engine over its complete operating window, but the completion of fired-engine testing beyond the scope of this research is required to complete and verify the model.

In this chapter the friction model is successfully adjusted to fit the motored data for total engine friction. Simulations of the running engine using the MVEM proved very difficult with only limited fired-engine data available, but easily incorporate the modeled friction. The next and final chapter provides concluding remarks as well as suggestions for future research related to this topic.

Chapter 6

6. Conclusions and Recommendations for Future Research

6.1 Conclusions

The objectives of this research included the design and construction of a dedicated engine dynamometer test stand for the purposes of engine friction characterization. Such a test stand was successfully built, incorporating the following capabilities:

- motoring of the Ford 2.0L engine to 3400RPM,
- repeatable torque-to-turn measurement at speeds up to 2600RPM,
- heating of engine to and beyond operating conditions corresponding to an oil temperature of 90˚C, and
- securely and safely mount and contain all test equipment.

This compact test stand is well suited to measuring the power required to motor almost any automotive related rotating equipment at low to moderate speeds. In the case of a 4-cylinder engine like the one tested, measurements at speeds below 1000RPM are difficult due to torque changes throughout the engine cycle. This would not be an issue for testing of equipment with a constant torque profile. The test stand is therefore seen to be an excellent tool for testing engines, but has further potential for testing related equipment such as transmissions or accessory engine components including the alternator, power steering pump, or air conditioning compressor.

After the dynamometer test stand was used to measure the frictional losses of the Ford 2.0L engine, a physical component based friction model was compared to and adjusted to fit the collected data. This model was found to fit the measured data quite well, and only minor adjustments were needed to achieve a good model fit.

A mean value engine model (MVEM) was presented for simulation of the Ford 2.0L engine under running conditions. This model was simplified for simulation of the operating conditions encountered during a standardized power-test conducted at Ford for which limited fired-engine data was available. The data-verified friction model is added to the MVEM and the power-test simulated. It is seen that augmenting the MVEM with the more detailed friction model is straightforward, while the MVEM itself is a useful tool for engine simulation. The simplified version of the MVEM as presented is extremely sensitive to the volumetric and thermal efficiencies which are input in a scaled form from the fired-engine data. Additional fired-engine test data would be needed to improve the MVEM predictions while extending its useful range to the full operating window of the engine.

6.2 Recommendations for Future Research

This research successfully characterized the internal friction losses of the complete Ford 2.0L engine at regular operating temperature. The first suggestion for future work is to use the existing experimental setup to investigate frictional losses of the engine for a range of oil temperatures from room temperature (~20˚C) to operating conditions already tested (~90˚C).

The fit of a component based friction model was investigated within this work. The remaining primary recommendations for future work relate to the experimental verification of the model fit corresponding to its individual component terms. The following arrangements for partial disassembly of the engine are recommended for testing according to the methods of this research.

(1) Both camshafts and the timing chain should be removed from the engine so that intake and exhaust valves remain closed at all times. In this arrangement the pistons are subject to full compression and expansion on alternate strokes. Friction terms related to the valvetrain and pumping losses are removed in this arrangement. The additional work related to the heat of compression lost to the cylinder walls should be considered. Measurements will apply to friction model terms for the crankshaft, reciprocating component group including piston gas pressure loading terms, and auxiliary losses of the oil pump.

(2) Both cylinder heads should be removed and replaced by custom-machined block-off plates to maintain flow of oil and coolant. This arrangement eliminates valvetrain and pumping losses as in the first case, with the additional elimination

of the piston ring gas loading terms. Measurements will apply to friction model terms for the crankshaft, reciprocating component group (excluding piston gas pressure loading terms), and auxiliary losses of the oil pump.

(3) The losses attributable to the valvetrain should be isolated by replacing the crankshaft with a custom-machined straight shaft, with all pistons removed, such that the valvetrain operates as normal. This arrangement eliminates the crankshaft losses except for those of the oil seals and remaining bearings used to support the straight shaft. Reciprocating group terms including piston gas loading are also eliminated. Measurements will apply to friction model terms for the modified crankshaft, valvetrain, and auxiliary losses of the oil pump.

(4) Custom weights equivalent to the mass of the piston and connecting rod should be attached to the crankshaft in place of 2 of the pistons (ex, the first and third). This arrangement would fully rebalance the crankshaft with half of the pistons removed, and allow the reciprocating group friction to be inferred. The valvetrain components can also then be isolated for the removed pistons without affecting airflow. Measurements will apply to friction model terms for the crankshaft, auxiliary losses of the oil pump, and half of the reciprocating group, pumping, and valetrain terms, dependent on final state of assembly.

(5) Custom weights equivalent to the mass of the piston and connecting rod should be attached to the crankshaft in place of all 4 pistons, and the valvetrain disabled by removal of the timing chain. This arrangement allows direct measurement of the sum of the crankshaft losses and auxiliary losses of the oil pump.

The torque sensor used in this research was damaged during testing. More durable units need to be investigated. A non-contact (wireless) transmission sensor may be considered as a further upgrade.

Finally, the mean value engine model (MVEM) presented in this research was simplified and fit to the Ford 2.0L engine for the conditions of a limited amount of available fired-engine data. The MVEM may be expanded to the initially suggested form and the fit improved with data provided from additional fired-engine testing. This suggested testing would be required to take place on a running-engine dynamometer and is therefore beyond the scope and methodology of the motored testing presented herein.

References

[1] A. Schafer, J.B. Heywood, and M.A. Weiss, "Future fuel cell and internal combustion engine automobile technologies: A 25-year life cycle and fleet impact assessment," *Energy 31*, pp. 2064-2087, 2006.

[2] J.B. Heywood, *Internal Combustion Engine Fundamentals*. New York, N.Y.: McGraw Hill Inc., 1988.

[3] H, Heisler, *Vehicle and Engine Technology*. Great Britain: The Bath Press; on behalf of SAE, 1999.

[4] R. Stone, *Introduction to Internal Combustion Engines*. Great Britain: SAE International, 1999.

[5] D. Sandoval and J.B. Heywood, "An Improved Friction Model for Spark-Ignition Engines," *SAE Paper 2003-01-0725*, 2003.

[6] R.E. Gish, J.D. McCullough, J.B. Retzloff, and H.T. Mueller, "Determination of True Engine Friction," *SAE Paper 580063*, vol. 66, pp. 649-661, 1958.

[7] P.J. Shayler, D.K.W. Leong, I.G. Pegg, and M. Murphy, "Investigations of Piston Ring Pack and Skirt Contributions to Motored Engine Friction," *SAE Paper 2008-01-1046*, 2008.

[8] S.F. Rezeka and N.A. Henein, "A New Approach to Evaluate Friction and Its Componenets in Internal Combustion Engines," *SAE Paper 840179*, 1984.

[9] H. Nehme, N.G. Chalhoub, and N. Henein, "Development of a Dynamic Model for Predicting the Rigid and Flexible Motions of the Crank Slider Mechanism," in *Transaction of the ASME Vol. 120*, 1998, pp. 678-686.

[10] N.G. Chalhoub, H. Nehme, N.A. Henein, and W. Bryzik, "Effects of Structural Deformations of the Crank Slider Mechanism on the Estimation of the Instantaneous Engine Friction Torque," *Journal of Sound and Vibration*, vol. 224, no. 3, pp. 489-503, 1999.

[11] D. Taraza, N. Henein, A. Naeim, and W. Bryzik, "Experimental Determination of the Instantaneous Frictional Torque in Multicylinder Engines," *SAE Paper 962006*, 1996.

[12] H.K. Nehme, N.G. Chalhoub, and N.A. Henein, "Effects of Filtering the Angular Motion of the Crankshaft on the Estimation of the Instantaneous Engine Friction Torque," *Journal of Sound and Vibration*, vol. 236, no. 5, pp. 881-894, 2000.

[13] G.A. Kfoury, N.G. Chalhoub, N.A. Henein, and W. Bryzik, "Enhancement of the Accuracy of the P-W Method Through the Implementation of a Nonlinear Robust Observer," *Journal of Sound and Vibration 291*, pp. 1080-1103, 2005.

[14] R.K. Rajput, *A Textbook of Automobile Engineering*. Daryaganj, New Delhi: Laxmi Publications Ltd., 2007.

[15] S.N. Kurbet and R.R. Malagi, "Review on Effects of Piston and Piston Ring Dynamics Emphasis with Oil Consumption and Frictional Losses in Internal Combustion Engines," *SAE Paper 2007-24-0059*, 2007.

[16] J.E. Forbes and E.S. Taylor, "A Method of Studying Piston Friction," NACA Wartime Report, March 1943.

[17] W.A. Leary and J.U. Jovellanos, "A Study of Piston and Ring Friction," NACA Wartime Report, November 1944.

[18] J.C. Livengood and C. Wallour, "A Study of Piston Ring Friction," NACA Technical Note No. 1249, 1945.

[19] S. Furuhama and M. Takiguchi, "Measurement of Piston Frictional Force in Actual Operating Diesel Engine," *SAE Paper 790855*, 1979.

[20] M.F. Richez, B. Constans, and K. Winquist, "Theoretical and Experimental Study of Ring-Liner Friction," *9th Leeds-Lyon Symp.*, pp. 122-131, 1982.

[21] D.A. Parker, D.R. Adams, and G. Donnison, "The Measurement and Reduction of Piston Assembly Friction," in *2nd Int. Conf. Combustion Engines - Reduction of Friction and Wear, Instn. Mech. Engrs. Conf. Pub 1989, Paper C375/017*, 1989, pp. 27-34.

[22] I. Sherrington and E.H. Smith, "The Measurement of Piston-Ring Friction by the Floating Liner Method," *IMechE., Experimental Methods in Engine Research and Development*, pp. 1-11, 1988.

[23] R. Cerrato, R. Gozzelino, and R. Ricci, "A Single Cylinder Engine for Crankshaft Bearings and Piston Friction Losses Measurement," *SAE Paper 841295*, 1984.

[24] Y. Wakuri, T. Hamatake, M Soejima, and T. Kitahara, "Piston Ring Friction in Internal Combustion Engine," *Tribol. Int.*, vol. 5, no. 25, pp. 299-308, 1992.

[25] T. Kikuchi, S. Ito, and Y. Nakayama, "Piston Friction Analysis Using a Direct-Injection Single-Cylinder Gasoline Engine," *JSAE*, vol. 1, no. 24, pp. 53-58, 2003.

[26] R.A. Mufti and M. Priest, "Experimental Evaluation of Piston-Assembly Friction Under Motored and Fired Conditions in a Gasoline Engine," *Journal of Tribology*, vol. 127, no. 4, pp. 826-836, 2005.

[27] S. Cho, S. Choi, and C. Mae, "Frictional Modes of Barrel Shaped Piston Rings Under Flooded Lubrication," *Tribol. Int. 33*, pp. 545-551, 2000.

[28] H.M. Uras and D.J. Patterson, "Measurement of Piston and Ring Assembly Friction by Instantaneous IMEP Method," *SAE Paper 830416*, 1983.

[29] Y.G. Ku and D.J. Patterson, "Piston and Ring Friction by the Fixed Sleeve Method," *SAE Paper 880571*, 1988.

[30] T. Goto, S. Aoyama, S. Nagumo, Y. Nakajima, and M. Onoda, "Measurement of Piston and Piston Ring Assembly Friction Force," *SAE Paper 851671*, 1985.

[31] L.L. Ting, "Development of a Reciprocating Test Rig for Tribological Studies of Piston Engine Moving Components - Part I: Rig Design and Piston Ring Friction Coefficients Measuring Method," *SAE Paper 930685*, 1993.

[32] J. Dearlove and W. K. Cheng, "Simultaneous Piston Ring Friction and Oil Film Thickness Measurements in a Reciprocating Test Rig," *SAE Paper 952470*, 1995.

[33] J. Song and K. Boo, "Performance Evaluation of Traction Control Systems using a

Vehicle Dynamic Model," in *Proc. Instn. Mech. Engrs Vol. 218 Part D: J. Automobile Engineering*, 2004, pp. 685-696.

[34] E. Hendricks and S.C. Sorenson, "Mean Value Modelling of Spark Ignition Engines," *SAE Paper 900616*, 1990.

[35] I. Rasmussen, "Emissions from Cars, In Danish," The Laboratory for Energetic, The Technical University of Denmark, Lyngby, Denmark, Ph. D. Dissertation 1971.

[36] C.F. Aquino, "Transient A/F Control Characteristics of the 5 Liter Central Fuel Injection Engine," *SAE Paper 810494*, 1981.

[37] E. Hendricks, D. Engler, and M. Fam. (2010, February) Elbert Hendricks' Homepage at The Technical University of Denmark. [Online]. http://www.iau.dtu.dk/~eh/

[38] E. Hendricks et al., "Modeling of the Intake Manifold Filling Dynamics," *SAE Paper 960037*, 1996.

[39] K.J. Patton, R.G. Nitschke, and J.B. Heywood, "Development and Evaluation of a Friction Model for Spark-Ignition Engines," *SAE Paper 890836*, 1989.

[40] I.N. Bishop, "Effect of Design Variables on Friction and Economy," *SAE Paper 640807*, 1964.

[41] Image only. (2011, September) xorl. [Online]. xorl.wordpress.com/2011/03/page/3/

[42] B. Yasukazu and H. Mitsuru, "Analysis on Driving Forces of Oil Pumps for Internal Combustion Engines," *SAE Paper 860230*, 1986.

[43] T.J. Kovach, E.A. Tsakiris, and L.T. Wong, "Engine Friction Reduction for Improved Fuel Economy," *SAE Paper 820085*, 1982.

[44] R.G. Bayer, *Mechanical Wear Prediction and Prevention*. New York: Marcel Dekker Inc., 1994.

Appendix A: Electrical wiring diagram

Figure A-1 below shows the electrical wiring of the complete experimental setup. Everything from the high power wiring of the electric motor and its controller to the thermocouple wires for monitoring temperature is included. Beginning in the top left corner of the diagram the 480VAC 3-phase power wiring is depicted. After passing through proper fuses these wires connect to a latching circuit involving a contactor block, industrial control transformer, and appropriate door switches as shown. The control transformer produces 120VAC power which is then used to switch the 480VAC on and off. Moving lower on the diagram the 480VAC power is seen to enter the 2400 Series Charging Unit, as well as powering the cooling fan for the electric motor. The 120VAC produced at the transformer is fed through a thermostat to the cabinet's cooling fan, to the Omega DMD-465 Bridgesensor that conditions the signal from the torque sensor (as shown in the top right of the diagram), and to provide auxiliary power to the 2400 Series Charging Unit. The 2400 Series Charging Unit connects to the 2400 Series Inverter as depicted in the large blocks in the center of the diagram, as well as to the Resistor Block that is used to dissipate any energy fed back into the electric motor. The electric motor and associated optical encoder connects directly to the 2400 Series Inverter as shown. Remaining connections to the 2400 Series Inverter are made from either the Analog Port or the Parallel I/O Strip to the PCI-6229 DAQ card as shown in the lowest portion of the figure. The Analog Port provides access to the +/- 10V input and output signals, while the Parallel I/O Strip provides digital control switches and operating mode feedback.

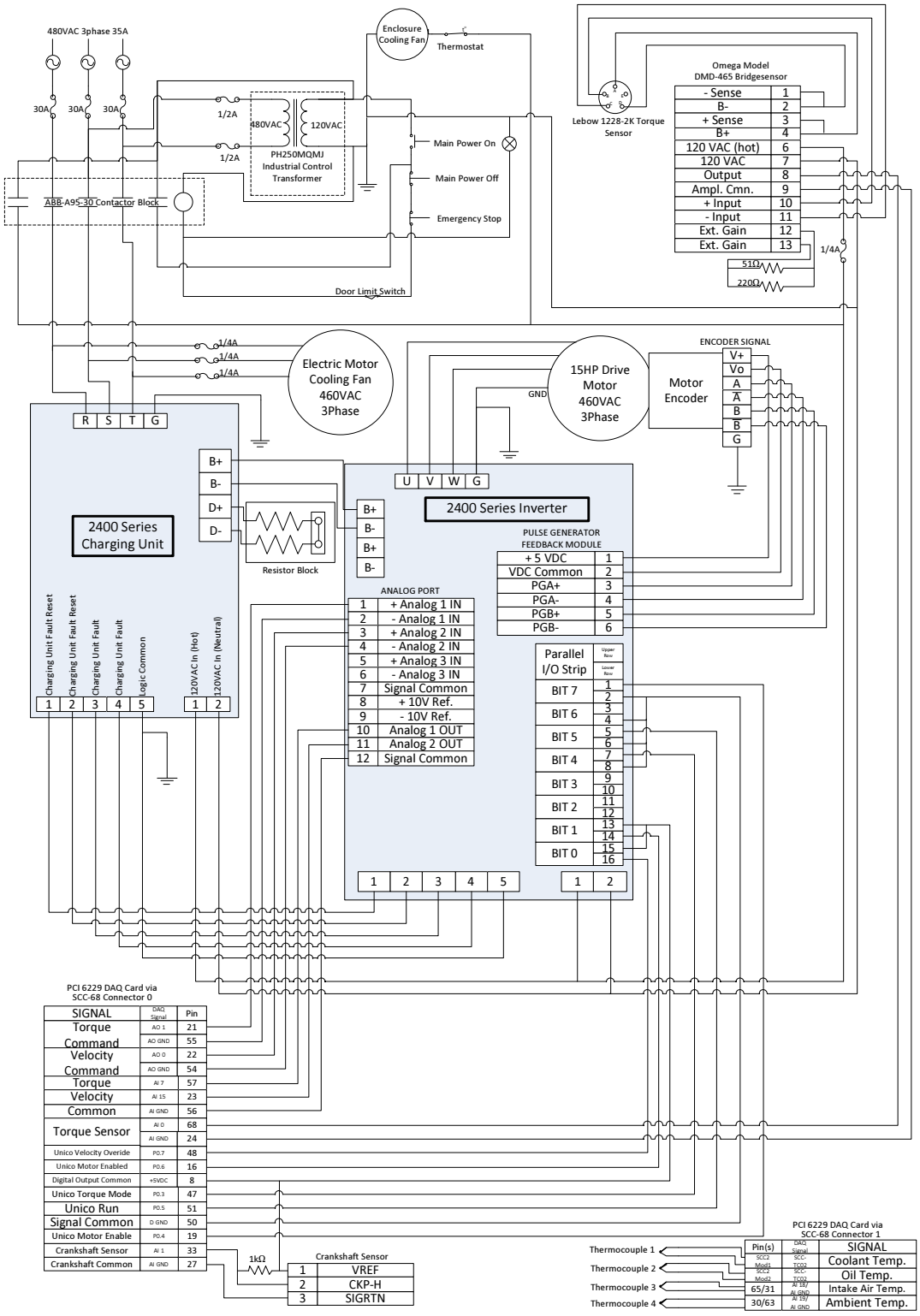

Figure A-1: Experimental setup electrical wiring diagram

Appendix B: Select component specifications

Table B-1 and Table B-2 below give selected specifications for the torque sensor and its corresponding signal conditioner that were used in this research.

Table B-1: Honeywell Model 1228-2k torque sensor specifications

Characteristic	Value
Torque Range	0-2000 lb-in
Max Speed	5000 RPM
Non-linearity	+/-0.15% of rated output
Hysteresis	+/-0.15% of rated output
Repeatability	+/-0.05% of rated output
Output at rated capacity	+/-2mV/V (nominal)
Excitation (maximum)	20Vdc or Vac RMS
Bridge resistance	350 ohm (nominal)
Number of bridges	1

Table B-2: Omega DMD-465 signal conditioner specifications

Characteristic	Value
Bridge excitation range	4 to 15 Vdc
Current output	120 mA max
Line and Load regulation	(0 to 100mA) 0.05% max
Output noise	0.5 mV RMS
Gain range	40 to 1000
Dynamic response	DC to -3 dB = 3Hz
Max output	+/-10 Vdc